

LBNL/PUB-5506

Conceptual Design Report of the Top-Off Upgrade of the Advanced Light Source at Lawrence Berkeley National Laboratory

Berkeley, December 23, 2004



Lawrence Berkeley National Laboratory,
1 Cyclotron Road, Berkeley, CA 94720

This work was supported by the Director, Office of Science, Office of Basic Energy Sciences, of the U.S. Department of Energy under Contract No. DE-AC03-76SF00098.

1	Motivation.....	5
1.1	Science at the Forefront	5
1.2	Increased Brightness with Top Off and Advanced Undulators	8
1.3	More Beamlines to Exploit the Brightness	11
1.4	Advantages to the user programs	12
2	Overall Scope of Project, Introduction of Subproject Parts.....	13
2.1	Present injection mode.....	14
2.2	Parameters and operation with Top-off	17
2.3	Introduction of the Subparts of the CDR	18
3	Detailed Description of all Parts of the Top-off Upgrade.....	20
3.1	User requirements	20
3.1.1	Operational Tests	21
3.2	Radiation Safety.....	25
3.2.1	Top-off Radiation Issues/challenges.....	25
3.2.2	Current Radiation Practices and Results.....	25
3.2.3	Top-off Radiation Issues/Challenges	29
3.2.4	Collimation/Scraper System	36
3.2.5	Radiation Monitors	39
3.2.6	Top Off Mode, Radiation Safety System.....	40
3.3	Accelerator Physics Studies.....	45
3.3.1	Vertical emittance reduction in the Storage ring	45
3.3.2	Operation with smaller vertical gaps in the storage ring	49
3.3.3	Linac to booster transfer efficiency	50
3.3.4	Booster to Storage ring transfer efficiency	50
3.3.5	Minimizing radiation levels	52
3.4	Injector Reliability	54
3.4.1	Scope.....	54
3.4.2	Injection System Components	54
3.4.3	Injector Operating Mode.....	55
3.4.4	Injection System Component Failures	55
3.5	Pulsed Magnets	59
3.5.1	Introduction.....	59
3.5.2	Pulsed magnet operation.....	59
3.5.3	Booster bumps analysis:	62
3.5.4	Booster Fast extraction Kicker:	68
3.5.5	Booster and Storage ring Thick and Thin septum magnets	72
3.5.6	Storage ring ‘fast’ bump magnets.....	90
3.5.7	Summary of pulse magnets study:	93
3.6	DC and Slow Ramped Magnets.....	94
3.6.1	Power Supplies.....	94
3.6.2	DC Cabling	95
3.6.3	AC Power.....	96
3.7	Timing System	97
3.7.1	Injector Timing	97
3.7.2	User Gating System	97
3.8	Booster RF System	98

3.8.1	Overall System Introduction & Description	98
3.8.2	Booster RF Power Requirements for Top-Off Mode of Operation	101
3.8.3	Final Amplifier/Transmitter with Controller	104
3.8.4	High Voltage Power Supply	104
3.8.5	RF Cavity Window	105
3.8.6	RF Transmission Line.....	105
3.8.7	Controls & Interlocks.....	106
3.8.8	Utilities.....	106
3.8.9	Structure Core Drilling	107
3.8.10	Spares	107
3.9	Diagnostics.....	108
3.9.1	Booster Diagnostics	108
3.9.2	BTS Diagnostics	113
3.9.3	Storage Ring Diagnostics.....	118
3.10	Computer Control System.....	121
3.10.1	Magnet Power Supplies	121
3.10.2	BTS Diagnostics	122
3.10.3	Booster Diagnostics	122
3.10.4	Booster RF	123
3.10.5	Radiation Protection.....	123
3.10.6	Collimation Controls.....	123
3.10.7	Software Effort.....	123
3.10.8	IOC software effort.....	123
3.10.9	Control Room Application Development	124
3.10.10	New IOCs.....	124
3.11	AC Power Utilities.....	126
3.11.1	AC Power Utilities-Booster Ring	126
3.11.2	Description-General.....	126
3.11.3	Booster RF AC Power	127
3.11.4	Booster to Storage Ring (BTS).....	127
4	Cost, Schedule, Installation.....	130
4.1	Project Organization	130
4.2	Work Breakdown Structure	131
4.3	Cost Estimate	132
4.4	Draft Schedule	134
4.5	Installation.....	139
4.6	Commissioning.....	140
5	Acknowledgments.....	141
6	References.....	142
6.1	List of Figures	143
6.2	List of Tables	146
7	Appendices.....	148
7.1	Parameter List	148
7.1.1	Storage Ring Performance Parameters	148
7.1.2	Booster Performance Parameters	148
7.1.3	Technical Parameters	149

7.2 Full Cost Estimate..... 150

1 MOTIVATION

One of the first third-generation synchrotron light sources, the ALS, has been operating for almost a decade at Berkeley Lab, where experimenters have been exploiting its high brightness for forefront science. However, accelerator and insertion-device technology have significantly changed since the ALS was designed. As a result, the performance of the ALS is in danger of being eclipsed by that of newer, more advanced sources. Enhanced brightness is the key not only to remaining competitive but also to setting a new performance standard.

Significant brightness improvements can be realized in the core soft x-ray region by going to top-off operation, where injection would be quasi-continuous. In top-off mode with higher average current, a reduced vertical emittance and beta function, and small-gap permanent-magnet or superconducting insertion devices, one to two orders of magnitude improvement in brightness can be had in the soft x-ray range. These improvements also extend the high energy range of the undulator radiation beyond the current limit of 2000 eV. Most important, top-off avoids the penalty of a much reduced lifetime that would otherwise come with increased brightness, a penalty that is totally unacceptable to the user community.

In brief, the ALS upgrade that we are planning includes full-energy, top-off injection with higher storage-ring current and the replacement of older first-generation insertion devices with newer state-of-the-art insertion devices and four new application-specific beamlines now being identified in a strategic planning process. The upgrade will involve no major disruption to the experimental program of the ALS, since it can be accomplished in a phased sequence of short (less than 2 month) shutdown and commissioning periods. The first phase of the ALS upgrade is to transition to top-off operation with higher beam currents and smaller vertical beamsizes. It is the top-off upgrade that is the focus of this report. Before describing the upgrade, some examples of different types of science that are enabled with higher brightness are presented.

1.1 Science at the Forefront

Exploitation of the high brightness of a third-generation synchrotron light source translates into four areas: (1) high resolving power for spectroscopy; (2) high spatial resolution for microscopy and spectromicroscopy; (3) high temporal resolution for diffraction and spectroscopy; and (4) high coherence for experiments such as speckle and lensless imaging. Capabilities in these areas will also enable the ALS to support the Molecular Foundry, a U.S. Department of Energy Nanoscale Science Research Center that is now under construction at Berkeley Lab with construction, equipment installation, and commissioning expected by the end 2006. The ALS offers a variety of characterization and diagnostic capabilities applicable to nanoscale science and technology, including diffraction, photoemission, absorption, and fluorescence spectroscopy, often with temporal as well as spatial resolution.

The physics of complex materials studied by photoemission with high energy and high momentum resolution has benefited enormously from the availability of high brightness sources. Improvement in the energy resolution from 50 meV to 10 meV has enabled investigation of low-energy excitations, such as the dispersion “kink” [1] and bilayer splitting in the high T_c superconductors [2]. Seven photoemission papers have made it to the “ten most cited physics papers” at one time or another. Further improvement in resolution down to the meV range will provide even sharper experimental incisiveness for the understanding of complex materials ranging from strongly correlated electron systems and magnetic materials to systems with reduced dimensionality.

Inelastic x-ray scattering (IXS) is a complementary but more demanding spectroscopy. As a photon-in/photon-out technique, it has the advantage over photoemission of greater penetration and the ability to look at bulk properties and buried interfaces. IXS is the only direct probe of charge-charge correlations that offers momentum resolution. Moreover, unlike photoemission, it is possible, to apply a magnetic field to the sample. The disadvantage of IXS is its inherently low cross-section, so that the state-of-the-art resolution is 250 meV. We have dedicated the last remaining straight section at the ALS to MERLIN, a new beamline mainly for IXS that will reach a resolution of 10 meV. (A second dedicated end station will be for photoemission with sub-meV resolution). This performance will be achievable only below a photon energy of 100 eV, so that only momentum transfers close to the Brillouin-zone center ($q=0$) can be investigated. To reach the zone edge it would be necessary to work closer to 1000 eV. This can in principle be done but only after the upgrade described below.

Understanding fundamental magnetic interactions is at the frontier of solid-state physics but also driven by the technology of thin-film magnetic devices. At the ALS we have pioneered the development of new techniques, one example being magnetic imaging for the elucidation of exchange bias in the coupling of the antiferromagnetic (AF) to ferromagnetic (FM) materials that lies at the heart of magnetic spin valves. This problem could only be solved with our new ability to image AF and FM domain structures at high spatial resolution, with interfacial sensitivity, and with elemental and chemical selectivity, by means of photoemission electron microscopy (PEEM). These techniques are revolutionizing our understanding of thin-film magnetism [4-8], and we expect PEEM 3, the next generation microscope, to begin commissioning in 2005 [9].

Manipulation of spin directly by optical or electrical means leads to the concept of “spintronics”[10]. The fundamental lateral length scale now shrinks to the magnetic exchange length measured in nanometers with a temporal scale set by magnetization precession time of picoseconds. On the horizon are devices such as spin transistors, spin-transfer devices or even spin-based quantum computers. Together with complementary laser probes, time-resolved soft x-ray probes will lead to major advances. Experiments in this domain are brightness limited and are at the edge of viability at the ALS today. They would become practical with the enhancements envisioned for this upgrade.

The structure of condensed matter is not static, and to understanding the behavior of condensed matter at the most fundamental level requires structural measurements on the time scale on which atoms move. The evolution of condensed matter structure, via the making and breaking of

chemical bonds and the rearrangement of atoms, occurs on the fundamental time scale of a vibrational period, ~ 100 fs. Atomic motion and structural dynamics on this time scale ultimately determine the course of phase transitions in solids, the kinetic pathways of chemical reactions, and even the efficiency and function of biological processes. A thorough understanding of such dynamic behavior is a first step to being able to control structural evolution and will have important scientific applications in solid-state physics, chemistry, materials science, and biology [11]. The tremendous potential scientific impact of this research area is largely unfulfilled, owing to the inadequacy of present zeroth-generation short-pulse x-ray sources (roughly analogous to rotating-anode sources in comparison with modern synchrotrons).

We have made considerable progress on the construction of a user facility, Beamline 6.0.1, which will fill a critical need for the growing ultrafast x-ray research community [12]. It will also serve as a stepping stone for developing femtosecond techniques in advance of the LCLS x-ray laser at the Stanford Linear Accelerator Center. An in-vacuum, permanent-magnet undulator/wiggler will radiate both soft and hard x-rays from 120 eV to 10 keV. The device has 50 periods with a period of 30 mm and a peak magnetic field of 1.5 T. There will be two branch lines, one with a variable-line-space grating spectrograph and the other with a Ge (111) or Si (111) crystal monochromator. On the soft x-ray branch, a streak camera will serve as the detector for measurements on picosecond time scales. The ultrafast facility will make use of an already installed wiggler (which now serves a protein-crystallography beamline) for generating femtosecond x-rays via laser-modulation (slicing) of the stored electron beam. A 40-kHz femtosecond laser system will be located at the end of the beamline and will serve the dual purposes of providing laser pulses for slicing the synchrotron beam and providing tunable “pump” pulses for sample excitation. Based on the present storage-ring parameters, we expect that x-ray pulses of 200 fs duration will be produced.

The high brightness of an optimized third generation source not only translates directly into high average coherent x-ray flux but the quasi-dc nature of synchrotron radiation is essential for many experiments. For example, the diffraction of a coherent x-ray beam from a sample has information at the spatial scale of the wavelength and over a lateral dimension of the coherence width. Two ways to use the information encoded are illustrated below. The upgrade is key in providing much higher coherent flux at the optimum energies.

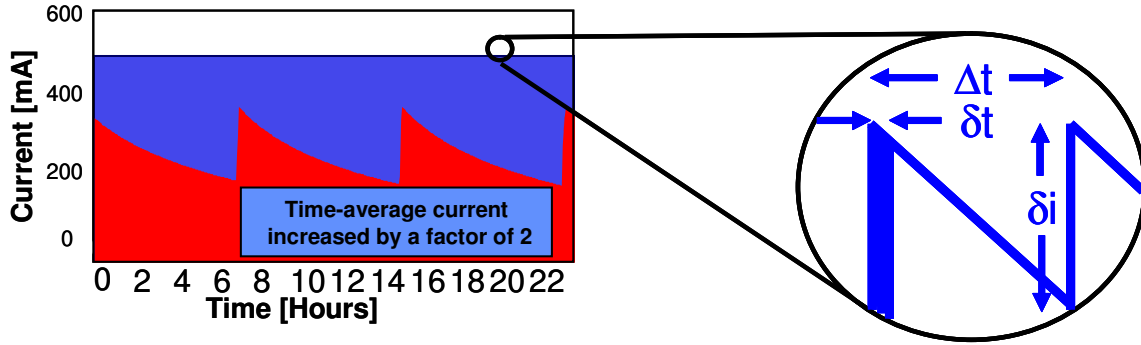
Zone plate-based x-ray microscopes can now achieve spatial resolutions down to 18 nm at soft x-ray energies, and with improvements in fabrication, some further progress can be expected. However, for the imaging of three-dimensional objects, the thickness of the object places severe restrictions on resolution because the depth of field scales as the square of the resolution. For many applications, such as cellular biology, materials engineering, in-situ study of materials in reactive conditions, and nanotechnology, there is a pressing need to find a technique that can look at thick objects at nanometer resolution. It has recently been found that coherent diffraction patterns can be reconstructed back into real space without prior knowledge of phase information. The key is that the transform of a non-periodic object is continuous in Fourier space and can be “oversampled.” Electron-density positivity and the sample boundary are then sufficient constraints for convergence on a unique phase set and hence an image [12, 13]. We now have the prospect of being able to image thick objects at nanometer resolution in liquids or under reaction conditions. This capability will give us a revolutionary new tool.

The interplay between spin, charge, lattice, and orbital degrees of freedom produces very complex phase diagrams and nanoscale phase behaviors in transition metal oxides. These micro-phases are thought to play a key role in the properties of high-temperature superconductivity in the cuprates and colossal magnetoresistance (CMR) in the manganites. Again, these length scales map directly to soft x-ray probe wavelengths. Soft x-ray coherent x-ray scattering offers important advantages, such as high coherent flux, excellent chemical contrast, an adequate scattering wave vector to probe nanoscale features, and access to core levels of interest, such as oxygen and the transition metals. These advantages should enable a much more complete characterization of these materials, including their response to external control parameters, such as field, temperature, and current, as well as their related dynamical properties.

1.2 Increased Brightness with Top Off and Advanced Undulators

At present, the ALS is operated in a mode where beam is injected three times daily to 400 mA. In the eight hours between fills, the beam decays to 200 mA with a time-averaged current of about 250 mA. Machine performance of the ALS is lifetime limited. While substantial improvements in brightness and current have always been technically feasible, they incur the penalty of a much reduced lifetime, an option totally unacceptable to our users. In top-off mode, injection would be quasi-continuous, so that the lifetime impediment is less important. In addition, because of the nearly constant current in the storage ring, beamline optics would not suffer the large thermal fluctuations associated with large changes in storage-ring current. These greatly reduced thermal fluctuations of beamline optics would result in enhanced photon position stability at all ALS beamlines.

It is also possible to increase the current in the machine to 500 mA (Figure 1.2-1). In terms of raw flux, the combination of top-off and increased current would therefore double our capacity in a very cost effective way. More important than capacity, however, is enhanced capability. The proposed upgrades will enable the newer and more revolutionary experiments briefly outlined above.



<u>coupling</u>	δi	Δt	σ_h	σ_v	σ'_h	σ'_v
After Top-off	1.5mA	32.0s	298 μ m	8 μ m	22 μ rad	3 μ rad

Figure 1.2-1: Parameters of top-off injection after the upgrade with reduced vertical emittance.

Parameter	Present	Future
Time Average Current (mA)	250	500
Vertical Emittance (nm•rad)	0.15	0.03
Vertical Beta Function (m)	3.6	2.25
Vertical Magnetic Gap (mm)	14	5

Table 1.2-1: Comparison of Present and Future Storage-Ring Parameters

The other half of the enhanced-brightness strategy is the insertion device. At present, the “workhorse” at the ALS is a 4.45-m-long, linearly polarizing undulator. The ALS has five of these insertion devices with periods of 5, 8, and 10 cm that were designed and installed about a decade ago. Each of these devices require one full storage ring straight section. With subsequent significant advances in undulator technology, the currently favored design is the 2-meter elliptically polarizing undulator (EPU). Of these, we have two installed, one under construction, and one proposed. Together with one wiggler, these undulators fill nearly all available ALS straight sections.

However, insertion-device technology continues to advance, with small-gap, short-period, in-vacuum undulators and superconducting undulators emerging as the insertion devices of choice. So, in addition to top-off operation with higher average current, further brightness improvements can be realized in the core soft x-ray region by reducing the vertical emittance and beta function of the storage ring, which allow us to install such small gap, permanent-magnet or superconducting insertion devices.

In Table 1.2-2 and Figure 1.2-2, we compare the brightness of the old workhorse with the present storage ring parameters to four new small-gap devices with the upgraded ring parameters shown in Table 1.2-1.

Photon Energy	Present Brightness	Future Brightness	ID length, period, technology	Improvement
500 eV	5.70×10^{18}	2.04×10^{19}	short, 30 mm, IVU	3.58
		6.93×10^{19}	long, 30 mm, IVU	12.2
1000 eV	3.49×10^{18}	1.88×10^{19}	short, 30 mm, IVU	5.39
		4.29×10^{19}	long, 30 mm, IVU	12.3
		5.83×10^{19}	short, 14.5 mm, SCU	16.7
		2.02×10^{20}	long, 14.5 mm, SCU	57.9
2000 eV	6.07×10^{17}	3.71×10^{19}	short, 14.5 mm, SCU	61.1
		1.25×10^{20}	long, 14.5 mm, SCU	206
4000 eV	not accessible with undulators	2.35×10^{19}	short, 14.5 mm, SCU	—
		4.81×10^{19}	long, 14.5 mm, SCU	—

Table 1.2-2: Comparison of Present and Future Brightness (photons/sec/0.01 %bw /mm²/mrad²)

The new devices all have a vacuum gap of 5 mm, in contrast to the 9 mm of the older undulators. The first two are 30-mm-period in-vacuum devices of lengths 4.3 m (long) and 1.8 m (short), respectively. These two devices could be constructed with hybrid permanent magnets [14, 15]. The second two are 14.5-mm-period superconducting devices of lengths 4.3 m (long) and 1.5 m (short), respectively [16, 17].

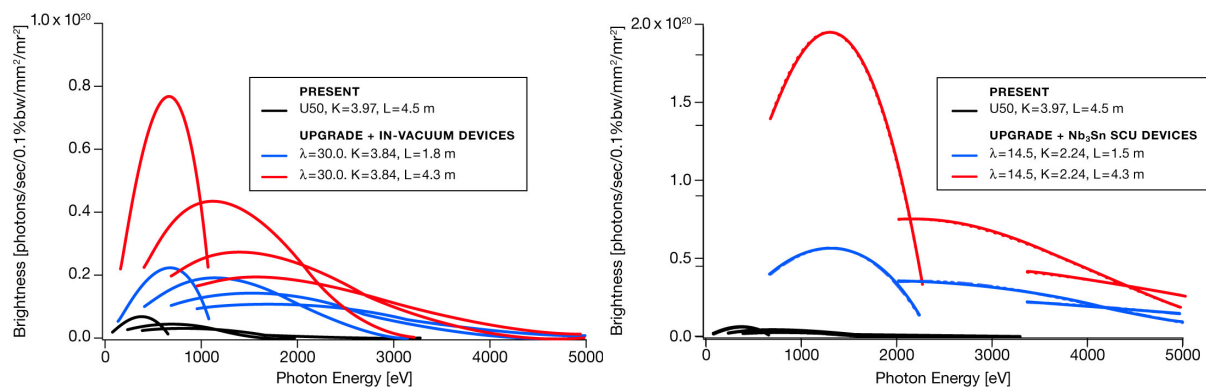


Figure 1.2-2: Brightness comparison of new ALS insertion devices to current insertion devices.

We see that there are one to two orders of magnitude improvement in brightness obtainable in the soft x-ray range. In reducing the vertical emittance after the upgrade, we also reduce the wavelength at which the undulators become diffraction limited to 0.57 nm, i.e., the ALS will be diffraction limited in the vertical direction throughout the whole of the soft x-ray energy range. It should also be noted that the proposed upgrades extend the high-energy range of the undulator radiation, which is currently limited at 2000 eV.

1.3 More Beamlines to Exploit the Brightness

The ALS, unlike the larger x-ray machines, has a severely limited number of straight sections. This has meant that several world-class programs, which would normally command one or more insertion devices, have multiple end stations sharing a single beamline. It would be preferable to design optical systems fully optimized to the type of science on each beamline.

Consequently, an important aspect of the later stages of the upgrade (beyond the scope of this CDR) is to replace some full-length, linearly polarized undulators with chicaned straights containing two shorter, more advanced devices. With the increased flux and brightness available, each of these devices will perform far better than the current devices, but at the same time allow simultaneous operation of two fully optimized, independent, application-specific beamlines.

Our plan is to replace five workhorse insertion devices with nine newer more advanced insertion devices plus four new beamlines that are responsive to the scientific drivers, such as those discussed above (Figure 1.3-1). A strategic planning process involving the full complement of ALS management, scientific staff, user community, and advisory bodies has been under way with the aim of identifying the scientific areas that would benefit from such independent beamlines and the types of beamlines needed to serve them.

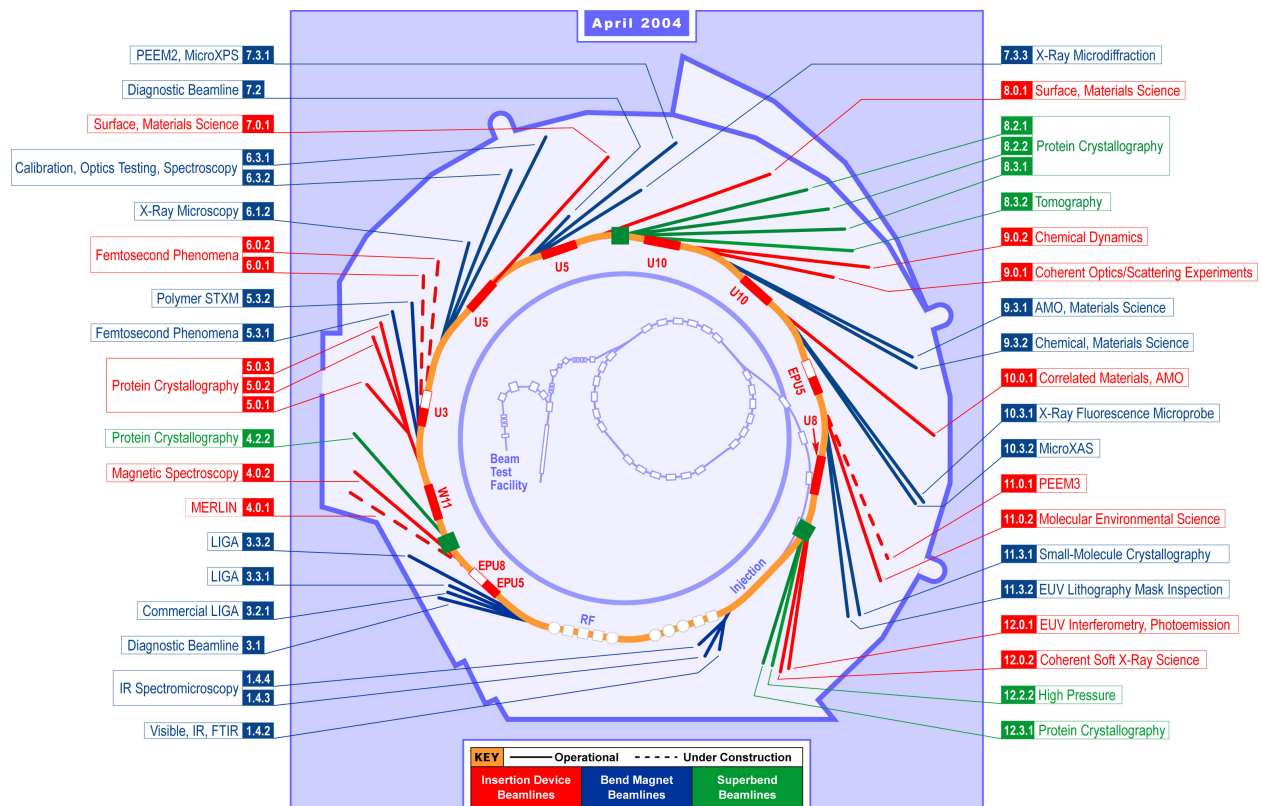


Figure 1.3-1: Beamlines at the ALS. In the upgrade, the five “workhorse” 4.45-m-long U5, U8, and U10 undulators would be replaced with nine shorter, small-gap devices with higher brightness in an orderly, phased manner to minimize disruption of the experimental program.

1.4 Advantages to the user programs

Continual topping-off by intermittent injection of small increments to the beam current in the storage ring will appear to many ALS users as an operational mode at constant current. For these users, the decay of the stored beam will become invisible. They will operate continuously with constant photon flux. The planned value of the current in top-off mode is 500mA. This is an increase of about a factor of two in the time-averaged flux for all experiments.

Continuous operation avoids the breaks in data taking necessary when the storage ring is refilled. A common experience of ALS users under pre top-off conditions is that low-rate data-taking under a particular set of conditions does not complete before the scheduled fill. Requests are often made to delay the fill, usually granted, but not by more than about ten minutes. This inconvenience will be eliminated.

With constant thermal loading of beam line components, there will no longer be a risk of thermally driven variations of mirror alignment, which can lead to variations of the photon flux at an experiment. The surface of an optic in an intense x-ray beam develops a thermal bump. To first order this resembles a change in the radius of the optical surface and affects the optical scheme like a change in the focal length of the optic. After top-off, these effects are constant on bend-magnet beam lines and can be compensated. Many of these first bend-magnet mirrors are bent, so the bending can be adjusted to remove most of the thermal effects. (Undulator beam lines must still be designed for variable thermal loading, because of the variability of the undulator gap.)

With top-off, there is no longer a strong requirement to maximize the lifetime of the stored beam. And there are three benefits to be exploited. First, the vertical emittance coupling can be reduced, to increase the vertical source brightness. Brightness limited experiments can enjoy higher count rates. Second, deliberate bunch lengthening may not be necessary, so that the natural bunch length could be recovered. This means that time resolved experiments requiring time resolution of the order of tens of picoseconds can exploit the ALS time structure. Faster experiments involving time resolved detectors or laser slicing can exploit the increased peak current within the shortened bunch. Third, the minimum gap of the undulators can be reduced. This will require replacement of the vacuum chamber for our existing undulators. Sector 6 will have a new in-vacuum undulator designed for this smaller minimum gap. The low energy limit is extended for all small-gap undulators, so that those users limited by the lowest energy of an undulator can gain access to a larger operational range. The extended limit allows greater freedom to optimize the period length of future devices.

2 OVERALL SCOPE OF PROJECT, INTRODUCTION OF SUBPROJECT PARTS

In this section we discuss the scope of the project and introduce the subproject parts. The scope of the top-off requires upgrading the injection system to full energy and injecting continuously with the shutters opened. Beyond that there are several additional components that make up the scope. The overall scope of the top-off upgrade is listed below:

- Upgrade injector to enable full energy injection, including necessary modifications to controls and timing.
- Where necessary for operational reliability (with the higher requirements in top-off), improve diagnostics and other existing systems.
- Install radiation safety system and conduct studies necessary for injection with shutters open.
 - Acquire DOE approval for necessary Final Safety Analysis Document (FSAD) changes.
- Minimize injection transients to reasonable levels.
 - Provide user gating signal.
- Migrate to higher current (400 → 500 mA) operation with smaller vertical beamsizes (150 → 30 pm rad emittance).
- Enable bunch cleaning in booster to make top-off compatible with two bunch operation.
- Transition to Top-off with minimal negative impact to users
 - Upgrade in a typical annual shutdown and commissioning period (<2 months)
 - Minimize the initial teething period
- Ensure that all subsystems within this project are upgraded in a safe manner, protecting the workers, the public, and the environment.

Because top-off is critical to upgrading the ALS, it is desirable to complete the upgrade as soon as possible. If we receive the funding in time we plan to go to upgrade to full energy injection by Mid 2006. Subsequently we would transition to top-off injection and commission the bunch cleaning. The total cost of the project is 4.85 M\$. To achieve this schedule requires receiving 2.4 M\$ by March 2005 and the remaining funds at the beginning of FY06.

In order to discuss the scope of the project it is useful to first describe our present mode of operation.

2.1 Present injection mode

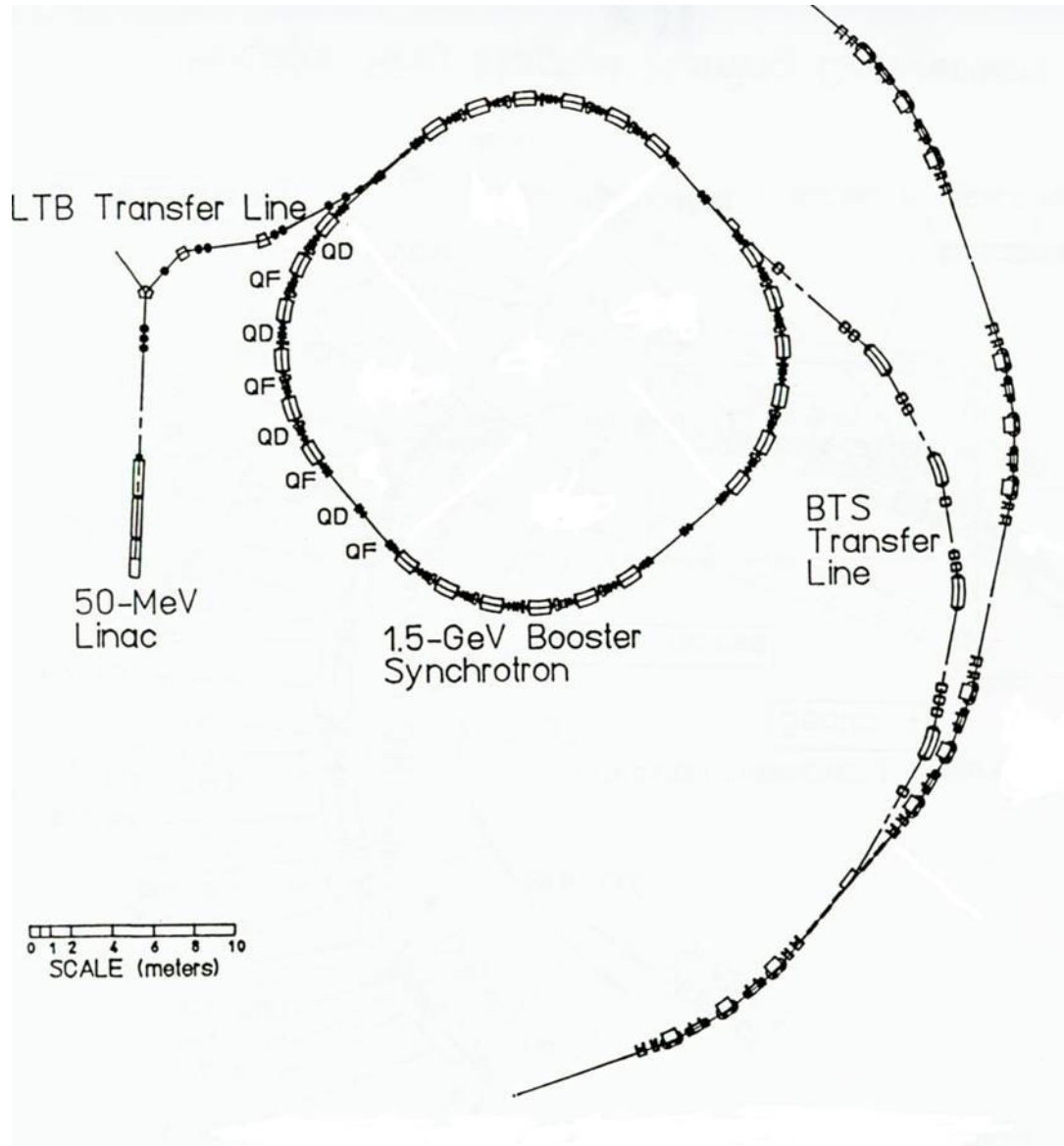


Figure 2.1-1: Layout of our present injection system

Our present injection system is shown in Figure 2.1-1. It consists of a 120 kV thermionic gun followed by a 50 MeV linac, and a 0.05 to 1.5 GeV Booster. The gun can extract 1 to more than 10 bunches of electrons spaced 8 ns apart. The electron bunch length is compressed before entering the linac where the electrons are further accelerated up to 50 MeV. Next the bunches pass from the linac to the Booster through the Linac-to-Booster (LTB) transfer line where they are injected into the Booster synchrotron. A Booster injection kicker is excited when the electrons

enter the booster ring and causes the electrons to be injected on-axis. The injection kicker flat top is long enough to allow more than 10 bunches (spaced 8 ns apart) to be injected into the Booster.

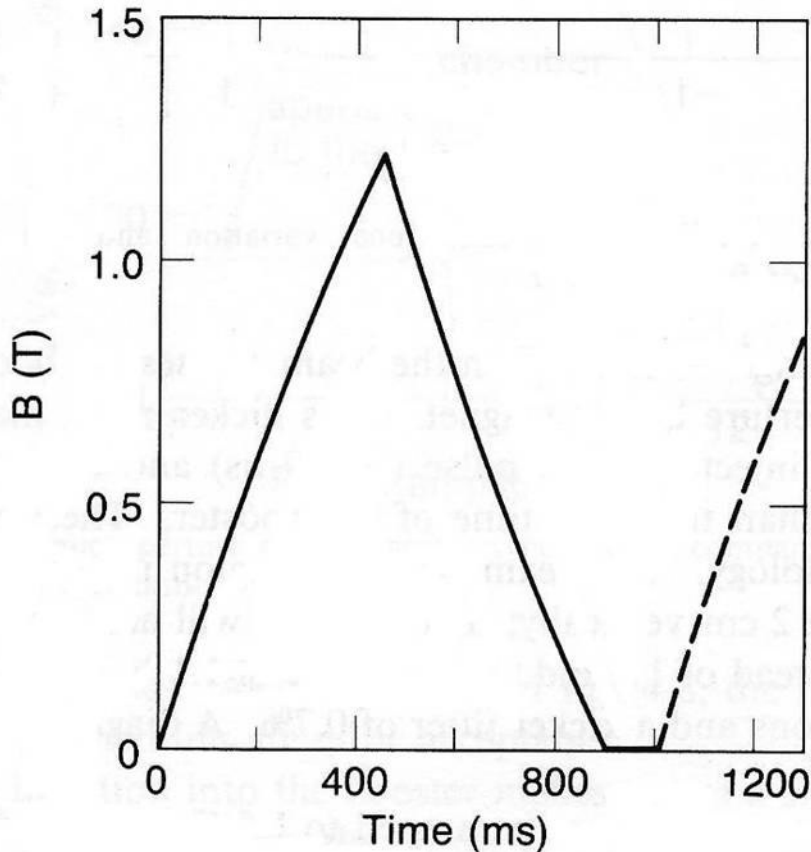


Figure 2.1-2: Booster ramping cycle.

The lattice of the Booster is a FODO structure consisting of 24 dipoles, 32 quadrupoles, and 20 sextupoles. The Booster lattice is 4-fold symmetric with 4 straight sections – one for injection, one for extraction, one for RF, and the other for diagnostics (such as the DCCT, a direct current current transformer). The Booster ramps the electron energy from 50 MeV to 1.5 GeV and the electrons are extracted. The Booster can cycle at 1 Hz between 50 MeV and 1.5 GeV. The Booster bend magnet ramping cycle is shown in Figure 2.1-2.

The Booster extraction consists of 3 bump magnets to move the stored beam towards the septa magnets, a fast (single-turn) extraction kicker, and thin and thick septa magnets where the electrons enter the Booster-to-Storage Ring (BTS) transfer line. The electrons then pass through the BTS line to the storage ring where they are injected into the storage ring

The electrons are injected into the storage ring in straight 1. In that straight section there are four bump magnets and a thin and thick septum magnet. The electrons passing down the BTS magnets enter the thick and thin septa magnets while at the same time the electrons in the storage ring are bumped toward the septa magnets by the 4 fast bump magnets. After entering the ring

the injected electrons oscillate radially about the stored electron beam. This oscillation is slowly damped (~ 15 ms) due to radiation damping. After one second a fresh bunch train of electrons can be injected. Once the storage ring is filled, the storage ring is ramped up in energy from 1.5 GeV to 1.9 GeV.

The storage ring is 196 m long and with a 500 MHz RF system it is possible to fill up to 328 bunches. There are two basic bunch fill patterns – multibunch and 2 bunch. In multibunch pattern a long train of bunches is filled (usually 276 bunches) followed by a gap. Sometimes in multibunch fill mode one bucket in the gap is filled – the so called camshaft bunch. The bunch current is 400 mA at the top of the fill with 10 mA in the camshaft and the remainder of the current evenly distributed between the other 276 bunches.

In 2-bunch fill mode two bunches on either side of the storage ring are filled (up to 30 mA / bunch). This fill pattern is used for experiments requiring a long gap between pulses for timing experiments. The current in the gap needs to be much smaller than that of the filled bunches ($< 0.01\%$). The ratio of the current of the non-targeted to the targeted bunches is called the bunch purity. Non-targeted bunches are filled because some of the non-targeted bunches in the injector also contain current. So after injection and bringing the ring up to full energy, beam is ejected out of the non-targeted bunches through resonant excitation. After the non-targeted bunches are cleaned the beam is given to users.

In 2 bunch mode, the time between fills is 2 hours rather than 8 hours due to the shorter lifetimes. The lifetime in the ALS is primarily determined by intrabeam scattering and is shorter in 2-bunch mode because of the higher beam currents per bunch.

At present the injector is run in either in single bunch injection mode or with a bunch train of 3 to 4 bunches. When the injector is well tuned up it will inject more than 1.5 mA in 4 bunches into the storage ring every second.

At present the lifetime is increased to acceptable levels by decreasing the electron bunch density. The vertical beam size is increased by introducing some vertical dispersion with skew quadrupoles. The longitudinal beam size is doubled through the use of a third harmonic RF system.

2.2 Parameters and operation with Top-off

With top-off operation we plan to double the time average current by keeping the current constant at 500 mA. In addition we plan to reduce the vertical emittance from the present value of 150 pm-rad to 30 pm-rad. Figure 1.2-1 shows the planned parameters after top-off operation. During special accelerator physics shifts, the ALS has run with vertical emittances as low as 5 pm-rad **Error! Reference source not found.**. So 30 pm-rad are easily achievable in normal user operation.

Because of the higher currents and lower vertical beam sizes the lifetime will become shorter. With our parameters, the lifetime at 500 mA will be 3 hours as opposed to 8 hours at 400 mA with the present parameters. In the intrabeam (so-called Touschek) dominated regime, the time between fills ΔT is related to the drop in current ΔI from the initial current, I_i , to the final current, I_f , by the relation

$$\Delta T = \tau_i \left(\frac{\Delta I}{I_f} \right)$$

where τ_i is the beam lifetime at the top of the fill. For present operation in 8 hours the current decays by 200 mA. In top-off operation the beam will decay by 1.5 mA in 32 seconds.

These parameters are the baseline parameters. Note that one can adjust them based on the needs of the users. It will also be possible to run with different sets of operating parameters during different running periods.

During top-off we assume that we can inject 1.5 mA per pulse. Presently it is possible to achieve 1.5 mA per pulse in 4 bunches. This is done with insertion device gaps opened and with a minimum vacuum chamber aperture of 8.9 mm full gap. With top-off we need to inject with insertion devices closed. Also the minimum vacuum chamber aperture will be as small as 5 mm. Our preliminary machine studies have shown a 40% reduction in injection efficiency with IDs closed and a vertical scraper with a 5 mm aperture. The plan for Top-off is to inject with a longer train, up to 10 bunches, and to improve the injection efficiency. Studies of the longer bunch trains and to improve the injection efficiency will be performed as part of the precommissioning.

Present Operation	After Top-Off
<ul style="list-style-type: none"> • Injection at 1.5 GeV and then ramp • Inject with insertion devices open • Average beam current is 250 mA • Vertical emittance is 150 pm rad • Lifetime is 8 hours at 400 mA 	<ul style="list-style-type: none"> • Full energy injection (1.9 GeV) • Inject with insertion devices closed • Average beam current is 500 mA • Vertical emittance is 30 pm rad • Lifetime is about 3 hours at 500 mA

<ul style="list-style-type: none"> • Injection period every 2 to 8 hours <ul style="list-style-type: none"> – 1 Hz injection for 4 minutes <ul style="list-style-type: none"> • From 200 to 400 mA • Photon shutters are closed during injection • Parasitic bunches cleaned in the storage ring 	<ul style="list-style-type: none"> • Injection period about every 30 seconds <ul style="list-style-type: none"> – 1 pulse <ul style="list-style-type: none"> • From 498.5 to 500 mA • Photon shutters remain open during injection • Parasitic Bunches cleaned in the booster
--	---

Table 2.2-1: Difference between present operation and operation after the top-off upgrade

Bunch cleaning in the storage ring is not an ideal solution with top-off because the cleaning process perturbs the stored beam. The plan is to clean the bunches in the Booster and cleanly inject into the storage ring. Injecting clean bunches is essential for using top-off with 2 bunch operation. This has been achieved at the APS, ESRF, and is in routine operation at Spring-8.

Table 2.2-1 shows the difference between present operation and operation after the top-off upgrade. There are several major changes from present operation to operation with top-off. A major issue that is being addressed is radiation safety with top-off. With top-off operation we will need to inject with the personnel safety shutters opened. It is important that when we inject with the personnel safety shutters opened that we prevent “freshly injected” electrons from passing down the beam line. In addition we need to mitigate the increased radiation levels due to injected electrons striking the storage ring vacuum chamber near the beamlines, the increase in normal stored losses, and the increase in levels due to RF trips. Finally, it is important to minimize the radiation levels near radiation sensitive equipment such as permanent magnet insertion devices, electronics equipment, etc. The plan for addressing these issues is described in section 3.2.

A very important aspect of the upgrade is to ensure that the transition to top-off operation is smooth with minimal impact to the present users. Therefore we plan to use our 1 and 2-day monthly shutdowns plus typical annual shutdowns of < 2 months for the installation of the components for the project. In addition we need to ensure that we minimize the teething period after the installations.

2.3 Introduction of the Subparts of the CDR

In Section 3 we provide a detailed description of the various parts of the top-off upgrade project. In Section 3.1 we discuss the user requirements including operational tests performed to evaluate any negative impact from injection transients on the different types of user experimental techniques. In Section 3.2 we discuss radiation safety issues. Section 3.3 presents accelerator physics studies done in preparation of top-off as well as some precommissioning studies. In Section 3.4 we discuss the injector reliability – what is the present reliability of the injector and what are the issues for top-off. In Section 3.5 we discuss the necessary upgrades to the pulsed magnets. A lot of work was done this past year to determine what was necessary to upgrade. Fortunately most of pulsed magnets are fine with small modifications. In Section 3.6 the upgrades of the DC and

slow ramped magnets are discussed. The magnets themselves are capable of 1.9 GeV operation. The power supplies need to be upgraded. In Section 1.1 we discuss the upgrades needed for the timing system for the injector as well as the user gating system. The user gating system will provide a warning to users that an injection pulse is coming so that they may gate out that time. The Booster RF system is discussed in Section 3.8. Upgrading the RF windows and amplifier/transmitter is necessary and is one of the larger systems that need to be upgraded for the project. Diagnostics are discussed in Section 3.9. Upgrades in diagnostics are necessary for top-off as well as to perform bunch cleaning in the booster. Computer control system upgrades are discussed for the various systems in Section 3.10. In Section 3.11 we discuss the present utilities. Because we do not require 1 Hz injection (we plan to run with 1/3 Hz injection), it is not necessary to upgrade the utilities. Finally, in Section 4 the cost, schedule, and installation of the upgrade project is discussed.

3 DETAILED DESCRIPTION OF ALL PARTS OF THE TOP-OFF UPGRADE

3.1 User requirements

Figure 1.2-1 shows the pre top-off and the proposed post top-off current profile in the storage ring. Pre top-off, the shutters are closed, the undulators are opened and the storage ring is refilled about every 8 hours. Post top-off, the time between injection pulses is Δt and the current is increased each time by δi . The injection transient duration is δt . Likely post top-off values are tabulated here.

δi	Δt	δt	ϵ_v	σ_h	σ_v	σ'_h	σ'_v
1.5 mA	32.0 s	50 ms	30×10^{-12} m rad	298 μm	8 μm	22 μrad	3 μrad

Table 3.1-1: Operational parameters chosen as goal for the ALS top-off upgrade.

Table 3.1-1 shows an intermediate coupling situation where the vertical brightness is increased up to the point where the vertical source RMS size shrinks to $8\mu\text{m}$ in the center of the straight section. This seems a reasonable place to operate, because smaller sources impose a figure requirement on the first optic that can be very difficult to maintain. For example, a sagittally focusing, horizontally deflecting first mirror on a soft x-ray undulator beam line typically deflects through 3 degrees. Such a mirror would be internally cooled with carefully engineered channels carrying water perhaps 1.5mm below the optical surface. It would be manufactured out of copper or silicon. Located inside the shield wall, its thermal deformation at full current with the undulator closed might give rise to an rms sagittal slope error, weighted by the illumination intensity of the useful radiation, of about 10 microradians. This deformation depends on the undulator gap and must blur the source by a negligible amount. That would be about $4\mu\text{m}$ in this example.

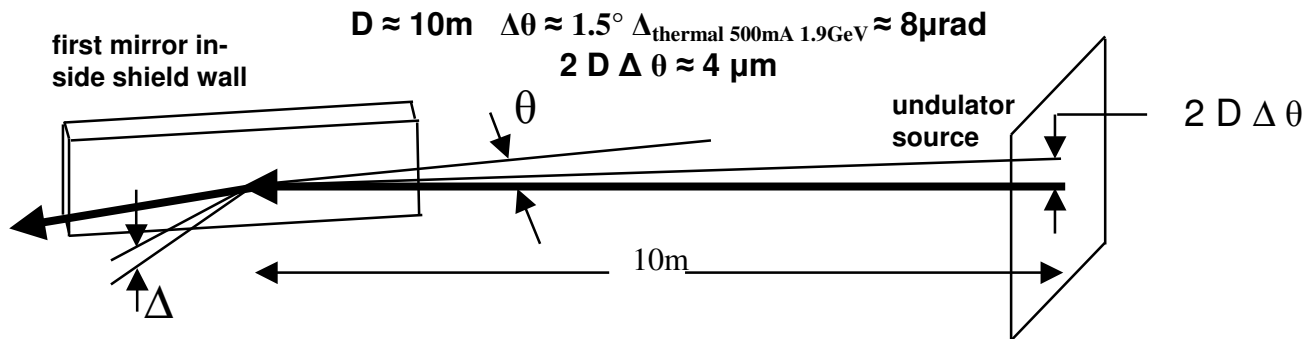


Figure 3.1-1: Heating induced focusing error on sagittally focusing mirror.

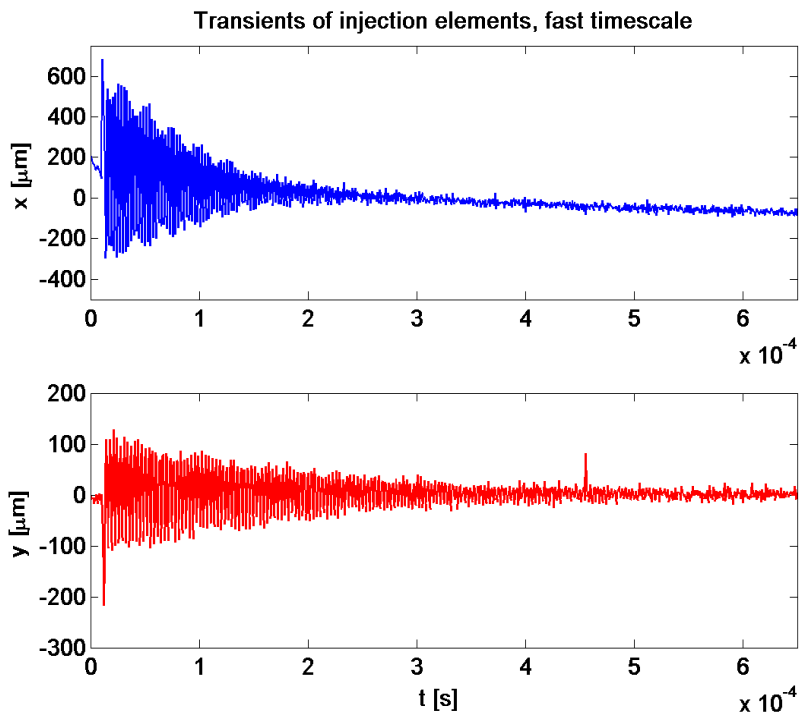
The time between injection is set by the need to inject 1.5mA each time. This is the limit from a single booster pulse. Polling users during the operational tests revealed a desire for widely spaced injections with a short transient. For those experiments requiring an inhibit-gate, 30 seconds between injections seemed reasonable.

3.1.1 Operational Tests

Operational tests suggest that there will be some users who will notice the effects of the top-off injection process, because of the sensitivity of their experiment to the position of the electron beam. Transient perturbations of the closed orbit around the ring are likely at the time of top-off injection. These orbit perturbations can cause a transient change in the flux delivered into those experiments that make use of an image of the source on an aperture. A gating signal will be provided, which will mark the timing of the top-off injection. Those experiments sensitive to the injection transients must find some way to inhibit data-taking during injection.

This past year a number of measurements were done to evaluate the impact of the injection process on the users. During three accelerator physics shifts, experiments were performed with representatives from various beam lines - 1.4, 4.0, 5.3.2, 6.3.2, 7.0, 7.3, 8.3.1, 10.0, 10.3.2, 11.0.2, and 12.0. During these experiments, data was taken with the injection elements turned on and compared with the case where the injection elements were not turned on. These results were presented at several meetings including a spring UEC meeting. The results are summarized in light source note LSBL-709.

In top-off, the beam line shutters remain open during injection and the injection process itself is not completely transparent to all users. In particular, the injection magnets perturb the stored beam during injection. At present there is a fast oscillation caused by non-closure of the pulsed injection bump magnets, as well as a slower closed orbit distortion caused by decaying eddy currents in the main septum magnet.

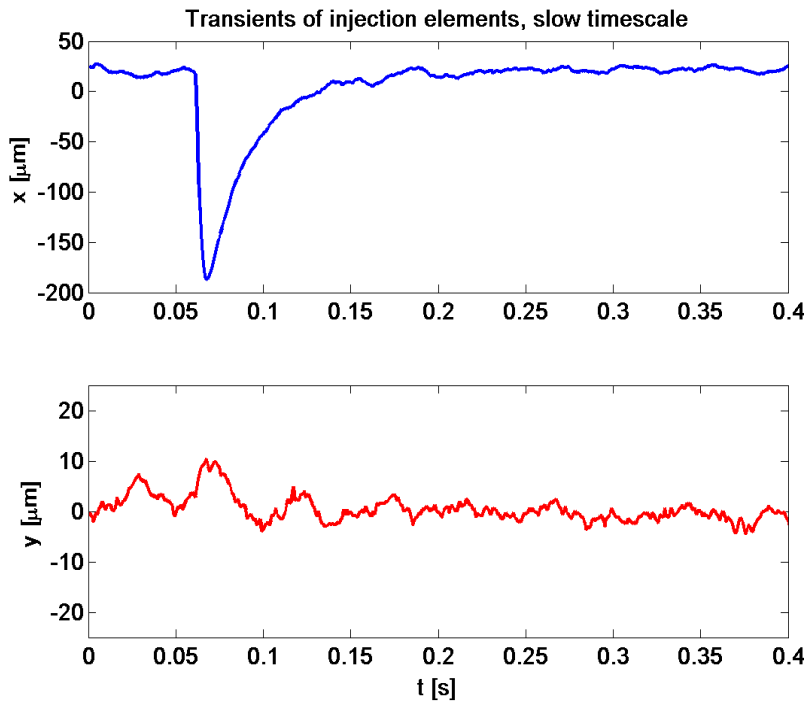


In terms of
beamsize

$\sim 1.3 \sigma_x$
peak

$\sim 4 \sigma_y$
peak

Figure 3.1-2: Fast (vertical and horizontal) oscillation of the beam, due to mismatch of the bump magnets. This lasts less than 1 ms.



In terms of
beamsize

$$\sim 2/3$$

$$\sigma_x$$

$$< 1/3$$

$$\sigma_y$$

Figure 3.1-3: Slower (horizontal) closed orbit distortion, due to the septum magnet eddy currents, that lasts about 0.1 s.

The results of these studies were that most of the experiments did not see the injection transients. Scanning instruments with short integration times were most affected. By far the most sensitive technique was STXM, with transient intensity fluctuations from 5% to 40%, depending on whether the septum magnet was pulsing. The infra-red beam line could also detect these injection transients. Some spectroscopy counting experiments (for example at beam line 4.0) saw the effect of the pulsed septum magnet, but not the fast bumps. We are currently in the process of reducing the impact of the septum on the beam transients.

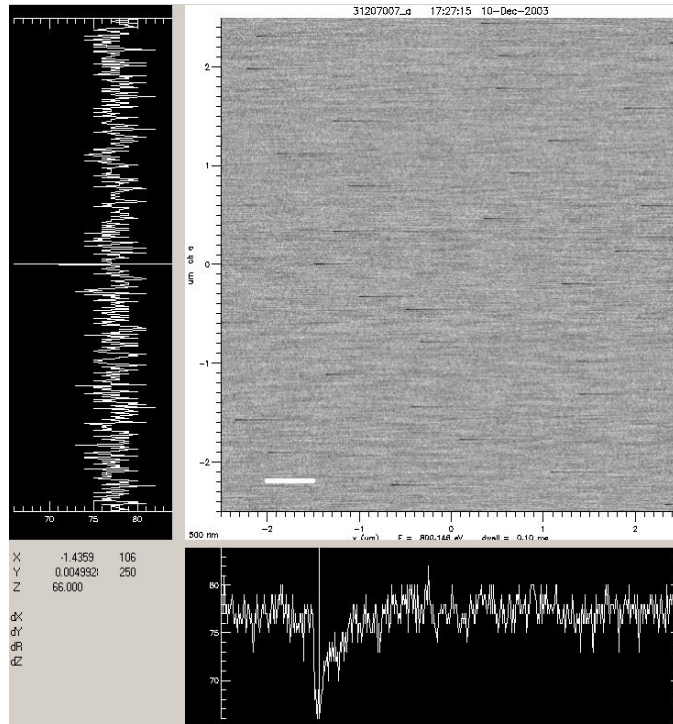


Figure 3.1-4: Injection transients causing an intensity fluctuation during a horizontal line scan in STXM at beam line 11.0.2 (second test 7 Dec 2003). Septum magnet turned off. One horizontal line scan takes 60 ms.

Gating seems to be a requirement for these sensitive experiments. For example, in STXM the microscope scans a horizontal line of the image and the vertical image position is stepped one pixel while the horizontal scanner resets for the next horizontal line. The inhibit gate will inform the microscope computer that an injection has occurred and the next vertical step will be inhibited. The next horizontal line scan will be a repeat and the corrupted line will be overwritten.

3.2 Radiation Safety

3.2.1 *Top-off Radiation Issues/challenges*

Gamma radiation or neutrons are generated in the ALS when electrons collide with vacuum chamber components or gas particles. The manner with which electrons are lost can be divided into three categories.

1. Injected electrons not being captured in the storage ring.
2. Slow loss of electrons from the stored beam - mostly due to intrabeam scattering.
3. Loss of the whole stored beam when the RF is suddenly turned off – RF trip.

The scope of the ALS top-off upgrade has several changes in operation that will have an impact on the radiation levels.

1. Injection will take place with the personnel safety shutters opened and the insertion device gaps closed.
2. The average current will be increased by a factor of 2.
3. The beam size will be decreased by a factor of 2 to 3.

The first is a fundamental change that is unique to top-off. All three of these changes will increase the amount of electron beam loss in the ALS. In addition to personnel safety issues, higher radiation losses near permanent magnet or hybrid insertion devices result in a more rapid rate of deterioration of those insertion devices.

In this section we will describe our plan to mitigate the radiation issues resulting from the top-off upgrade. We first describe our current radiation practices and results. Next we will discuss the issues of top-off and our plan for dealing with each of them. Finally we will present our future plan and our preparations for a safety review to modify the ALS safety envelope.

3.2.2 *Current Radiation Practices and Results*

3.2.2.1 Radiation Monitoring Systems

Presently there are a variety of passive and active monitoring systems located around the ALS. The locations of these monitors are shown in Figure 3.2-1. There are two types of active systems that are constantly monitoring the radiation levels:

- 12 interlocked neutron/gamma monitors
- ~25 beamline 1st optics gamma monitors

The 25 beamline optics monitors are not interlocked. They alarm in the control room if the level reaches or exceeds 5 mrem/hr.

There are three types of passive monitors.

- ~50 in-close dosimeters
- 12 peripheral dosimeters
- ~50 badged staff

The first two are measuring radiation levels around the clock for the entire year. The ALS dosimetry policy requires people to wear dosimetry if they expect to spend more than 10% of their time inside the area defined by the outer storage ring shield walls. This typically excludes users from the requirement to wear dosimeters.

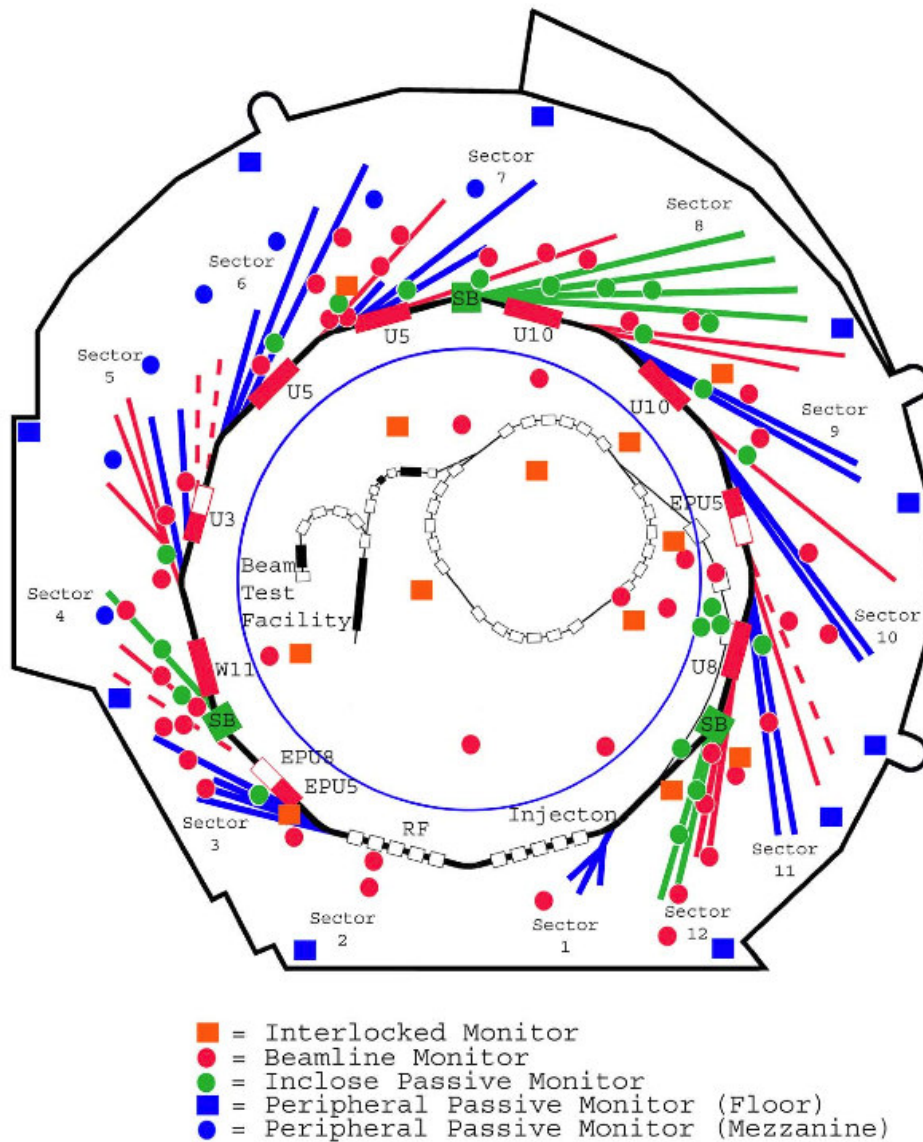


Figure 3.2-1: Locations of Radiation Monitors at the ALS.

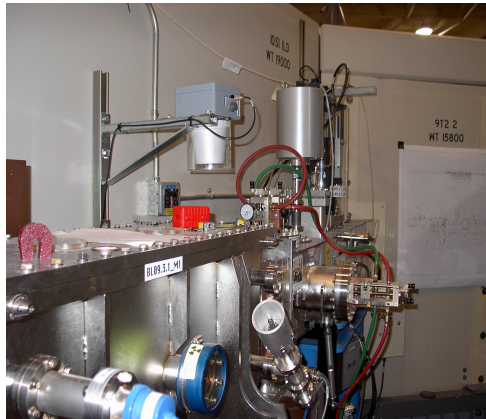


Figure 3.2-2: Active Radiation Monitors: Interlocked Neutron/Gamma Monitors (left) and Optics Gamma Monitors (right).



Figure 3.2-3: Passive Radiation Monitors: In-close dosimeters (left) and Peripheral dosimeters (right).

The in-close dosimeters are located throughout the experimental floor. The majority of the dosimeters are positioned close to the shield wall near first optics tanks where we expect the highest scatter from gas bremsstrahlung. Some are also located at the end of beamlines where users spend the majority of their time. The in-close dosimeters are read every 4-6 weeks

ALS 3-Pack Summary Report

January, 2004 CR-39 in field from 1'

Gamma: Neutron:

Location Description	Issue	Return	Net (mrad)	CR-39 #
ALS-01	1/3/08	2/20/08	3	0
ALS-02	1/3/08	2/20/08	2	7
ALS-03	1/3/08	2/20/08	0	0
ALS-04	1/3/08	2/20/08	0	2
ALS-05	1/3/08	2/20/08	0	0
ALS-06	1/3/08	2/20/08	0	0
ALS-07	1/3/08	2/20/08	0	4
ALS-08	1/3/08	2/20/08	0	0
ALS-09	1/3/08	2/20/08	0	0
ALS-10	1/3/08	2/20/08	0	0
ALS-11	1/3/08	2/20/08	0	3
ALS-12	1/3/08	2/20/08	0	0
ALS-13	1/3/08	2/20/08	0	0
ALS-14	1/3/08	2/20/08	0	0
ALS-15	1/3/08	2/20/08	0	2
ALS-16	1/3/08	2/20/08	8	13
ALS-17	1/3/08	2/20/08	0	1
ALS-18	1/3/08	2/20/08	4	2
ALS-19	1/3/08	2/20/08	0	2
ALS-20	1/3/08	2/20/08	0	0
ALS-21	1/3/08	2/20/08	0	1
ALS-22	1/3/08	2/20/08	0	1
ALS-23	1/3/08	2/20/08	0	7
ALS-24	1/3/08	2/20/08	2	2
ALS-25	1/3/08	2/20/08	0	3
ALS-26	1/3/08	2/20/08	7	16
ALS-27	1/3/08	2/20/08	0	6
ALS-28	1/3/08	2/20/08	0	0
ALS-29	1/3/08	2/20/08	0	9
ALS-30	1/3/08	2/20/08	0	1

Table 3.2-1: A January 2004 summary report of the in-close gamma and neutron monitors.

and the neutron monitors are read every 3-4 months. In Table 3.2-1 a summary report is shown for January 2004. Results have been corrected for background. This report represents a typical average period and demonstrates the low stray radiation levels on the ALS experimental floor.

There have been no readings above background in the peripheral neutron/gamma monitors in more than 10 years of operation of the machine. There have been no readings above background of the 50 badged permanent staff directly related to ALS operations.

The difference between annual doses as measured by the in-close dosimeters and the combined results of both the peripheral dosimeters as well as staff dosimeters indicates the conservative placement of the in-close dosimeters as well as an indication of the personnel occupancy factor – the fraction of a year a person actually spends on the experimental floor, particularly in the re-

gion of ID first optics tanks. Our approach has been to provide passive monitoring around the locations of highest scattered radiation levels and when the levels exceed an annual dose of approximately a few hundred mrem, based on continuous (no occupancy factor) monitoring, to reduce the levels by providing local shielding around the source of scattered radiation.

Based upon the 10 years of results for the peripheral dosimeters and personnel dosimeters this approach seems sufficient for current operations. With the increased losses projected for top-off operations, a different approach is required – one which attempts to control or localize electron beam losses in the storage ring and then provides the necessary local shielding inside the storage ring shield walls in order to reduce potential radiation levels on the experimental floor and minimizes the impact of additional shielding that otherwise might be required on beamlines.

3.2.3 Top-off Radiation Issues/Challenges

3.2.3.1 Preventing “freshly” injected electrons passing down beam line

In our present operation the beam line personnel safety shutters (PSS) are closed when beam is injected. With top-off operation it is necessary to inject electrons with the personnel safety shutters opened. If injected electrons pass down the beam pipe they will strike the first optic in the beam line. If the full charge of a freshly injected bunch strikes a first optic the radiation dose can be unacceptably high. Figure 3.2-4 shows a calculation of the unshielded dose equivalent at 30 cm from one injected pulse of electrons carrying 1 nC of charge and striking a high Z material. This charge of 1 nC is roughly the amount of charge we anticipate injecting in a single shot into the storage ring. At large angles the dose equivalent is about 20 mRem however in the forward direction the dose equivalent can be 10-100 Rem. This is clearly an unacceptable accident condition that cannot be allowed to occur. Therefore it is critical that we demonstrate, or provide passive protection to insure that it is impossible to inject electrons down any beam line. Preventing electrons from being injected down the beam line is a condition that has been addressed at other facilities doing top-off such as the APS [19], SLS [20], and Spring-8 [21]. We have adopted a similar strategy to those facilities.

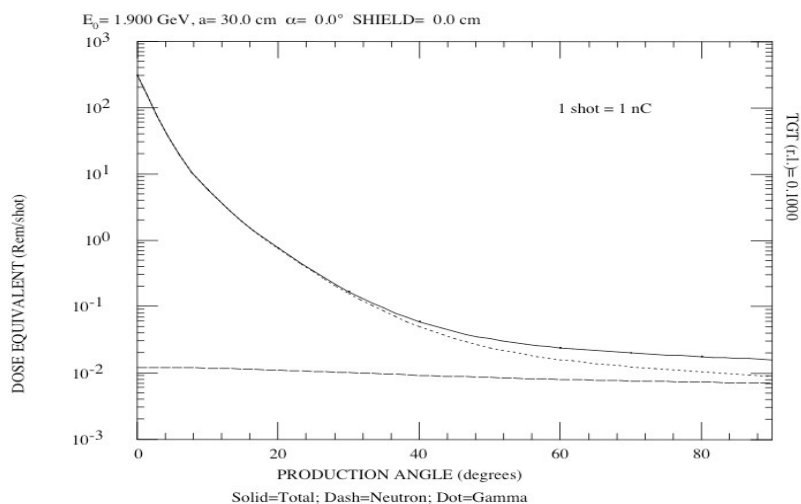


Figure 3.2-4: Passive Dose equivalent at 30 cm of one injected pulse of electrons carrying 1 nC of charge striking a high Z material.

One can easily conceive of a scenario where injected electrons can pass down a beam pipe. Any of the 36 bend magnets could be shorted such that an injected e- beam would be directed down the front end and into the beam line instead of its nominal 10 degree bend in the storage ring. Such a condition would preclude storing beam. Therefore the basis of all our tracking studies, as has been done elsewhere, is the requirement that there be stored beam. These studies are detailed in the following sections.

Another scenario whereby electrons might be directed down a beam line is the quenching of one of our Superbend dipoles. The ALS has installed three of these superconducting dipole bend magnets. The first beam port on a Superbend magnet is at 8 degrees. The nominal bend is 10 degrees. If the Superbend were at 80 percent of its nominal field, the injected electrons upon exiting the Superbend magnet would travel down the 8 degree bend magnet beam line. Simulations [22] have shown that a 1 percent change in the Superbend nominal field would result in the loss of stored beam. Recent measurements indicate that the time during a quench for the Superbend to drop to 80 percent of its nominal field is greater than 0.5 seconds. Beam loss would occur at 1 percent drop and in a fraction of a millisecond thereafter. The loss of stored beam could easily trigger the radiation safety interlock system to inhibit the next injected pulse.

In the next section the tracking studies are detailed and requirements for preventing electrons from being injected down a beam line are summarized.

3.2.3.2 Tracking Study Assumptions

Following similar approaches as used by the APS [19], ESRF [24], and others, we track particles backwards from the point or beam line of interest to the injection point of the storage ring. If it is determined that particles cannot be successfully tracked from a beam line front end to the injec-

tion point then the inverse must also be true – that injection into the storage ring cannot be directed down the beam line. The condition of stored beam is assumed.

Beam line 2.1, which is currently under design, will become the closest beam line to the storage ring injection point. Straight sections 1 and 3 will not have insertion devices as these straights are used for injection and rf cavities. Straight 2 may some day contain an insertion device however our current estimate is that it may prove more difficult to inject down 2.0 than 2.1 since by definition 2.0 is the 0 degree port and any electron beam must therefore pass through the B1 magnet with no deflection.

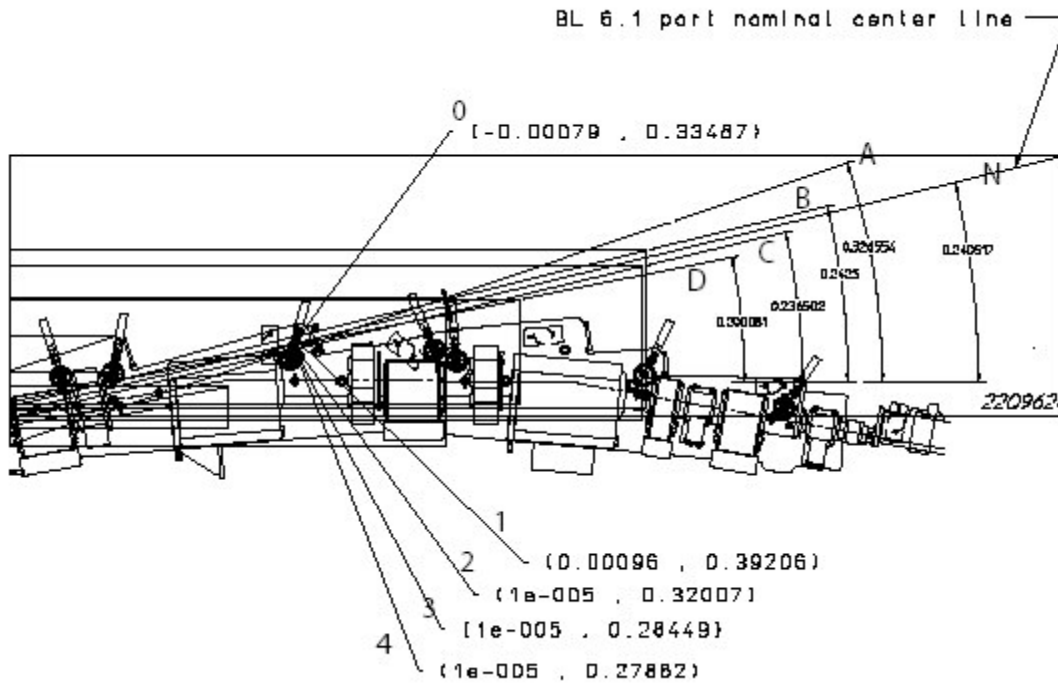


Figure 3.2-5: Geometry of x.1 beamline. Rays A-D mark the extremes in angle and offset that still pass through the frontend apertures. Ray N marks the nominal center of a x.1 beamline.

Line	T(rad)	T(deg)	dT(rad)	Point	Xo(m)	dX(m)	Z(m)
N	0.240517	13.780577	0.000000	0	0.334870	0.000000	-0.000790
A	0.326554	18.710122	0.086037	3	0.392060	0.057190	0.000960
B	0.242500	13.894194	0.001983	1	0.320070	-0.014800	0.000010
C	0.236502	13.550535	-0.004015	4	0.284490	-0.050380	0.000010
D	0.200081	11.463770	-0.040436	2	0.278820	-0.056050	0.000010

Table 3.2-2: Geometry parameters of the apertures for a x.1 beamline.

The geometry is outlined in Figure 3.2-5 and Table 3.2-2. The reference ray is Line N. The 4 lines (A ~ D) are defining the boundary marking the outer boundaries of the 2.1 exit port and limited by the downstream photon stops. With respect to Line N, the other 4 rays are in the range

of -40 mrad to 86 mrad. For conservatism we simply sample over -50 mrad to 100 mrad. Similarly for position offsets we sample over the range -70 mm to

Inverse Tracking from BL2.1

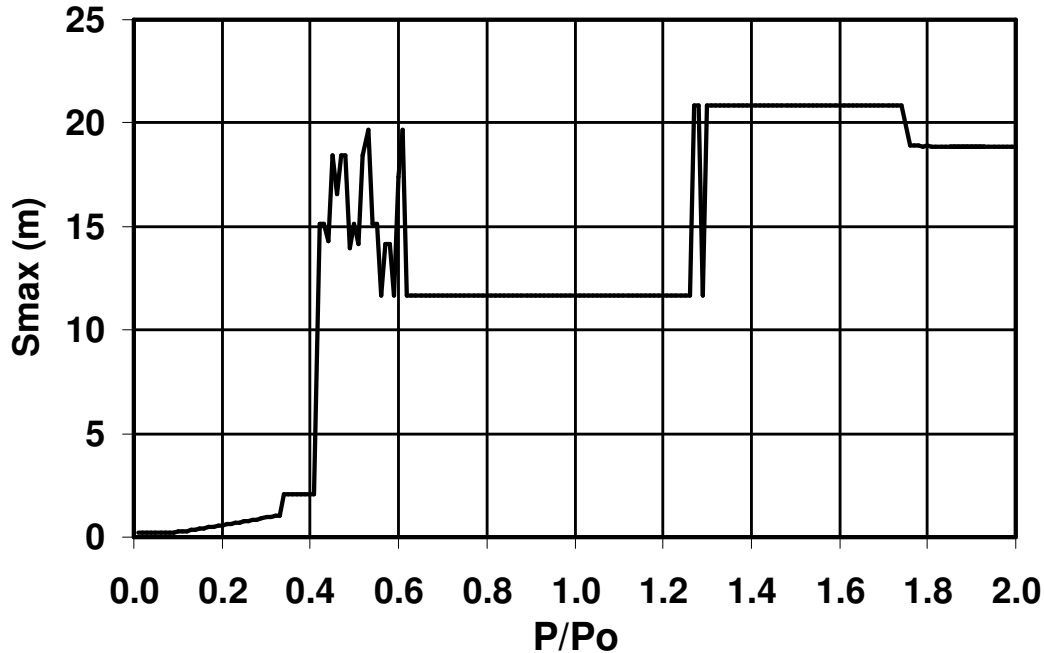


Figure 3.2-6: Maximum distance injected back to SR injection point.

70 mm. Particles are injected at the longitudinal location of BPM5 just downstream of the second bending magnet (at the locations marked as 0-4 in the Figure) on Line N. Realistic physical apertures and magnetic field profiles are used.

3.2.3.3 Tracking Study Results

Tracking results are summarized in Figure 3.2-6 for injected beam energy to stored beam energy ratios (P/P_0) ranging from 1% to 200%. It is clear from this plot that there is no condition for which the beam injected at beam line 2.1 can travel completely back to the injection point at 25 m. The results indicate that the nominal beam energy reaches less than half way to the injection point. There is however a range of P/P_0 (40% to 62% and $> 125\%$) for which the injected beam reaches within about 5 m of the injection point.

To demonstrate why this happens, the paths of several particles are selected and plotted together with the physical apertures. This is shown in Figure 3.2-7. Here it can be seen that nominal energy particles hit the entrance to the upstream straight section while there is a solution for extreme P/P_0 particles to produce a trajectory through the straight section. This indicates that the physical apertures provided by the straight section are very effective in filtering out particles of

approximately nominal energy. The results were repeated while varying individual quadrupoles in the storage ring by +/- 20%. The results did not significantly change the results.

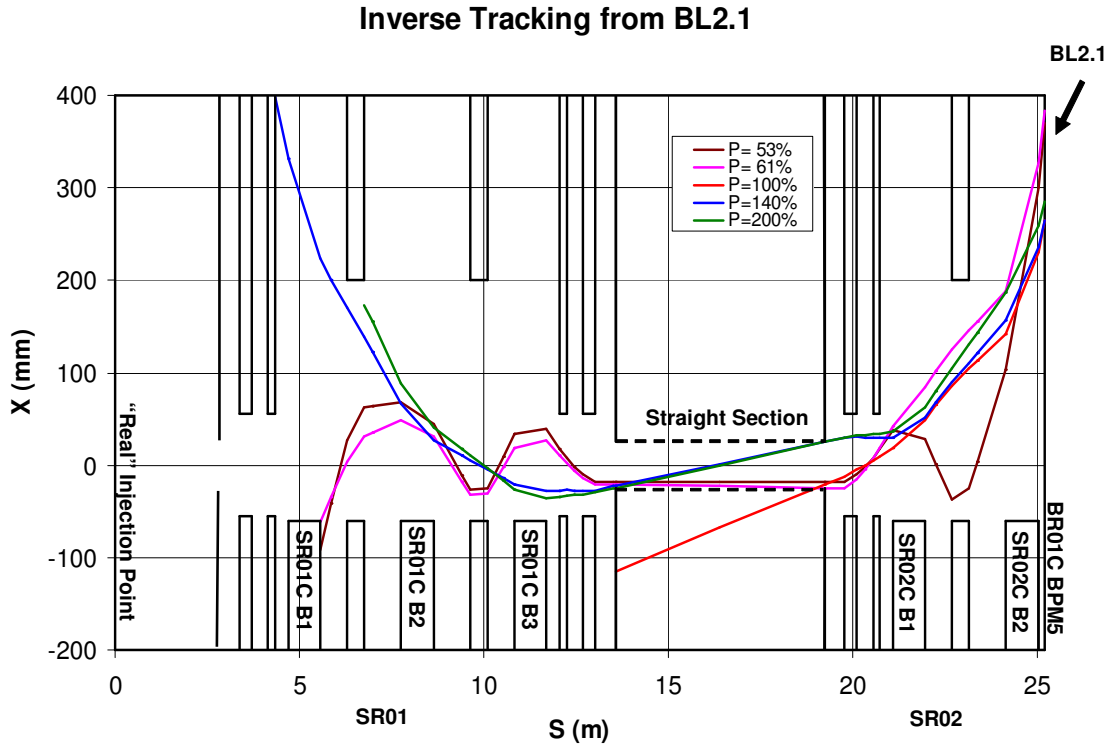


Figure 3.2-7: Trajectories of several important particles

3.2.3.4 Tracking Study Conclusions

Based on these analyses, the following condition is necessary to prevent from being inadvertently injected down a beamline:

- There must be stored beam in the ring. We plan to use a threshold current of 10 mA for the interlock system, which is easy to measure and small enough compared to normal operation conditions in two-bunch operation not to cause any unnecessary injection inhibits.

As additional precaution, we plan to insure that the match between the booster extraction energy and the storage ring beam energy is within 10%.

Horizontal collimators are being designed for installation in the booster-to-storage ring transfer line to remove the tails of the injected beam distributions, which due to the relatively large emittance of the booster and the limited dynamic aperture of the storage ring would not be captured. Future studies will include more intuitive forward calculations as well as verifying that beam line 2.1 represents the limiting case.

3.2.3.5 Stored Beam Losses

Aside from considerations for the worst case accident scenario, there will be increased stray radiation levels due to the increased number of electrons. Topping off the stored current every 30 seconds with 1.5 mA yields 1440 mA /shift. Since beam current will be kept constant at 500 mA this results in 1440 mA of electrons lost per 8 hr shift. Present operations result in a loss of approximately 200 mA. This leads to roughly a factor of 7 increase in beam loss and hence stray radiation levels.

Beam losses from Touschek scattering and from RF trips now are lost mainly in the small vertical gap insertion devices at 4.0 and 11.0 with smaller losses occurring elsewhere. Little effort has been made or has been required to locally collimate losses due to the low stray radiation levels. Increases in these levels by a factor of 7 or more dictates a strategy of providing collimation and then locally shielding the collimator(s). This section describes closed orbit distortion simulations to determine the effectiveness of vertical collimators placed in any of 6 available locations in one or more arc sector chambers. These locations are commonly referred to as Jackson holes. The locations of these are shown in Figure 3.2-8.

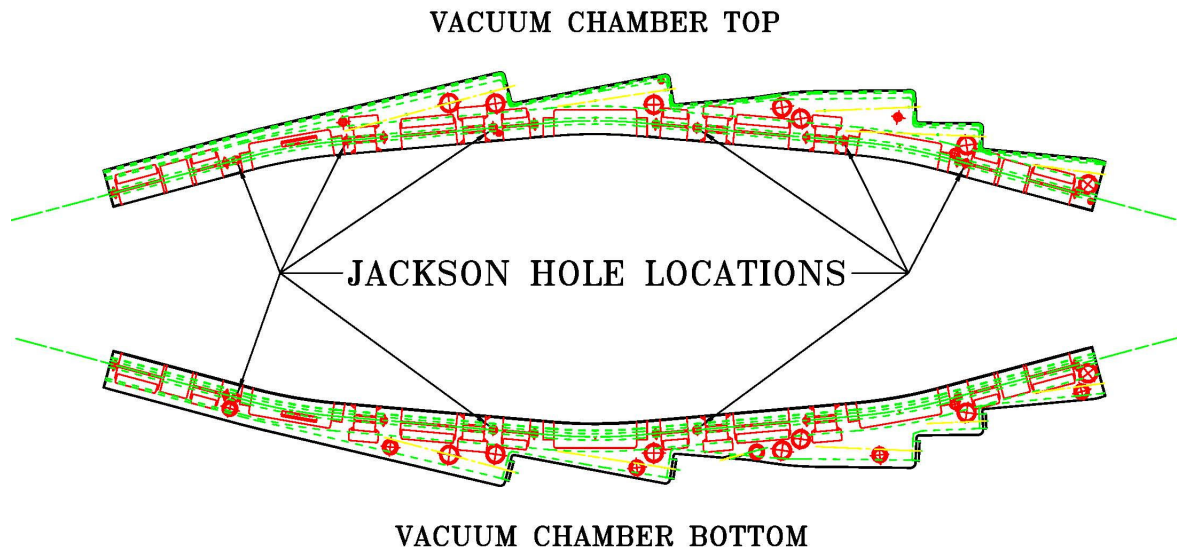


Figure 3.2-8: Jackson hole locations on arc sector

Closed orbit distortion calculations were carried out to determine the location of beam loss as a function of vertical collimator aperture heights assumed to be located in several Jackson holes (JH). The RF is assumed to be turned off instantly, allowing stored beam to lose energy via synchrotron radiation. Interaction between beam and unpowered cavities is ignored. During tracking apertures are checked at each JH location as well as at the entrance of each straight section. The process is repeated for 100 random seeds.

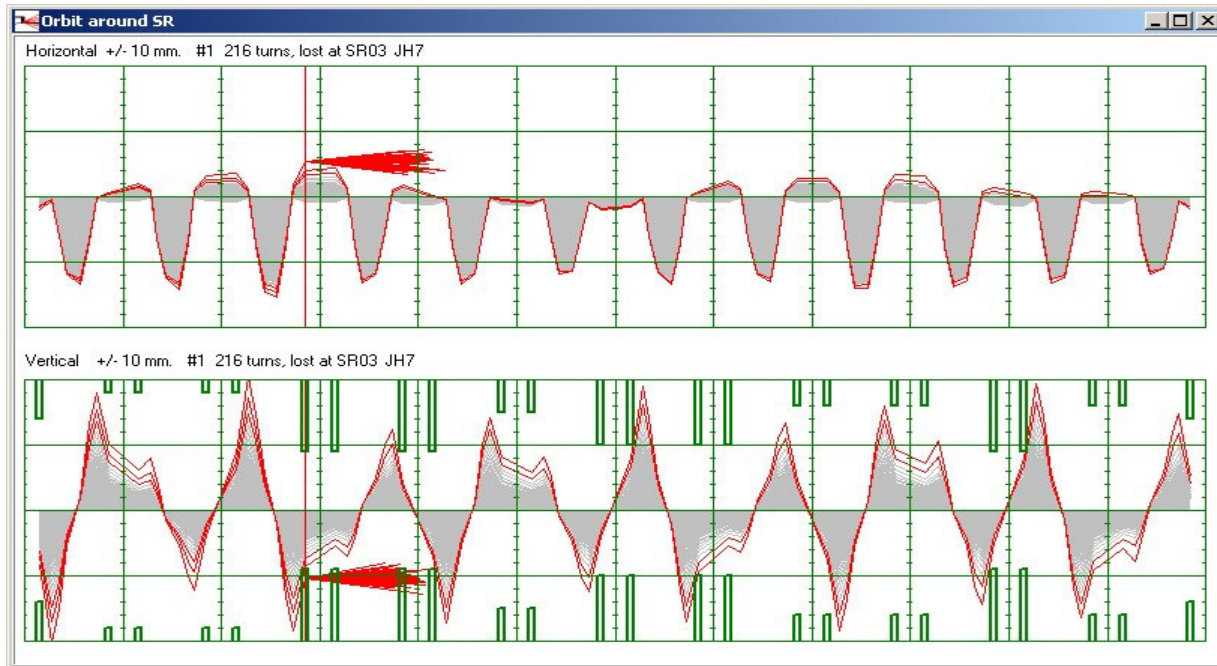


Figure 3.2-9: Closed orbit distortion following rf trip.

Figure 3.2-9 shows the tracing of one injected particle with no JH scrapers present. This demonstrates the horizontal and vertical orbit distortion increasing with subsequent loss at the ID4 entrance, consistent with present experience and measurements. Particles can survive on average several hundred turns before hitting a small vertical aperture.

Figure 3.2-10 gives a summary of beam loss for JH vertical scrapers located at SR02 JH6 and SR03 JH1. These are located at the exit of arc sector 2 and the beginning of arc sector 3, locations where betatron oscillations are the largest giving more flexibility in actual adjustment to scraper heights. This demonstrates that the proper location and adjustment of vertical collimators/scrapers located in existing Jackson holes can be used as an effective strategy in localizing beam losses.

Future work will determine optimal number and location of JH scrapers to localize beam losses from both Touschek scattering and RF trips. Simulations and measurements will also determine the effect of JH scraper heights on stored beam lifetime. These scrapers will be designed so that apertures can be changed but then locked into a position such that they cannot be inadvertently removed from their intended function of minimizing stray radiation levels on the experimental floor. Two sets of collimators will be installed. By placing two collimators apart by 90 degrees horizontal phase advance, one can collimate both in displacement and angle. With the use of those collimators, radiation levels for permanent magnet insertion devices and due to bremsstrahlung for user beamlines can be minimized.

Beam Dump at SR02 JH6/SR03 JH1

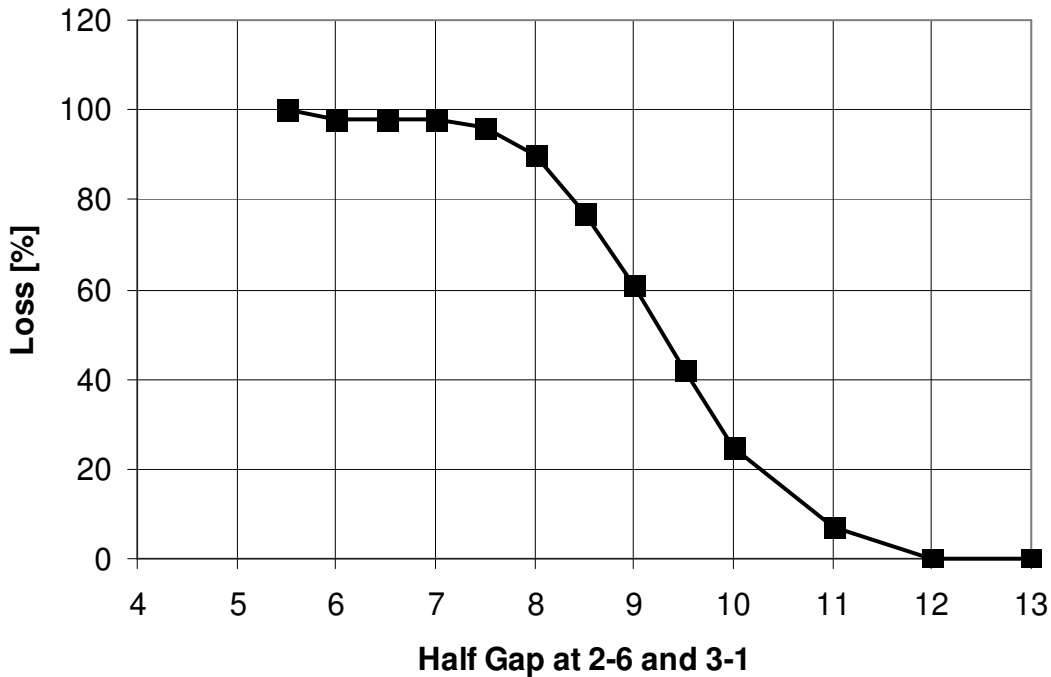


Figure 3.2-10: Beam loss at SR02 JH6 and SR03 JH1 as a function of JH half gap height.

3.2.4 Collimation/Scrapper System

3.2.4.1 Horizontal Collimators in the BTS line

The purpose for these collimators is to allow to remove particles at large horizontal amplitudes (i.e. in the tails of the beam distribution), which due to the relatively large emittance of the booster and the limited dynamic aperture of the storage ring would not be captured anyhow. By placing two of those collimators apart by 90 degrees horizontal phase advance, one can collimate both in displacement and angle. With the use of those collimators, radiation levels for permanent magnet insertion devices and due to bremsstrahlung for user beamlines can be minimized.

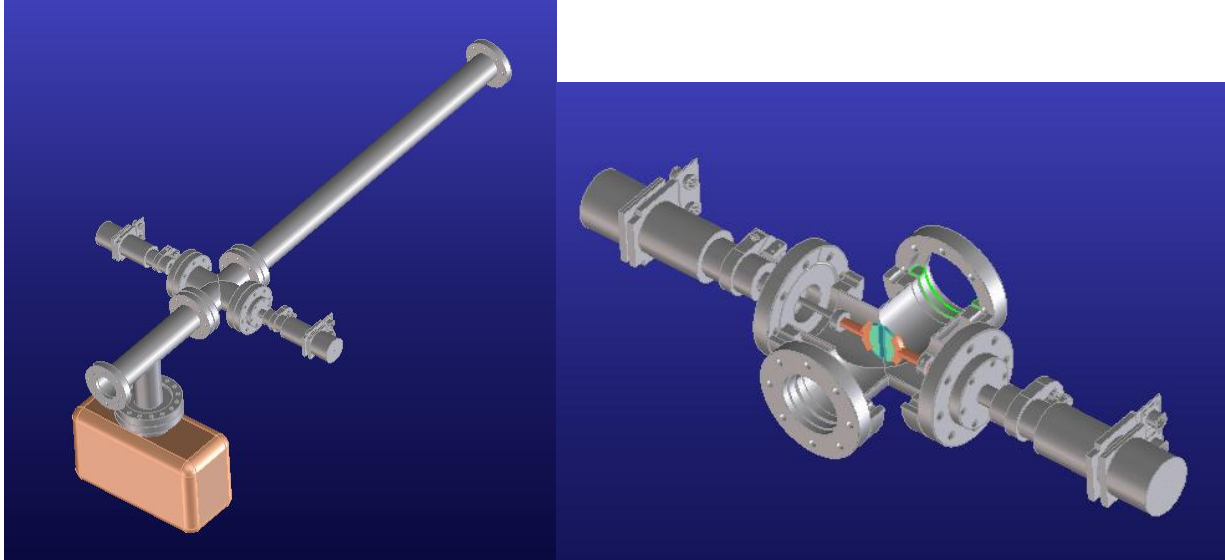


Figure 3.2-11: CAD drawing of the double sided horizontal collimator for the BTS transfer line.

3.2.4.2 Vertical Scrapers in the Storage Ring

In addition to the collimators in the BTS line we will also install vertical moveable collimators/scrapers in the ALS storage ring. They will serve 3 different purposes:

1. Localizing injection losses
2. Localizing stored beam (lifetime) losses
3. Localizing losses due to beam dumps (RF aborts)

In all of those cases, the particle losses in the ALS occur in the vertical plane, either due to particle diffusion/single particle resonances, or due to a resonant explosion of the vertical closed orbit when the vertical tune changes close to the half integer resonance in the case of an RF abort. The simulation investigating the effectiveness and optimum location for these scrapers are shown in Section 3.2.3.5. After the installation early next year, detailed beam studies will be conducted, including injection with one beamline shutter open to fully detail the effectiveness of the scraper system. Even though it is not envisioned that the scrapers will be an integral part of the radiation protection system (but rather a means to reduce steady state radiation levels to avoid posting of radiation areas), their mechanical design is done such that they could be easily locked in a position, which would enable their use in a radiation protection system. Using the combination of the collimators in the BTS line and the scrapers in the storage ring, it is expected that steady state radiation levels close to the first beamline optics and the deposited radiation doses in insertion devices will not increase with top-off, but stay about the same or even get smaller.

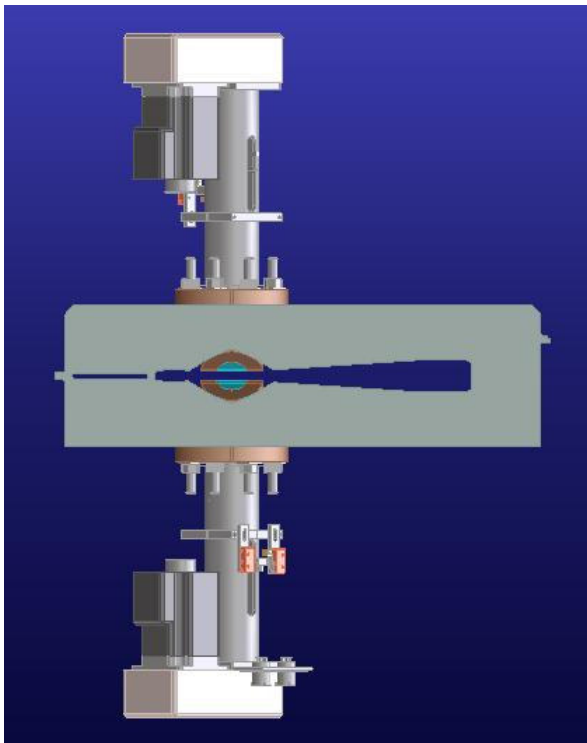


Figure 3.2-12: A pair of vertical scrapers installed in the so-called Jackson holes of one of the storage ring arc vacuum chambers.

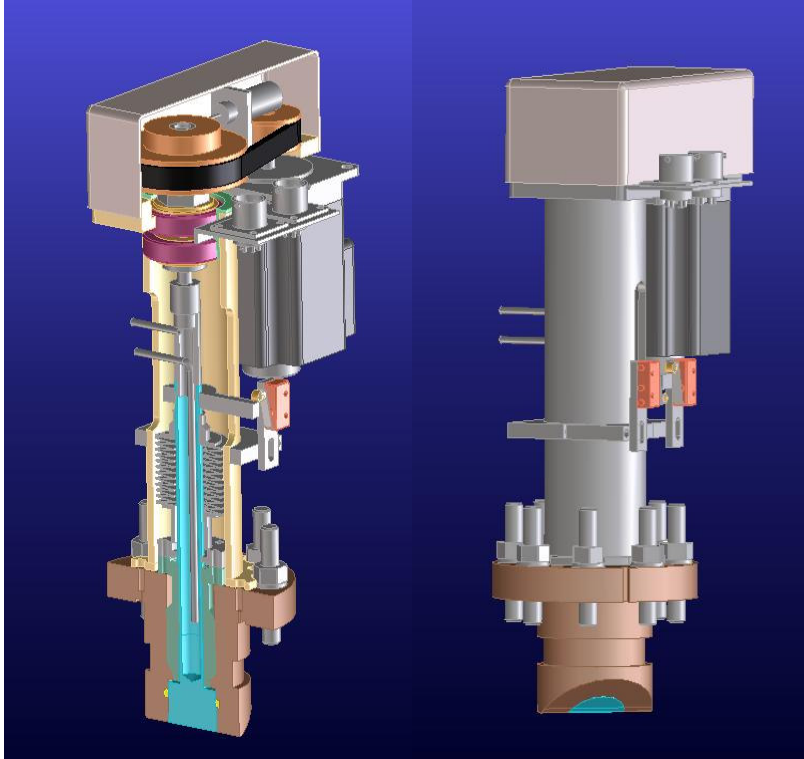


Figure 3.2-13: Drive system, cooling and inner structure of vertical scrapers.

3.2.5 Radiation Monitors

The existing system of beamline radiation monitors will be upgraded with a new (faster) readout electronics that also provides the capability to implement an interlock system. It has not been decided, yet, whether an interlock system is necessary. The decision will be based on injection radiation level measurements with one beamline shutter open during the coming year. However, all components that would be needed for a beamline interlock system are currently included in the scope, schedule and cost estimate of the project.

3.2.6 *Top Off Mode, Radiation Safety System*

Currently the ALS operates in two modes. During injection we run in fill mode. All the beamline Personal Safety Shutters (PSSs) are closed and the BTS bend power supplies (PS) for the first two bend magnets (B1, B2) in the transfer line between the booster and the storage ring are enabled to be turned on. After injection the operators switch the accelerator to stored beam mode. The BTS bend magnet PS are disabled and the beamline PSSs are enabled to open. (Please see Figure 3.2-14)

1. The storage ring beam current monitor interlock must be made up to a value yet to be determined.
 2. The injection energy must match the storage ring energy. The interlock circuitry will monitor and compare the currents of a BTS bend magnet PS with the current of the storage ring gradient PS.
- Top-off mode will enable the BTS bends to operate with the beamline PSSs open.

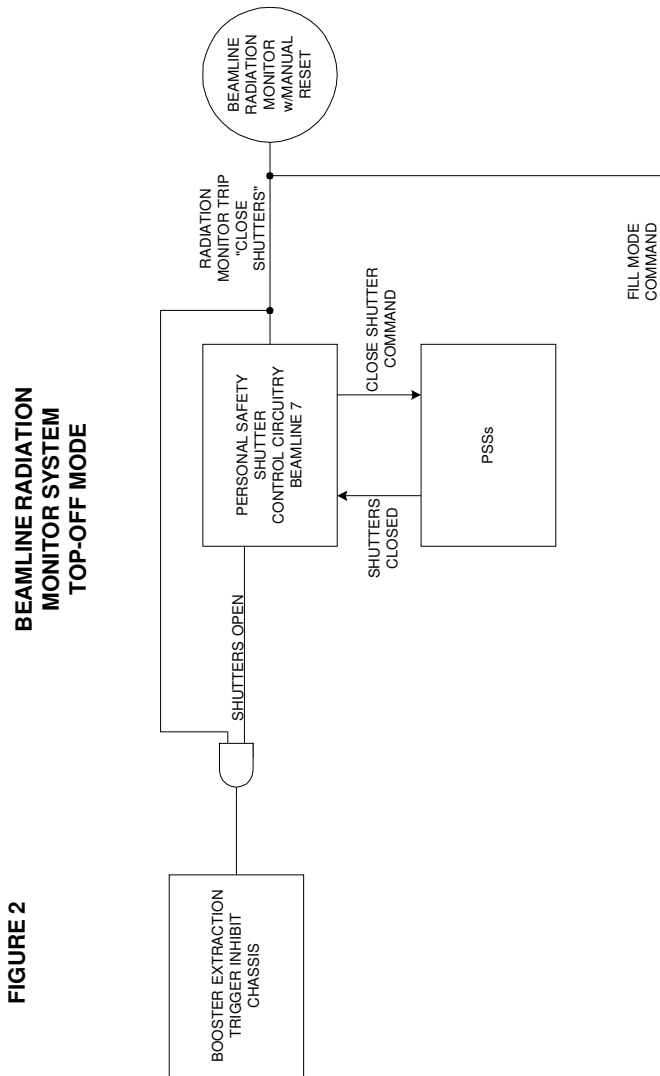


FIGURE 2

Figure 3.2-15: Logic of a (potential) beam line radiation monitor interlock system.

A number of radiation monitors will be added to the beamline area of the ALS in addition to the already existing system described earlier. All beamline radiation monitors could be interlocked and a possible reaction of the system to the detection of excessive radiation levels would be to

- 1 Send a “Close Shutter” command to all the beamline PSSs.
- 2 Generate a trigger inhibit signal to disable the booster extraction magnets and the storage ring injection magnets.
- 3 The accelerator will revert back to fill mode.

After all the beamline PSS report back that they are closed, the trigger inhibit signal would be turned off. The radiation monitor interlock would have to be reset manually at the beamline the radiation monitor resides at before resumption of top-off mode.

3.2.6.1 Top Off Mode, Radiation Safety System (cont)

The beam current interlock will utilize two sources for storage ring beam current monitoring.

1. The DCCT SR05
2. A BPM array by summing the four buttons.

The injection energy interlock will monitor two of the BTS bend magnet PS currents and then compare them to the SR gradient PS current ensuring the BTS line and the storage ring energies match.

One BTS bend PS will have a transducer added for monitoring and on the second BTS bend PS we will monitor the current signal from the PS itself. On the gradient PS we will once again monitor current utilizing a current transducer and then the PS current signal.

In addition to the new top-off mode interlocks outlined above, it will be necessary to design a new interlock system for the booster tunnel. Tunnel access will be prohibited with the booster RF on. Currently the booster RF power is low enough to allow access with the system on. The interlock scheme will resemble the storage ring, with a prohibited access high power mode and a limited access low power mode.

All personnel protection interlock systems mentioned in this subsystem will be implemented in a fully redundant way.

3.3 Accelerator Physics Studies

3.3.1 Vertical emittance reduction in the Storage ring

The main possibilities to increase the brightness of the ALS are increasing the time-averaged current, reducing the beam size, and reducing the insertion device gaps. Currently those changes would result in (unacceptably) short lifetime. With continuous injection (top-off), the importance of this lifetime impediment will become significantly reduced in the future. Figure 1.2-2 shows a comparison of the brightness of planned, new ALS insertion devices with the upgraded beam parameters to the typical brightness of a current ALS undulator. One of the main improvements comes from a smaller vertical emittance and the smaller physical gaps of the undulators.

3.3.1.1 Simulation of Emittance Correction

A number of simulations were performed to find the smallest number of individual skew quadrupoles, which still allow an effective emittance correction, as well as a good distribution of these skew quadrupoles and finally an optimum correction algorithm. The result was that 12 skew quadrupoles (one in each sector) were sufficient, six of them located at high dispersion points and six of them at lower dispersion points with a larger product of horizontal and vertical beta-functions. In the simulations many different minimization algorithms were used, but it turned out, that orbit response matrix analysis (using Matlab LOCO) to fit an effective skew quadrupole distribution gave results as good as the best other minimization algorithm. Since it has the advantage of requiring very few iterations and automatically providing a measurement of the local coupling everywhere along the ring it is perfectly suited to be used with measurement data on the real machine. The simulations were also used to optimize the parameters of LOCO like the weight factor of the dispersion function, the outlier rejection tolerance, and the number of singular values. Figure 3.3-1 shows the results of one of those simulation runs for 100 random seeds of misaligned machines. In this particular case it was possible to correct the vertical emittance below 5 pm using 12 skew quadrupoles for 25% of the error seeds. Some details of the random error distribution are pessimistic compared to the errors we find in the real machine. In addition, all seeds that in the simulations could not be corrected to emittances below 30 pm have one specific error type, which could if necessary be resolved relatively easily by realigning a few storage ring magnets.

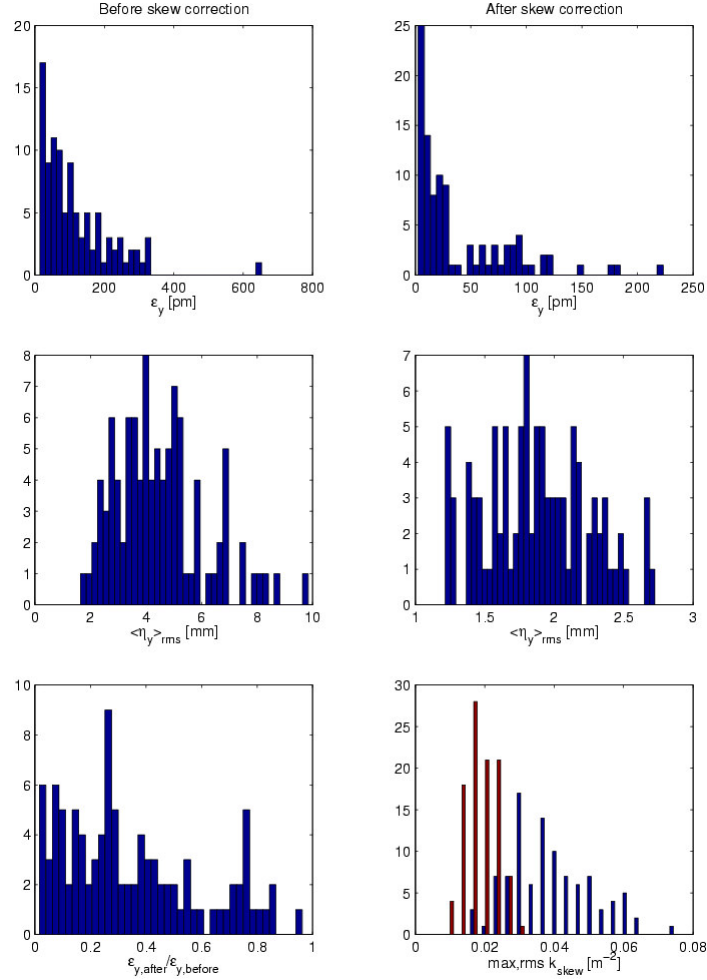


Figure 3.3-1: Histograms showing the results of simulated vertical emittance and dispersion correction for 100 randomly misaligned error seeds.

The skew quadrupoles at the ALS are integrated in the sextupoles and used to be connected in 4 chains. Based on the simulations, individual power supplies were installed two years ago, powering 24 individual skew quadrupoles - at least one in every sector. Two sectors have four skew quadrupoles each to generate a closed dispersion bump for the fs-slicing experiments.

3.3.1.2 Measurements

Because of the resolution limit even of x-ray beamlines it is quite difficult to measure emittances in the few pm range accurately. The primary beamline to measure emittances at the ALS uses an imaging optics with a KB-mirror pair, carbon filters to select the x-ray wavelength (1.5keV) and to attenuate, a BGO crystal to convert to visible light and a microscope with CCD. Even though the fundamental resolution limit would allow a direct measurement of emittances of a few pm, aberrations of the optics create a larger limit. Therefore we used three somewhat indirect but independent methods to measure the very small vertical emittances.

The first method was to determine the resolution of the beamline using Touschek lifetime measurements for various beamsizes. We then corrected the beamsize measurements for the beamline resolution to deduce the real vertical emittance. The second method was based on the analysis of an orbit response matrix, using a large number of skew gradient error fit parameters. With the calibrated machine model one can then calculate the vertical emittance using a lattice code. The final method used a scan of the RF-acceptance while measuring the Touschek lifetime. For low RF amplitudes, the Touschek lifetime is strictly proportional to the bunch volume. Therefore one can deduce a very small emittance from a beamsize measurement at moderate coupling.

All three methods gave consistent results. In the best case, the measured vertical emittance as determined by the three methods was 4-7 pm, corresponding to an emittance ratio of less than 0.1% at 1.9 GeV (natural emittance is 6.75 nm). Figure 3.3-2 shows an example of the change in beamsize and local tilt angle in one iteration of the emittance correction. The mean value of the emittance measurements of about 5 pm was to our knowledge a world record in 2003 for vertical emittances in electron/positron storage rings and is virtually identical to the design value for the NLC damping rings. It is interesting to note that emittances this small are within one order of magnitude of the theoretical limit due to the finite opening angle of the synchrotron radiation emission.

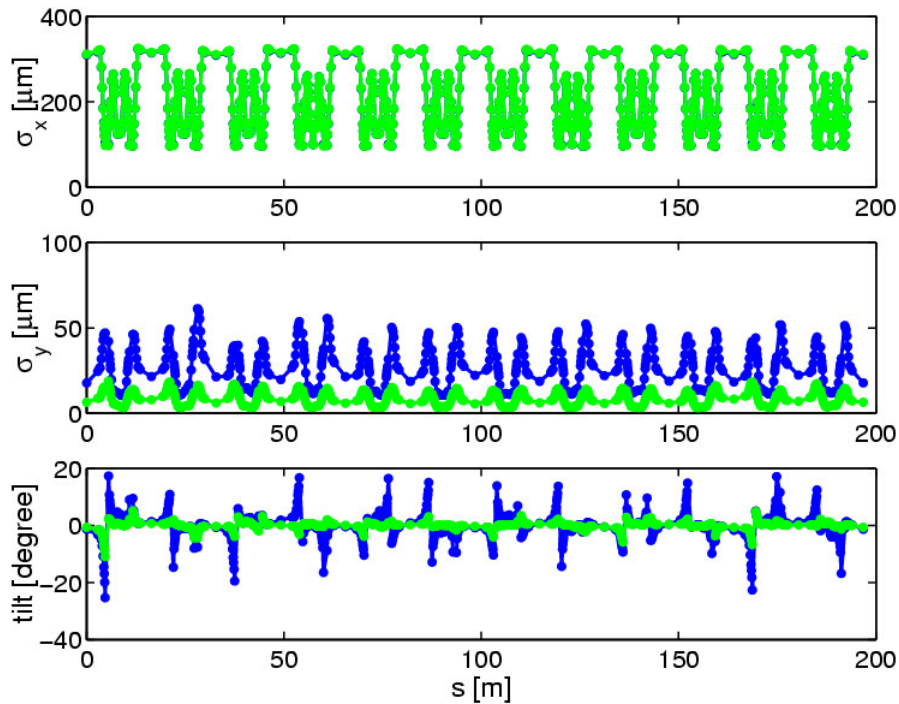


Figure 3.3-2: Horizontal/vertical beamsize and beam tilt as calculated from calibrated machine model using orbit response matrix analysis. The blue case is before coupling correction, the green one after one iteration.

3.3.1.3 Emittance Control

Until the full energy injector upgrade at the ALS is finished to allow top-off injection, it is important to still operate with artificially increased vertical emittance to achieve reasonable beam lifetimes for users. Historically at the ALS a controlled excitation of the nearby linear coupling

resonance has been used to increase the vertical beamsize. After installing the individual skew quadrupoles, we switched to a different scheme. The emittance and vertical dispersion is corrected and then 12 skew quadrupoles are used such as to introduce a global vertical dispersion wave, without introducing coupling. In that case, the vertical emittance is generated directly via quantum excitation. The local emittance ratio around the ring can be made fairly flat and all local tilt angles are small.

The main advantages of this method are a better beamsize stability (especially for scanning undulators/wigglers), better dynamic (momentum) aperture and less sensitivity of the momentum aperture to the vertical physical aperture. An example of the improvement in longtime beamsize stability can be seen in Figure 3.3-3.

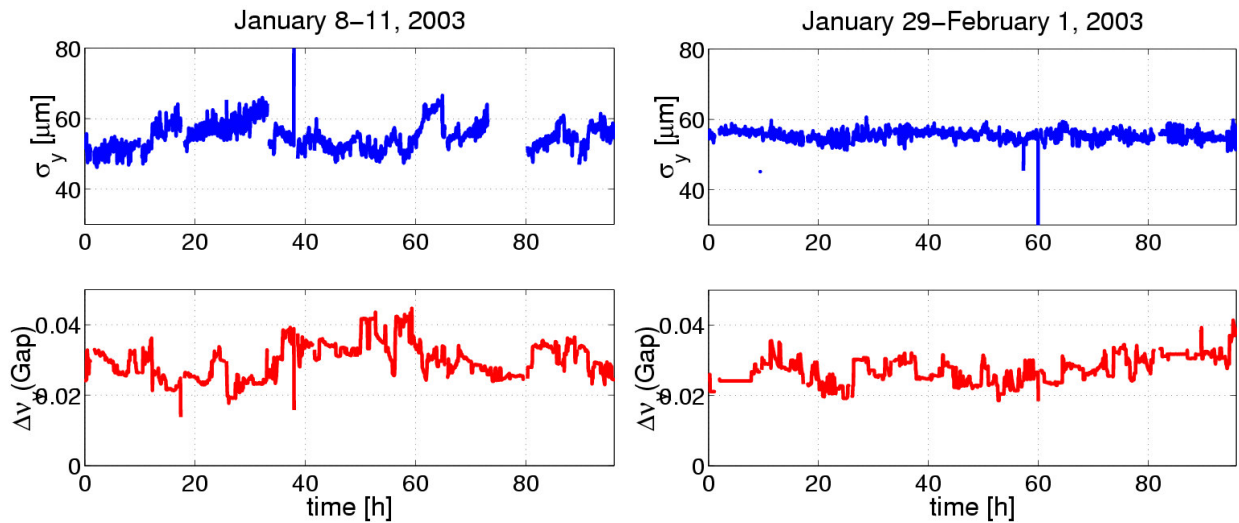


Figure 3.3-3: Vertical beamsize for two four day periods. Using a global vertical dispersion wave to increase the vertical emittance (right) leads to a much better beamsize stability than excitation of the coupling resonance (left).

3.3.1.4 Beam Dynamics at low Emittance

Since the lifetime at all (low energy) third generation light sources is (strongly) Touschek limited, the momentum aperture of the ring is very important. For top-off operation, injection efficiency becomes very important as well (i.e. on-energy dynamic aperture). For most light sources the dominant factor for the momentum aperture is the transverse single particle dynamics and in most cases the particles are lost on the narrowest vertical apertures. Therefore it is important to understand and optimize the dependence of the momentum aperture on the vertical physical aperture.

We found that for the current ALS lattice the dependence of the momentum aperture (lifetime) on the vertical physical aperture became much weaker both for the case with corrected vertical emittance and the case with vertical dispersion wave, compared to the case with artificially excited coupling resonance (compare Figure 3.3-4). Combined with the improvements in the lattice implemented two years ago and better correction of lattice symmetry errors this will enable the

ALS to reduce the physical gap of insertion devices from the current 8-9 mm down to about 5 mm.

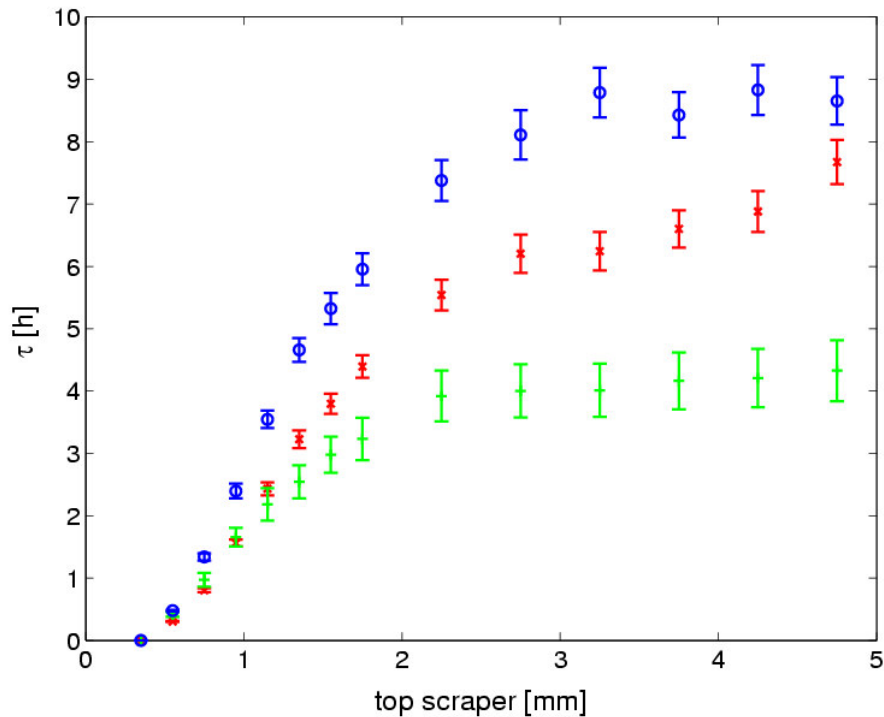


Figure 3.3-4: Measured lifetime of the ALS versus half aperture in one straight for three different cases: excited coupling resonance (red), corrected coupling and vertical dispersion (green), vertical dispersion wave (blue). The two cases with excited coupling resonance and dispersion wave were measured for identical vertical emittance.

Simulating the effects in tracking, we found good agreement between measurements and simulations. The simulations showed that a correction of the coupling reduces the sensitivity of the dynamic momentum aperture to the vertical physical aperture. The injection efficiency for smaller vertical gaps was studied as well and no show stoppers were found so far. It is planned to install a collimator system to protect all insertion devices in the ALS from injection losses during top-off operation.

3.3.2 Operation with smaller vertical gaps in the storage ring

For permanent magnet as well as for superconducting insertion devices the possible performance depends strongly on the possible minimum gap of the magnetic structure. Therefore it is important to determine the minimum physical vertical aperture which can be tolerated with respect to beam lifetime and injection efficiency. At the ALS the limit used to be a full vertical aperture of about 8 mm. With an improved lattice, better correction of the lattice symmetry and especially better control of coupling it was possible to reduce this limit to a full aperture of about 5 mm. This was verified by measurements using a scraper at the ALS. Figure 3.3-5 shows a scraper measurement in the ALS with corrected coupling and the vertical emittance increased to its cur-

rent nominal value of 150 pm by using a vertical dispersion wave. The lifetime reduction in those conditions is fairly small down to a full vertical aperture of about 5 mm.

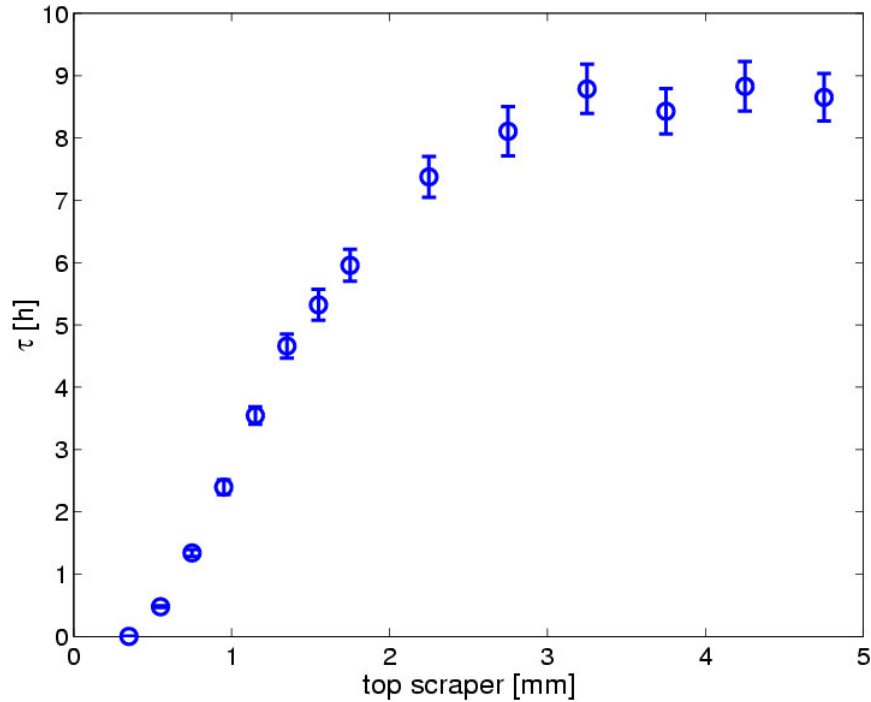


Figure 3.3-5: Lifetime of the ALS versus half aperture in one straight, measured using a scraper: The lifetime reduction for a lattice with corrected coupling and vertical dispersion wave to increase the vertical emittance is small down to a full vertical aperture of about 5 mm.

3.3.3 Linac to booster transfer efficiency

The injection efficiency into the booster is currently only about 25%. Because of this, the Linac is running with much larger per bunch charge than necessary, increasing its beam loading and therefore the output energy spread. This is an area where significant improvements seem possible. Therefore detailed studies have been started, investigating whether different RF settings (cavity coupling, synchrotron tune), different lattice settings (tune), better orbit correction or the use of the existing sextupoles to correct the chromaticity can improve the situation.

3.3.4 Booster to Storage ring transfer efficiency

During top-off we assume that we can inject 1.5 mA per pulse. Presently it is possible to achieve 1.5 mA per pulse in 4 bunches with nearly 100% injection efficiency into the storage ring. This is done with insertion device gaps opened and with a minimum vacuum chamber aperture of 8.9 mm full gap. With top-off we need to inject with insertion devices closed. Also the minimum vacuum chamber aperture will be as small as 5 mm. Our preliminary machine studies have shown a 40% reduction in injection efficiency with IDs closed and a vertical scraper with a 5 mm aperture. The plan for Top-off is to inject with a longer train, up to 10 bunches, and to improve the injection efficiency.

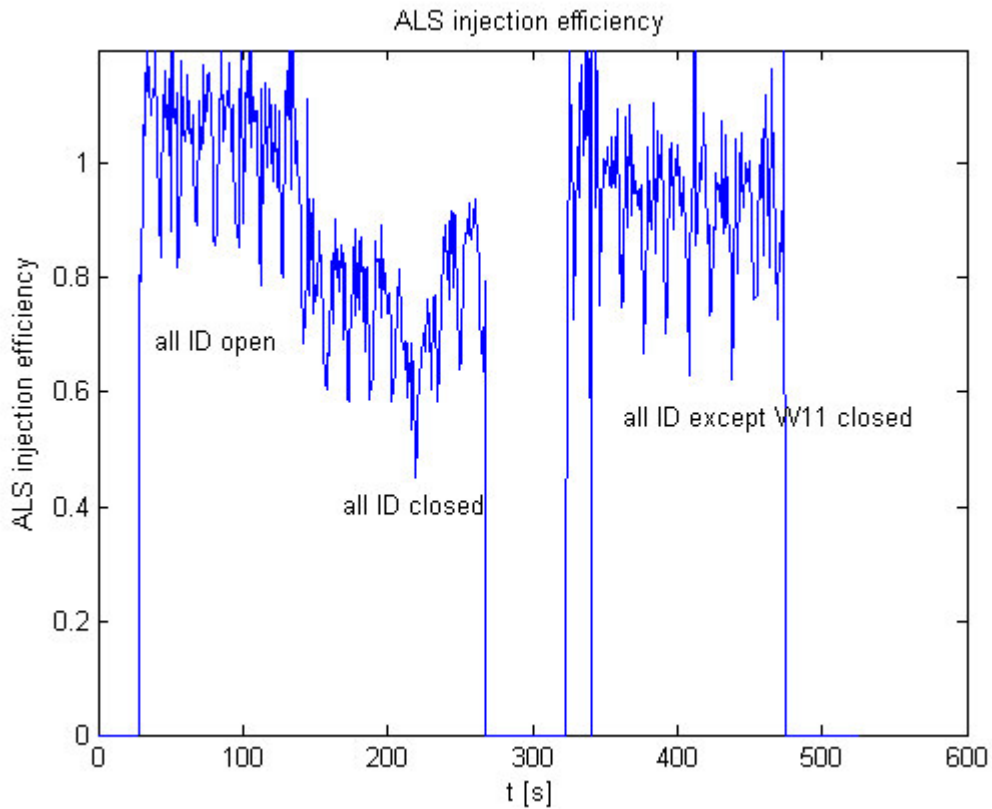


Figure 3.3-6: Dependence of ALS injection efficiency (without re-optimization) on insertion device settings. Only the W11 wiggler reduces the injection efficiency significantly. Because the integration time of the storage ring current monitor is not exactly matched to the injector period, the measurements have some jitter around the correct values. This also explains why some of the measurements indicate injection efficiencies above 100%.

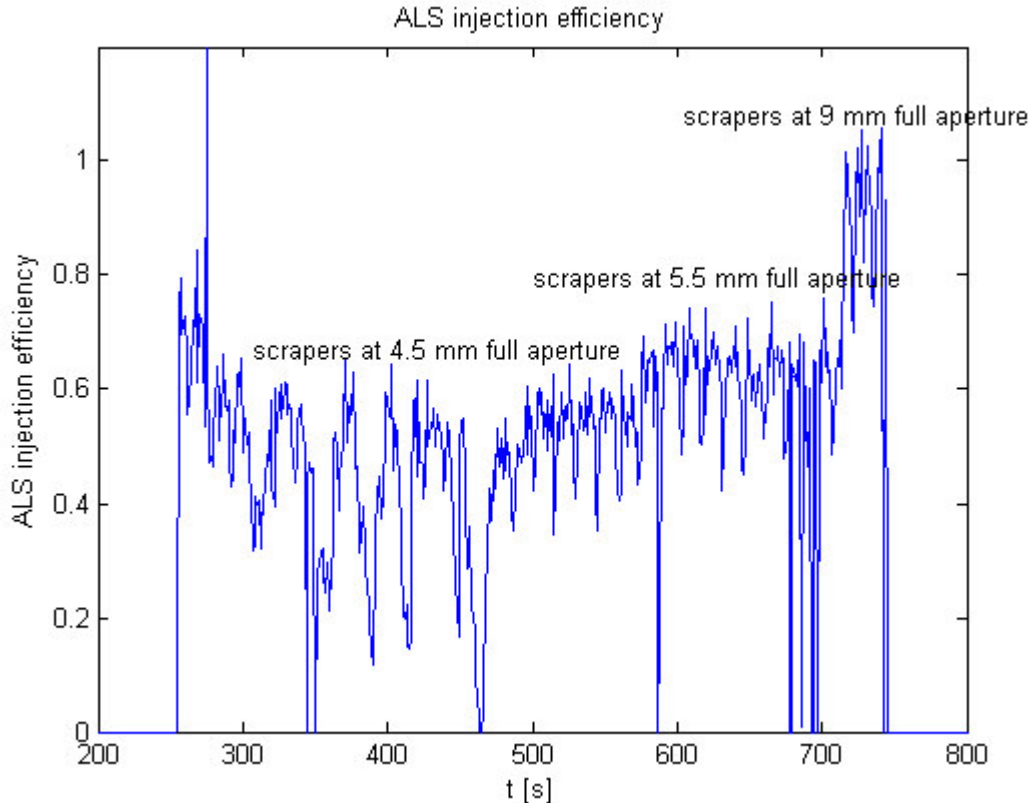


Figure 3.3-7: Dependence of ALS injection efficiency on the vertical physical aperture in the storage ring without any re-optimization. The aperture was changed by opening and closing two vertical scrapers in straight 3 at a beta function of about 6 m.

3.3.5 Minimizing radiation levels

Since the steady state radiation levels on the accelerator floor and the potential radiation damage to permanent magnet insertion devices are extremely important issues with top-off, accelerator physics studies of those issues were started early in the project and will continue further, eventually leading to a full radiation safety review.

At the ALS, most particle losses occur in the vertical plane, for all three main modes of particle loss, namely injection, lifetime losses, and (RF abort) beam dumps due to equipment failures. The mechanisms in all cases are somewhat different, but vertical scrapers can be used to localize losses for all three cases, thereby reducing the steady state radiation levels on the floor and protecting permanent magnet insertion devices.

The first mechanism studied in detail was RF beam aborts, which happen whenever there is any kind of equipment failure at the ALS, since the interlock systems simply switch off the RF power. We found both in simulations and using turn-by-turn beam position monitors, that after the particles start to lose energy (with the RF off), the beam loss happens around 200-250 turns and is not caused by position shift due to dispersion, or resonant single particle losses due to resonances, but rather due to the vertical tune getting close to the integer resonance and therefore the closed orbit exploding.

After understanding the loss mechanism due to RF aborts, we used the existing pair of vertical scrapers to attempt to minimize the radiation levels at the first beam line optics. The current

scrapers are installed at the end of straight 3, not too far upstream from one of the JH locations (3-1) found in the simulations in Section 3.2.3.5 to be effective, however at a lower vertical beta function (about 6 m versus 24 m). Using this one scraper and closing it slightly more than the narrowest existing aperture in the ring, it was possible to reduce the radiation levels at the beamline 4 first optics by about a factor of 4 (Figure 3.3-8). Even with just one scraper, this would more than compensate for the about 2 times higher dose rates due to the higher average currents at which beam dumps will occur in the future. Using larger numbers of scrapers will further improve the situation.

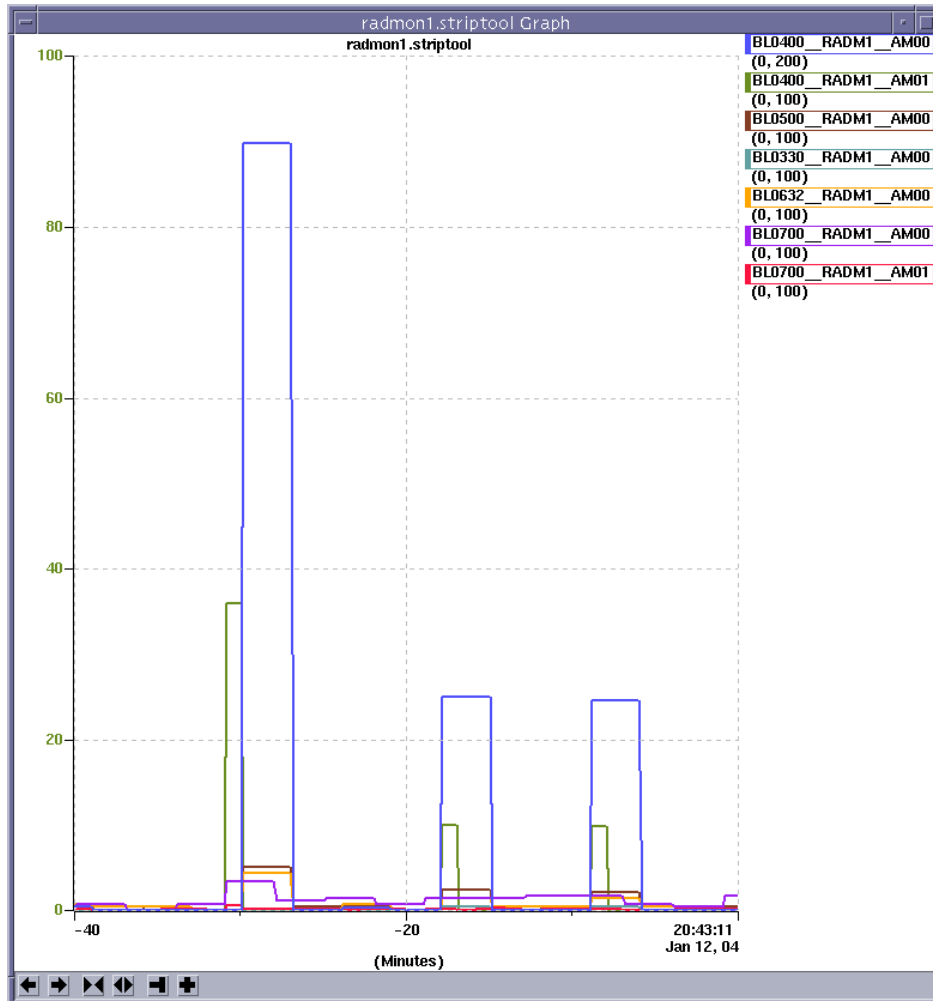


Figure 3.3-8: Reduction in radiation dose at first optics in beamline 4.0 due to ALS beam dump using a vertical collimator at the end of straight 3. The vertical axis shows average count rates of radiation monitors and the horizontal axis is time in minutes. Shown are 3 (intentional) beam dumps with equal stored beam current. After the first dump with scraper open, the scraper (at a vertical beta function of about 6 m) was set to a full aperture of 8 mm for the second, and 5 mm for the third beam dump.

Future studies will focus on the effectiveness of scrapers (both the existing ones and the ones to be installed next year) to localize injection and stored beam (lifetime) losses.

3.4 Injector Reliability

3.4.1 Scope

This section reviews the reliability of injection system components.

An overview of injection system components is presented in section 3.4.2. Section 3.4.3 describes the present mode of injection system operation and compares it to the mode proposed for top-off operation. Section 3.4.4 lists the component failures that occurred over a recent twelve-month period and discusses the typical times required to repair components.

3.4.2 Injection System Components

The injection system consists of six subsections: Electron Gun (**EG**), Linac (**LN**), and Booster Synchrotron (**BR**), and the three beam transport sections, Gun-to-Linac (**GTL**), Linac-to-Booster (**LTB**) and Booster-to-Storage Ring (**BTS**).

The electron gun operates at 120 kV and uses a dispenser type thermionic cathode that is positively biased with respect to the control grid. Electron bunches are generated with an 8 ns time structure by a 125MHz grid-to-cathode modulating voltage. The number of gun bunches per macro pulse is controlled by the length of time the 125 MHz voltage is gated on.

The linac is a 3 GHz traveling wave structure that accelerates the electron bunches to 50 MeV. It consists of two accelerating sections (**AS1** and **AS2**), each 2 m in length. The accelerating sections are powered by separate 30 MW klystrons (**KLY1** and **KLY2**), which are driven by pulsed power modulators (**MOD1** and **MOD2**). Attached to the front end of AS1 is an S-band buncher that is also powered by KLY1. Additionally, there are two subharmonic bunchers in the GTL section. One operates at 125 MHz (**SHB1**) and the other at 500 MHz (**SHB2**). A separate amplifier system drives each buncher.

The booster synchrotron has a FODO lattice structure with four-fold symmetry. It uses two families of quadrupole magnets (**QF** and **QD**) which are powered in series, with a separate power supply for each family. Likewise, a single power supply powers the bend magnets. The two families of sextupole magnets (**SF** and **SD**) have not been commissioned. The four horizontal (**HCM**) and four vertical (**VCM**) corrector magnets in each sector are powered by individual power supplies. A fast kicker magnet (**BR1 KI**) steers the beam on orbit at injection; three bump magnets, a fast kicker (**BR2 KE**), and thin and thick septum magnets (**BR2 SEN** and **SEK**) extract the beam. The RF accelerating cavity is powered by a 15 kW klystron.

The EG, GTL, LN, LTB and BTS sections have a total of 5 solenoid, 22 quadrupole, 8 bend and 32 corrector magnets. Each of these magnets is controlled with a separate power supply.

3.4.3 *Injector Operating Mode*

The injection system operates at 1 Hz rep rate. The storage ring is filled three times a day, at 8 hr intervals, and at other times if faults occur.

Normal user operations consist of 5-6 day periods of continuous, 24 hr/day operation. A one or two-day maintenance shutdown and/or one day of machine studies conducted by the Accelerator Physics group follows each user period. An experimental facility in the BTS area, designed to use booster beam when the booster is not needed for storage ring injection, runs periodically. When the BTS experiment is taking beam, the booster is pulsed 8 hr/day, 5 days/wk for one to two week intervals.

The egun cathode is kept at the nominal operating temperature at all times. The gun high voltage is turned off when beam is not needed for tuning or injection into the storage ring.

The bunchers, linac and booster RF systems are pulsed continuously at 1 Hz. The GTL, LN, and LTB magnets are at nominal operating currents at all times. The BR bend, quadrupole and corrector magnets are always on; booster pulsing is stopped when the system is not in use. The booster injection and extraction, and storage ring injection pulsed magnets are turned off when not needed for tuning or injecting beam into the storage ring. The BTS bend magnets are turned off when not needed for injection. All other BTS magnets are kept at their nominal operating currents.

Aside from the upgrade of the injection system to full energy (1.9 GeV), the operational conditions for top-off operation would not change significantly from the normal fill mode. The differences would be: (1) All magnet power supplies stay on continuously. During the periods between injection cycles, pulsed magnet triggers are disabled. (2) The gun HV remains on; gun output is blocked by inhibiting the gun gate trigger. (3) The booster ramp rate is reduced from 1 to 0.5 Hz. Because of the similarity of the two operational modes, the reliability of most components is expected to be similar. An exception is the pulsed magnets; the increased duty cycle of these components may increase the failure rate.

3.4.4 *Injection System Component Failures*

A review of injection system performance over a recent 12-month period provides an overview of the type of failures that can be expected. The table below shows the component faults/failures that occurred between 1 Oct 03 and 1 Oct 04. Also shown is the number of occurrences of the fault and the mean-time-to-repair (MTTR), or recover, from the event.

Table 3.4-1: Injection System Faults/Failures 1 Oct 03 to 1 Oct 04

	No. Events	MTTR
EG		
HV supply – current clamp at turn on (cleared by off/on cycle)	3	0.25 min
Heater fault - vacuum interlock chassis intermittent	6	3 min
GTL IP vacuum fault	1	5 min
MOD 1 and 2		
Waveguide and accelerator vacuum	8	3 min
PFN HV supply – overvoltage	4	5 min
PFN HV cable arc (replaced)	1	1.6 hr
Thyratron failure	1	3 hr
Computer controls (ILC)	1	
KLY 1 and 2		
800W RF amplifier failure	1	1 hr
RF input – 500MHz to 3GHz multiplying chassis failure	1	2 hr
Linac		
Water temperature controller failure	1	30 min
Solenoid power supply failure	1	1.2 hr
LTB		
Q4.1 power supply – AC breaker trip	2	5 min
Q4.1 power supply – defective fan, replaced supply	1	30 min
Booster		
Septum box vacuum fault	2	1 min
RF cavity IP spark down	2	2 min
Klystron, intermittent overtemperature fault (defective meter replaced during maintenance)	2	5 min
Girder water fault	1	21 min
SEN and SEK HV power supply failure	2	30 min
KI and KE HV power supply failure	5	30 min
KI arcing in PFN chassis (loose ground wire)	1	1.9 hr
QF power supply capacitor bank failure	1	3.5 hr
BTS		
Girder water flow meter failure (Keptrol controller replaced)	1	30 min
Corrector magnet power supply failure	1	30 min
Power supply rack water fault (flow turbine failure)		51 min
Bump magnet grounding and trigger chassis - relay failure	1	1.9 hr
Bump power supply – sled timing and firing	2	2.4 hr
Power supply rack, AC power phase fault (defective breaker)	1	3.5 hr

B1 bend magnet power supply overcurrent – firing circuit SCR failure	1	3.5 hr
SEK power supply airflow. Interlocked rack fan, not shown on print, off	1	4.5 hr
B4 power supply intermittent air flow fault (defective vane switch)	3	
Power supply computer controls (ILC)	4	

The electron gun is relatively trouble free. A cathode typically last about 5 years. Replacements are scheduled; no cathode has failed catastrophically. Should the 120 kV high voltage supply fail, it can be replaced in about 30 min.

Two recent E-gun problems involved cathode heater faults and overcurrent clamps of the HV power supply. The heater faults were intermittent and were caused by ripple on a power supply in a vacuum interlock chassis. Recovery time was minimal with the cathode returning to operating temperature within 2-3 minutes. The HV power supply overcurrent clamps occurred when the power supply was turned on. A simple off/on cycle of the supply cleared the clamp within seconds.

The subharmonic bunchers have rarely presented a problem; only SHB2 has had a significant failure. In Sept 97, the 100 W pulsed driver and a tube and resistor string in the power amplifier failed. The driver was replaced with a spare. The amplifier failures only caused the buncher gradient to sag over the 20 microsecond flattop of the pulse and could wait for a maintenance day to repair.

The most common linac modulator problems are arcing at connections in the pulse forming network or failure of the high voltage PFN charging supply. Arcing problems are usually resolved in 1-2 hr and involve cleaning and retightening the connection and occasionally replacing a damaged cable. If an HV charging supply fails, it can be replaced in about 30min. The thyatron that fires the PFN usually is good for about 2 yr. The tubes show signs of aging (time jitter or occasional break down) before failing and are usually replaced on a scheduled basis; replacement takes about 3 hr. PFN capacitor failures have not interrupted operation. Capacitors are periodically inspected during maintenance periods and those showing signs of leakage are replaced.

One of the klystrons (KLY1) is original to the facility and has logged approximately 77,000 hr of operation. The other, KLY2, was installed in Mar 98 and has logged approximately 47,000 hr of operation. The original klystron powering AS2 failed at approximately 30,000 hr. When replacement is required, a spare klystron can be installed in about two shifts. The most likely klystron component to fail is the buncher cavity, 800W RF amplifier. Replacing this amplifier takes about 1 hr.

The most common booster component failures are the kicker magnet HV charging supplies and thyratrons and the septum magnet HV supplies. Thyratrons take about 3 hr to replace and can usually be deferred for replacement until a maintenance day. Kicker and septum magnet HV supplies can be replaced in about 30 min. The booster quadrupole and bend magnet power supplies occasionally fail and can take hours to repair. Failed capacitors or SCRs can usually be identified and replaced in 3-4 hr. Other problems, such as those involving logic circuitry, can

take 8 hr or more to resolve. The booster RF system has been relatively trouble free. The only exceptions are two problems that occurred with the klystron HV supply that took 3-4 hr to resolve. One was arcing inside the supply at one of the connections. The other was failure of the vacuum contactor that connects the HV supply to the klystron.

The BTS elements requiring the longest time to repair are the high power supplies that power the bend magnets. The components most likely to fail in these supplies are the SCRs. Identification and replacement of failed SCRs can take 3-4 hr.

At the downstream end of the BTS line, in the storage ring injection straight, are the pulsed septum and bump injection magnets. The most common problem with the septum magnets is failure of an HV supply. Typically, an HV supply can be replaced in about 30 min. Bump magnet failures take more time to resolve and usually involve the sleds. Sled failures usually take 2-3 hr to resolve.

The power supplies powering individual injection system DC magnets rarely present a problem and are easily replaced. Most supplies can be replaced in about 30 min.

Other common faults are accelerator vacuum faults and magnet and power supply water faults. Vacuum faults typically result from an ion pump sparking down or drawing excessive current because of aging. Problems with high current draw are normally cleared in a few minutes by cycling the IP power. Water flow faults are often not the result of real flow problems but rather a problem with either the flow turbine or associated electronics. The turbine or controller can be replaced in about 30 min.

Most injection system failures can be resolved in less than an hour. Some components responsible for longer duration failures will be upgraded to accommodate the increased beam energy in top-off mode. These include the fast pulsed magnet power supplies (BR2 KE, BR and SR septa, SR bump), and the booster series magnet and BTS bend magnet power supplies. While the reliability of the upgraded systems will not be known initially, it is likely, due to the nature and complexity of the systems, that they will continue to be a source of injection system failures.

3.5 Pulsed Magnets

3.5.1 Introduction

ALS top-off mode of operation will require injection of the electron beam from the Booster ring (BR) into the Storage Ring (SR) at the full ALS energy level (1.9GeV). Currently Booster delivers 1.5GeV¹ beam to the Storage Ring where it is ramped to the full energy and then stored for the user operation. Higher Booster beam energy will require the Booster and Storage Ring pulse magnets to operate at proportionally higher magnetic gap fields. To better understand the breadth and scope of the pulse magnet capabilities and future requirements for ‘topoff’ our group posed the following basic questions:

- 1) What are the engineering design and installation (EDI) modifications necessary to operate at 1.9 GeV² ‘topoff’ mode? To have sufficient design margin
 - a) Can we use existing pulse magnets?
 - b) What’s required to drive the existing pulse magnets?
- 2) What are the EDI modification necessary to minimize storage beam instability during ‘topoff’ operations?
 - a) For the storage ring Septa:
 - i. Do we need to improve eddy current shielding of thick septum magnet?
 - b) For the storage ring Bumps:
 - i. Can we understand and minimize the vertical kick of the stored beam by the bump magnet operations?
- 3) What are magnitudes of the increased stresses and the estimates for life expectancy for the various pulse magnet systems?

Our work over the past seven months is reflected in the report that follows.

3.5.2 Pulsed magnet operation

Extraction from the booster ring into the transfer line and injection from the transfer line into the storage ring is achieved by activating a combination of slow bumps, kickers, septa magnets in the booster ring (BR) and set of fast bumps and septa magnets in the storage ring (SR). The configuration of these pulse magnets is shown in Figure 3.5-1 (booster extraction) and Figure 3.5-2 (storage ring injection).

The extraction/injection magnets are nominally used to fill the storage ring at a 1 Hz rate with three bunches spaced 8 ns apart during each booster ramping cycle. The nominal injection energy is 1.525 GeV. During the normal injection process the magnets are operated continuously at a 1 Hz pulse rate until the storage ring has been refilled from a nominal base level (200 ma) to a peak current of 400 ma. Depending on the injection rate (0.7 to 0.8 ma/shot) the process takes about six minutes or 360 shots to refill the storage ring. In the ‘topoff’ mode magnets will be

¹ The exact transfer energy is 1.522 GeV.

² As a design margin, throughout this section 2.0 GeV is assumed as the design energy for pulsed elements.

driven at 28% higher fields to accommodate the full injection energy of 2.0 GeV and will pulsed once every 20 sec, continuously.

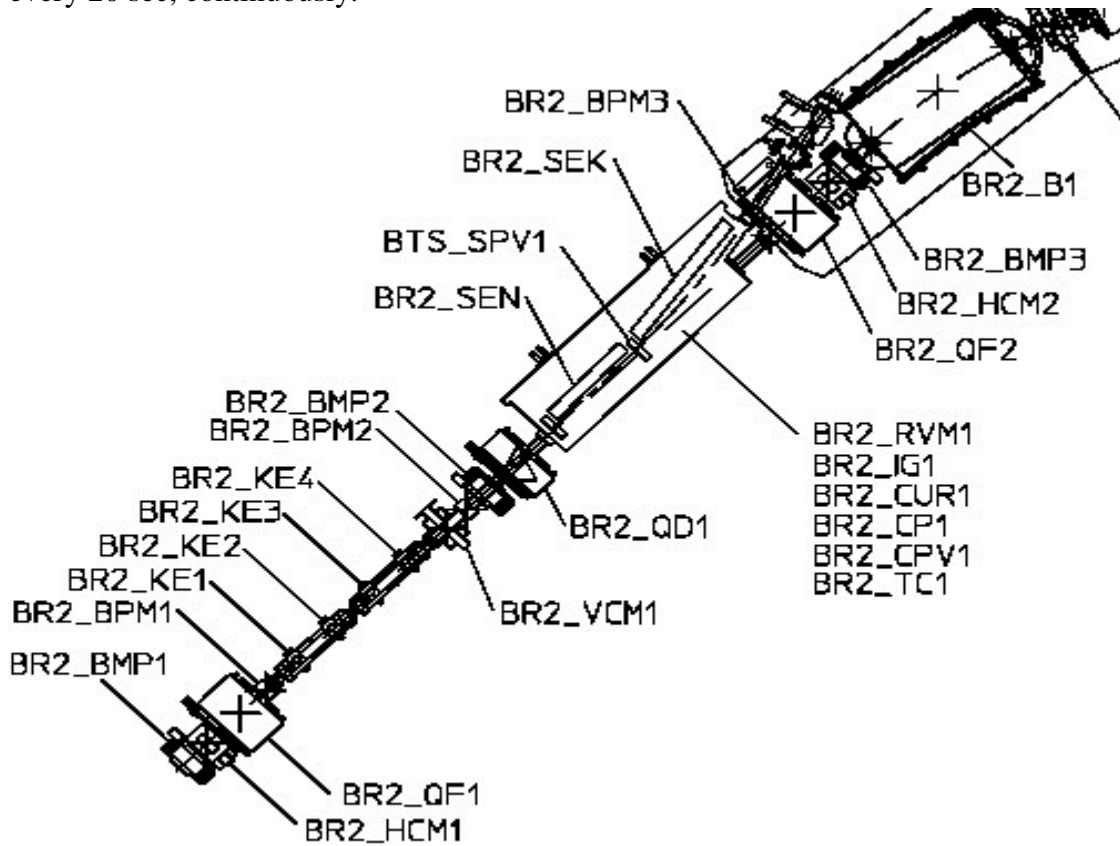


Figure 3.5-1: Booster extraction magnets.

Key:

BR2_BMP1-3 are the 3 booster bump magnets

BR2_KE1 - KE4 are booster kickers

BR2_SEN is thin septum

BR2_SEK is thick septum

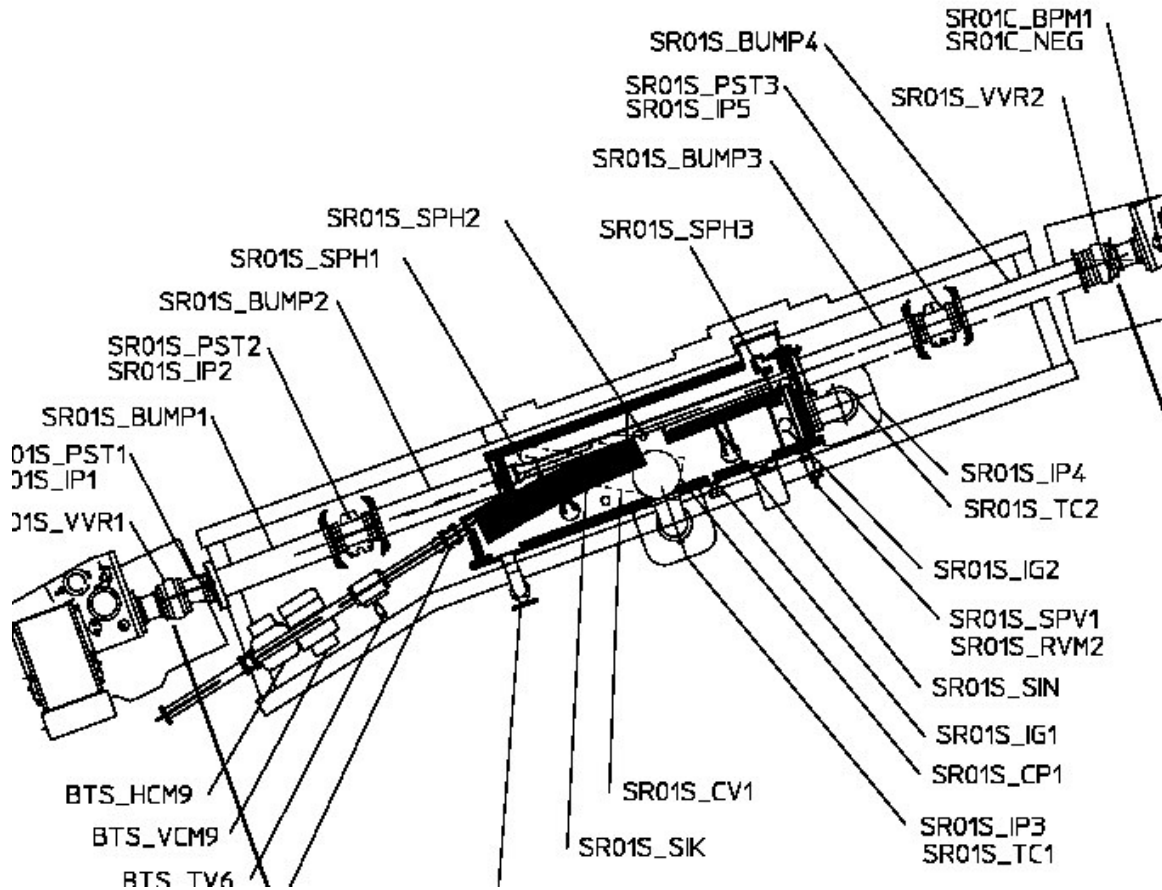


Figure 3.5-2: Storage Ring injection area.

Key:

SR01S_BUMP1 to BUMP4 are Bump magnets

SR01S_SIK is Thin Septum

SR01S_SIN is Thick Septum

A brief outline of the extraction/injection process follows and is shown in Figure 3.5-3:

- 1) 5 ms before beam extraction from the BR three 'slow' bump magnets are energized
- 2) 50 us before beam extraction two 'thin' septa magnets are energized
 - a. One in the extraction and one in the injection sections
- 3) 10 us before beam extraction the two 'thick' septa magnets are energized
 - a. One in the extraction and one in the injection sections
- 4) 2 us before beam extraction the four SR 'fast' bumps are energized
- 5) 75 ns before beam extraction the four BR 'fast' extraction kickers are energized

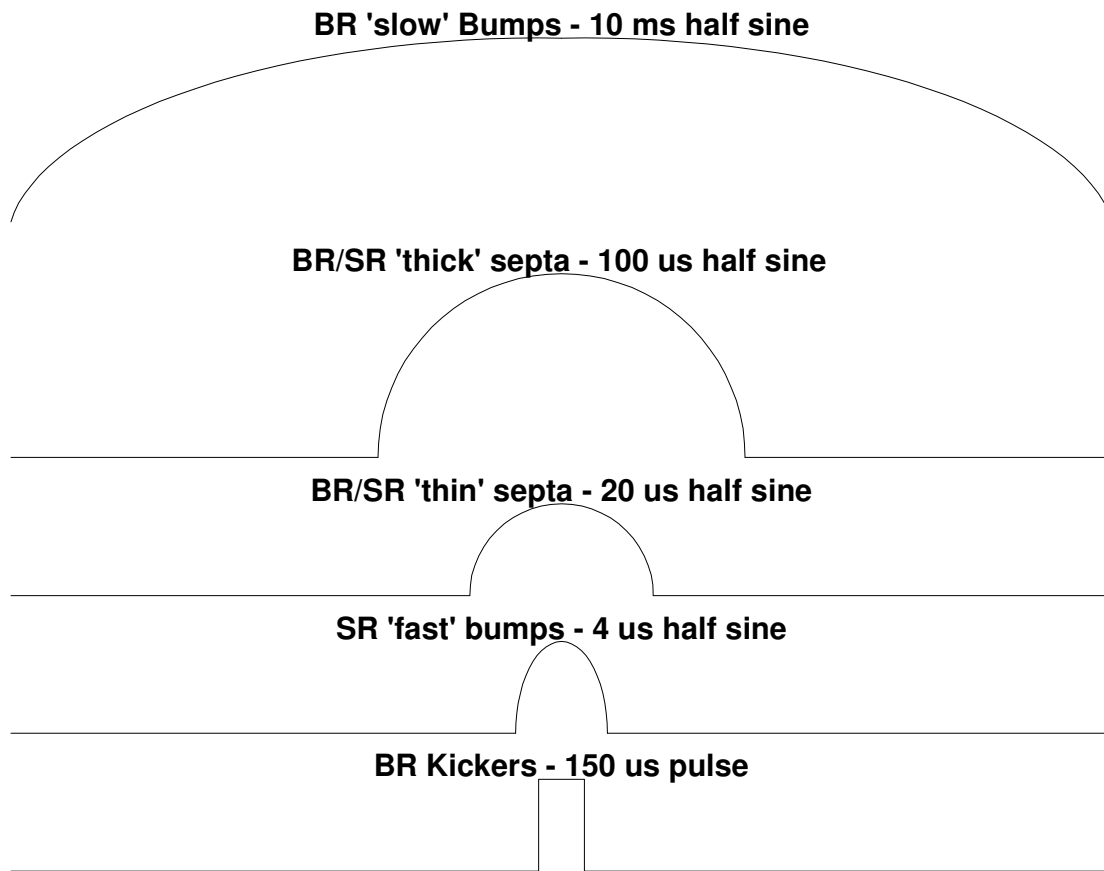


Figure 3.5-3: Timing diagram for booster/storage extraction/injection magnets. Time periods not to scale

Details of the magnet structures, our investigations and conclusions for each magnet will be discussed under their specific headings

3.5.3 *Booster bumps analysis:*

The extraction of the booster beam is initiated by a full-sinusoidal excitation ($T_{full} = 20\text{ms}$) of three corrector bump magnets in the booster. The magnets when excited produce a local closed orbit distortion in the extraction area of the Booster Ring where the fast kicker magnets can be energized to direct the beam into the extraction septa magnet channel. The location of the Bump Magnets in the Booster extraction line is shown in Figure 3.5-4.

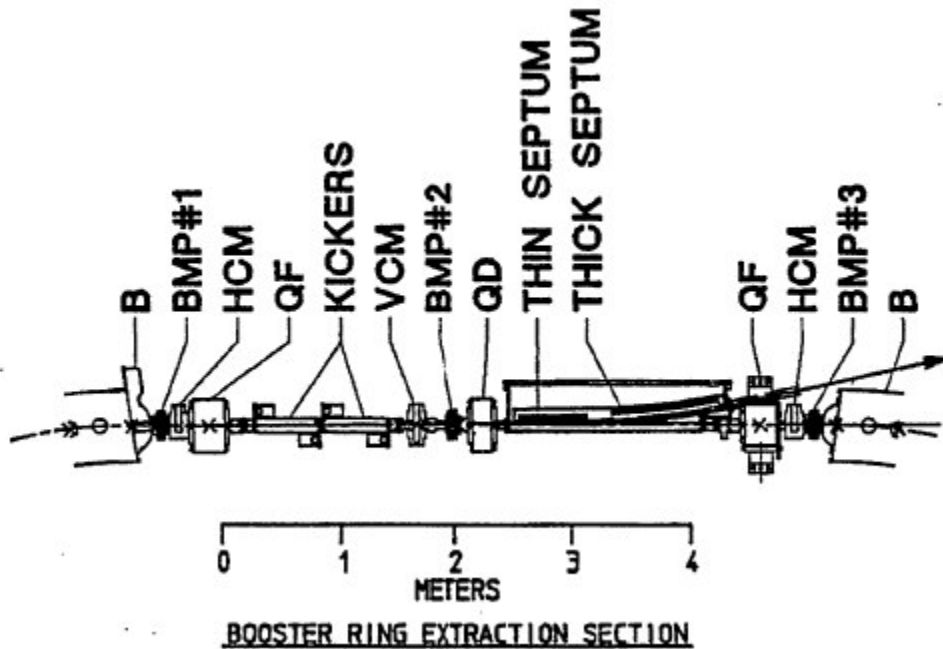


Figure 3.5-4: Location of booster extraction magnets.

Each of the three Bump Magnets has the same core and coil geometry³. See Figure 3.5-5. The magnets have laminated steel cores with a window frame design to minimize magnetic stores energy and pulse power requirements. The cores are split on the horizontal mid-plane to permit assembly of the coils and to allow installation of the magnets around the stainless steel vacuum chamber. The coils are made of square hollow copper conductor with saddle shaped ends and will operate satisfactorily at 1 Hz pulse rate with only natural convection cooling.

The one of three identical capacitor discharge circuits is shown in Figure 3.5-6.

³ Engineering Note: Light Source – Booster Extraction Bump Magnets. AL0323, M6852

firm that the driver and magnets could reach these values. The current nominal injection energy is 1.522 GeV and is listed as 1.5 in the subscript.

Magnet #	B _{1.5}	B _{1.9}	I _{1.5}	I _{1.9}	∠ _{1.5}	∠ _{1.9}
	(Kgauss)	(Kgauss)	(Amps)	(Amps)	(mrad)	(mrad)
B1	2.13	2.74	138	178	5.311	5.311
B2	-3.67	-4.72	-238	-306	-9.16	-9.16
B3	1.44	1.85	93	120	3.579	3.579

Table 3.5-1: Current and future operation parameters for booster extraction bump magnets.

Equipment used for evaluation of magnets at 2.0 GeV:

- a) **Gauss meter and sensor:** The model YR100-3-2 is a self contained, high linearity, high stability magnetic field to analog voltage transducer for one component of a magnetic field. It is particularly appropriate for magnetic fields up to 2T with better than 0.1% absolute accuracy at 1T and with a frequency response from dc to 10 kHz. Probe is guaranteed flat to 1.0 kHz
- b) **Magnet current sensor:** Pearson 101 current probe
- c) **Monitor scope:** TDS5000 digital oscilloscope

Results of magnetic field measurements:

The waveform for BR-2 the magnet with the highest required drive is shown in Figure 3.5-7. The transfer function of peak current vs. peak field is shown in Figure 3.5-8.

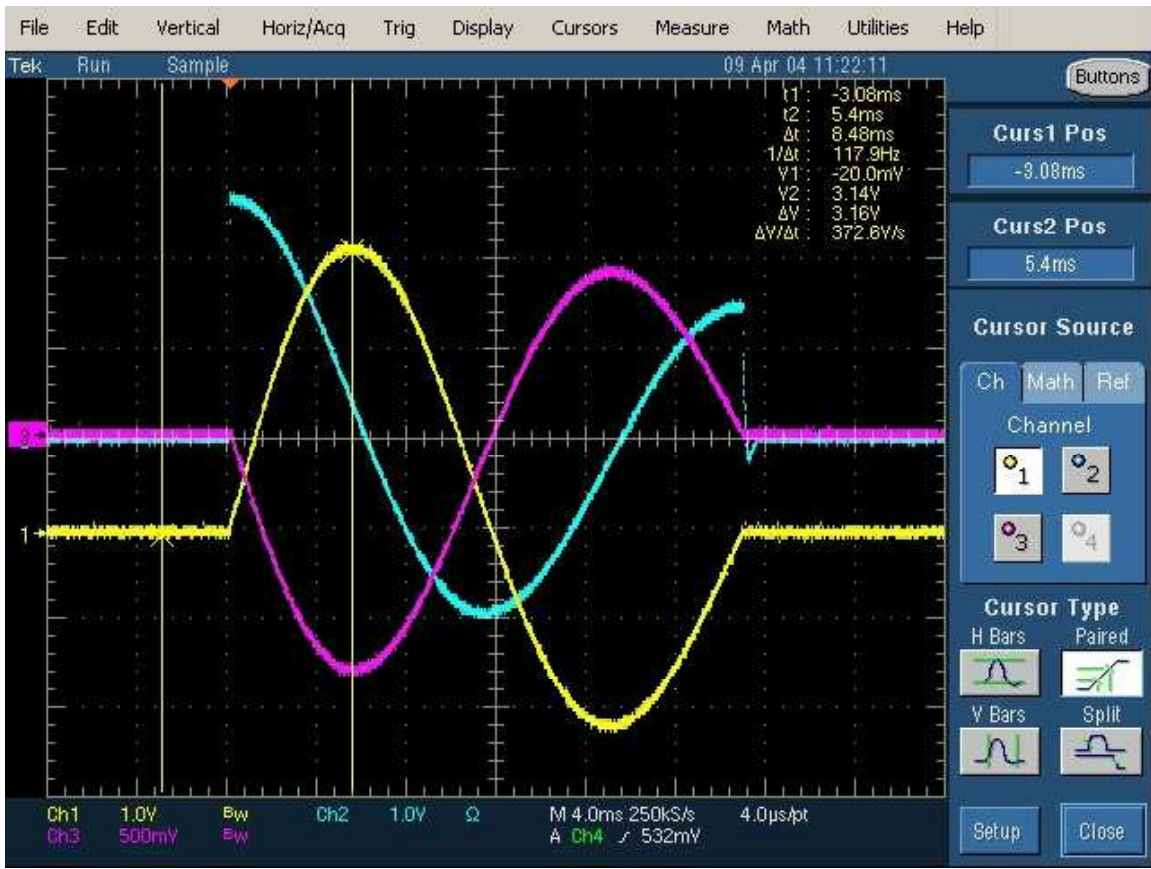


Figure 3.5-7: Waveform pictures taken at peak drive current of 312 amps

For magnet Bump #2.

Color code:

Yellow is magnet current @ 100 amp/volt

Turquoise is applied voltage @ 100 volts/volt

Purple is B field measured with Hall element @ 4000 gauss/volt

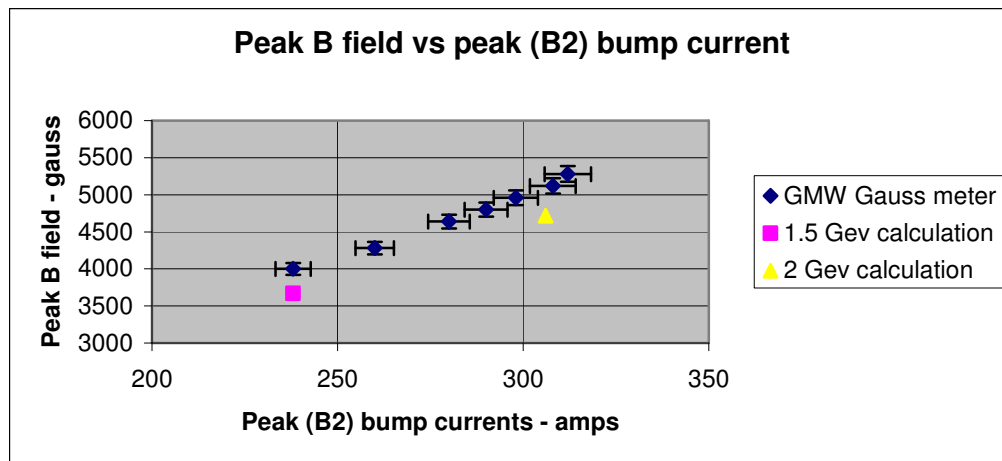


Figure 3.5-8: Field versus current transfer function for the second booster extraction bump magnet.

Key notes for graph #1:

- 1) The thin (~3mm) Hall probe was placed directly on top of the beam pipe on axis with the beam center line.
- 2) Only central bump magnet (B2) was measured for following reasons:
 - a. Only magnet where center axis of magnet above the beam tube could be accessed by Hall probe.
 - b. From calculations⁵ B2 has the highest current requirements.
- 3) Calculated data points for 1.522 and 2.0 are colored square and triangle
 - a. Both points are ~10% below the measured values. This discrepancy may be due to short length of the magnet and the difficulty in determining the true magnetic length of the magnet
- 4) Measurement anomaly: Off axis (from beam center line) B field measurements increased linearly up to approximately $1.5 \times 5280 = 7920$ gauss. This effect was not investigated but may be due E field coupling from the adjacent magnet conductors and Hall probe electronics during the pulse.

3.5.3.1

Summary:

- 1) From graph #1 above the nominal B fields for 2.0 Gev operation were reached with sufficient headroom.
- 2) Higher field measurements indicate some nonlinear effects in the measurement but this is well above the nominal operating point.
- 3) Conversion to water cooling at 2.0 Gev operation is not necessary
 - a. A 29% increase in current or 65% increase in power multiplied by 1/2 Hz cycle rate results in a -17.3% decrease in magnet power dissipation.⁵

⁵ G.Stover "Comparison of Booster ring "Bump magnet" B field measurements vs. calculations @ 1.522 and 2.0 Gev." ALS Top-Off Project Note 04/19/2000

3.5.4 Booster Fast extraction Kicker:

At approximated 145 ns before beam is extracted from the booster four Thyatron triggered, charge line type, kicker power supplies discharge a square pulse of current into four ‘very fast’ single turn window frame magnets in the booster ring to create the final link of the magnetic channel to the storage ring. During the initial ALS Top-Off design process a key question to answer was: “Do we need to modify the Booster fast extraction kickers for Top-Off operation?”.

Extraction Energy:	E	1.95[GeV]
Beam stiffness at 1.95GeV	B_s	6.5 [Tm]
Required deflection angle-	θ	4 [mRad]
Effective length of the kicker (4 units)	l_{eff}	1.07[m]

Required Induction in the kicker air gap:

$$B_{Air} = \frac{B_s \cdot \theta}{l_{eff}} = 0.024 \text{ T} = 240 \text{ G} \quad (3.5-1)$$

The cross-section of the ALS kicker is shown in Figure 3.5-9.

Since the magnetic flux is the same in the air gap and the ferrite core the average magnetic induction in the ferrite core equals:

$$B_{Ferr} = B_{Air} \cdot \frac{S_{Air}}{S_{Ferr}} = 1603 \text{ G} \quad (3.5-2)$$

The maximum value of the magnetic induction in the ferrite core was calculated using INSOFT software and the results are given in Figure 3.5-9.

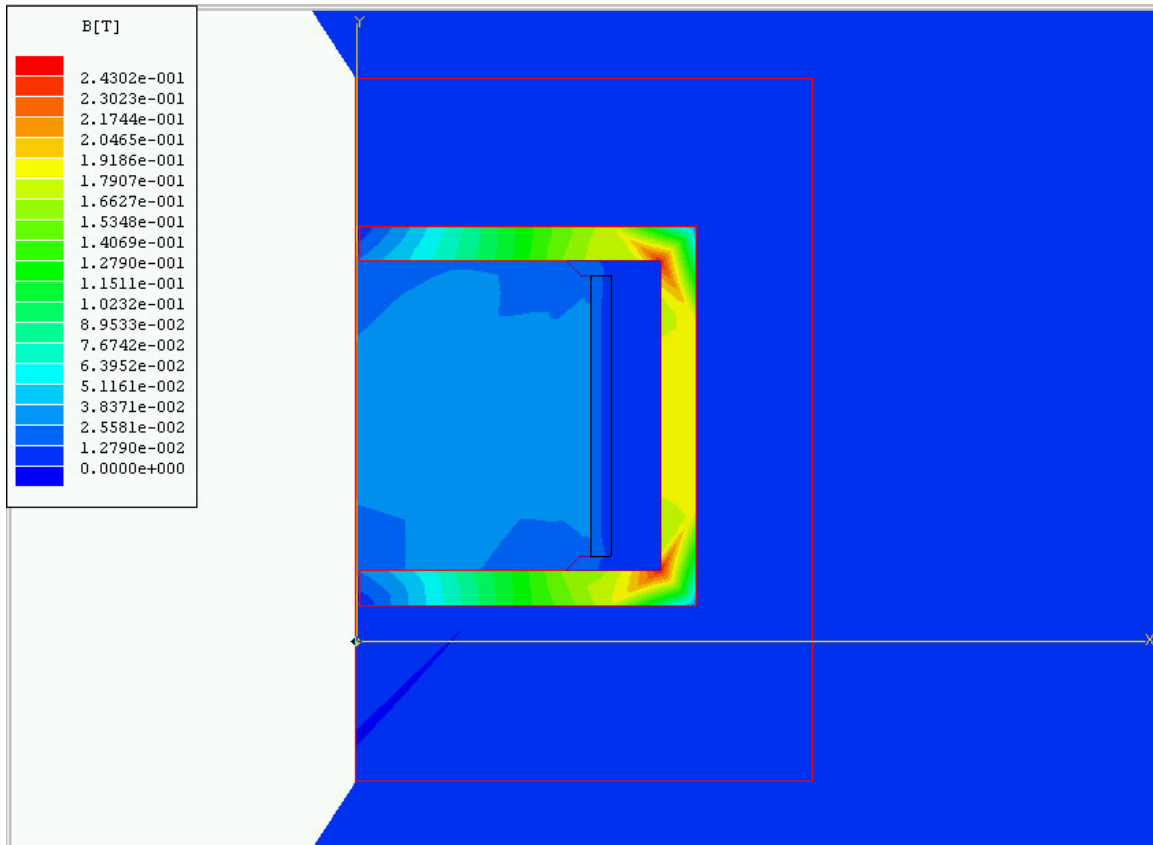


Figure 3.5-9: INSOFT Half magnet simulation of B field @ 2.0 GeV

The maximum B-field in the corners of the ferrite core reaches the value of 2400 G. What is still well below the saturation value for CMD 5005 ferrite (3200 G). Calculations also indicated that the nominal DC operating voltage for the Charge line and Thyatron would rise 30% from 12.5 KV to approximately 17.0 KV.

Several questions that had to be answered:

- 1) Could the existing Balan coupling transformer handle 17kV pulses?
 - a. According to ALS record several transformers failed during 13kV dc high-potting tests).
 - b. Construction of transformers is very involved and difficult.
- 2) Could the existing CX1157 thyatron operate at 17kVDC?
 - a. Operational experience has shown that the CX1157 in it's existing configuration was unable to operate above 16kVDC due internal sparking problems.
- 3) Could the various subsystem components (charge line cables, etc.) stand the higher DC operating voltage?

To answer these questions a kicker test stand shown in Figure 3.5-10 was constructed.

KICKER MAGNET TEST STAND

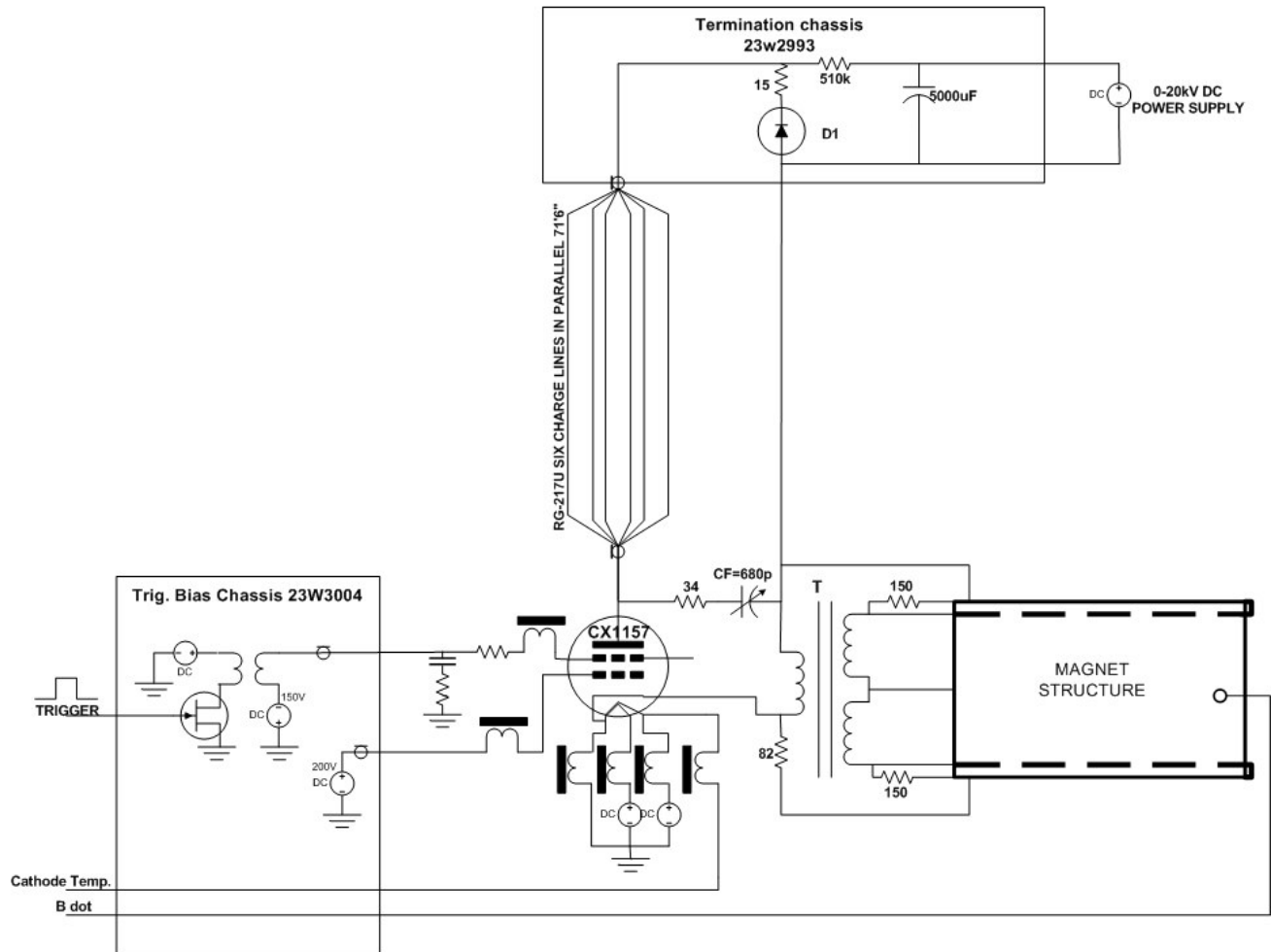


Figure 1

Figure 3.5-10: Drawing of kicker test stand arrangement.

High Voltage Tests results:

- 1) The power supply dc voltage was increased slowly from 0 to 20kVdc. At 16.5kVdc pulse front end forming capacitor (Cf in Fig1) failed. It has been replaced with two 1800pF ceramic capacitors each rated for 40kVdc connected in series.
- 2) For voltages around 17-17.5kV occasional discharge inside the brass cylinder containing CX1157 thyatron occurred. It has been noticed that the clearance between the thyatron body and the thyatron brass container tube was very small (less than 13mm). We insulated the brass containing tube with two layers of 0.03" thick Teflon sheets. Then we were able to increase the dc voltage to 20kVdc without any further incidents.

Life test results:

- 1) The kicker pulse amplitude was increased slowly from 5 to 17kV (5% above
- 2) the value required for Top-Off operation mode). We noticed linear dependence between the dc power supply voltage and the pulse B-field amplitude value over the whole 5 to 17kV range (no sign of saturation noticed). The test stand was operated at 17kV level with 1Hz repetition rate for 3 days.
- 3) On day four we increased the repetition frequency to 10Hz and it was run in these conditions for the next three weeks until:
 - a. **the reversing diode stuck failed** (D1 in Fig.1). This device was designed for current mode of operation and was rated for only 16kV (16 1kV diodes in series without reverse voltage balancing resistors).
 - b. D1 was replaced with 20kV rated device and the test continued up to the full 30days period (24 hours/day) without any further incidents.
- 4) Upgrading the existing Kaiser Systems Inc (KSI) charging power supply to a newer design is currently being investigated.
 - a. The design of a hardware interface is required.
 - b. Several spares with interfaces should be produced.

Summary:

The ALS extraction kicker successfully passed a 30 days endurance test at the B-field level corresponding to 2GeV ALS beam energy level. In order to use existing kicker magnets for Top-Off operation we suggest following modifications:

1. Change existing pulse front forming capacitors to higher voltage handling devices.
2. Insulate the thyatron containing tube against the possible high voltage discharges from thyatron tube.
3. Replace the existing reversing diode stacks with higher voltage handling devices.
4. The charge-line cables should be replaced

3.5.5 Booster and Storage ring Thick and Thin septum magnets

Fifty microseconds before the peak of the storage ring orbit bump, the two identical ‘thick’ septa magnets, one in the BR extraction straight and a mirror device in the SR straight, are energized. Thirty microseconds later the two identical ‘thin’ septa magnets one in the BR extraction straight and a mirror device in the SR straight are activated. See Figure 3.5-1 and Figure 3.5-2 above. The basic questions that we attempt to answer in this section are: What modifications to the septa magnets and drivers are required to operate at 2.0 Gev ‘topoff’ mode? Are there any changes to the system topology that can minimize storage beam instability during ‘topoff’ operations? And finally what are magnitudes of the increased stresses and the estimates for life expectancy for the septa magnet systems?

3.5.5.1 Electronic drive requirements for topoff:

Existing septa drives

The driving circuit for the thick septa is shown in Figure 3.5-11. A low inductance capacitor is resonantly discharged through a stacked array of six high voltage, high di/dt SCR’s and a series blocking diode. The resultant current and voltage waveforms are shown in Figure 3.5-12. The half sine period for the thick septum is ~100us and ~20us for the thin septum magnet. The thick septum uses an energy recovery inductor to minimize the charging power supply size and cost. The thin septum has no energy recovery and requires only two SCR’s in series. Both systems operate at one Hertz.

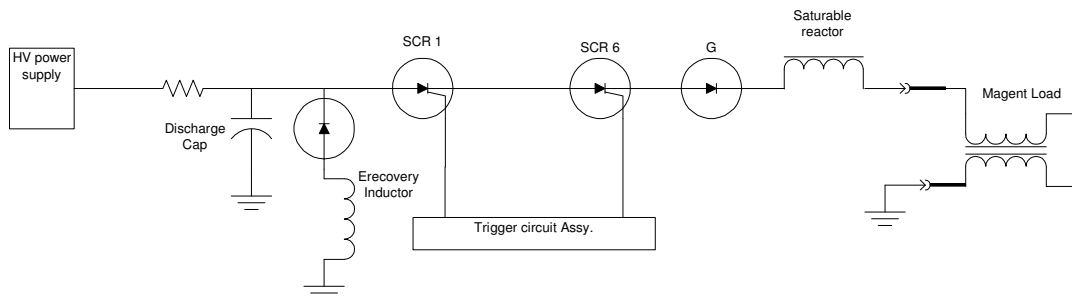


Figure 3.5-11: Basic discharge circuit for the thin and thick septum magnet



Figure 3.5-12: Basic discharge circuit waveforms for the thick septum magnet

Drive requirements for Topoff:

Description	Present	Top-Off	
Maximum Field, B	1.0	1.3	T
Magnet Current, I_{min} - I_{max}	4.0	5.21	KA
Pulse length, t	118 (half sine)	236 (full sine)	μs
Magnet Voltage, max., V	4.86	6.3	KV
Di/dt stress (SCR)	107	138	A/ μs

Table 3.5-2: Thick septum operational parameters for higher fields:

Description	Present	Top-Off	
Maximum Field, B	.29	.38	T
Magnet Current, I_{min} - I_{max}	3.5 (4.2)	4.55 (5.46)	KA
Pulse length, t	20	20	μs
Magnet Voltage, max., V	1.35 (1.62)	1.76 (2.11)	KV
Di/dt stress (SCR)	1.3 (1.6)	1.7 (1.9)	KA/ μs

Table 3.5-3: Thin septum operational parameters for higher fields (SR thin septum*):

The increase in the drive requirements for both magnets is 30%. This presents no real challenge for an upgrade to the drivers. The thick septa will require a new higher voltage charging supply, capacitors, and replacement of several lower voltage sub-components. The thin septum power supply will require a new higher di/dt SCR that is currently being specified and new charging capacitors. In addition the charging power supply for the SR thin septum needs to be upgraded. (*)This is due to an existing +20% over drive condition required for the SR thin septum magnet. The reason for the overdrive condition is not understood at this time. A discussion of possible reasons and future investigations is listed under the topic "Further studies to do". A new higher voltage spare driver has already been constructed for driving the spare pulse magnets. This unit is a swappable replacement for both the existing and future thin and thick septum drivers.

3.5.5.2 Septum magnets:

Mechanical description:

Each thin and thick septum magnet comprise a pulsed bending magnet system; one system is for extracting the beam from the booster and the other system, essentially identical, is for injecting the extracted beam into the storage ring. Figure 3.5-13 shows the injection top view layout, with each magnet sectioned through the horizontal mid-plane. The thick septum, named for its thicker septum plate, gives a 10.0 deg bend, and the thin septum gives a 2.0-degree bend. Both magnets are iron dominated, with C-shaped cores forming the main magnetic gap, as shown in Figure 3.5-14 the drive coil is wound around the back leg of the core. The thick septum has a laminated steel core which can pass a higher peak B field but requires a longer period (~100 us) discharge pulse, and the thin septum has a ferrite core which can pass a lower peak field, but employs a shorter (~20) pulse. Both magnets employ an eddy current septum design that consists of a thin copper sheet placed against the open end of the C-shaped magnet gap. The fast rise and fall of the main gap field generates sufficiently high eddy currents in the longitudinal direction in the copper septum plate to prevent the fringe field at the end of the gap from penetrating through the septum, thus allowing a circulating beam to be positioned close to the opposite side of the septum plate. The return leg eddy current travels through a similar copper plate on the opposing side of the magnet; these plates being electrically connected at each end and across the top and bottom with copper plates and form a "shield box" around the magnet. For sufficient thickness of the septum ($t > 3$ skin depths), the total current in the septum plate closely matches the drive current, which is the case for both magnets.

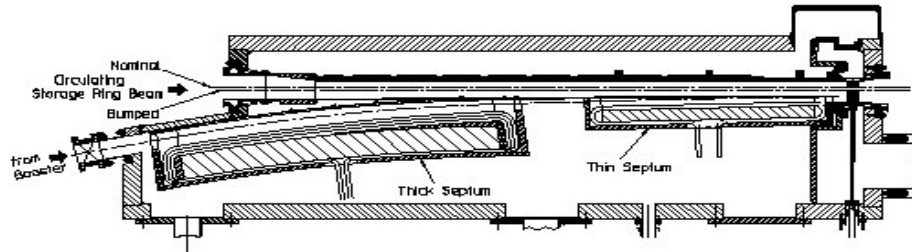


Figure 3.5-13: Top view of Septa magnet layout – SR straight. Each magnet sectioned through the horizontal midplane.

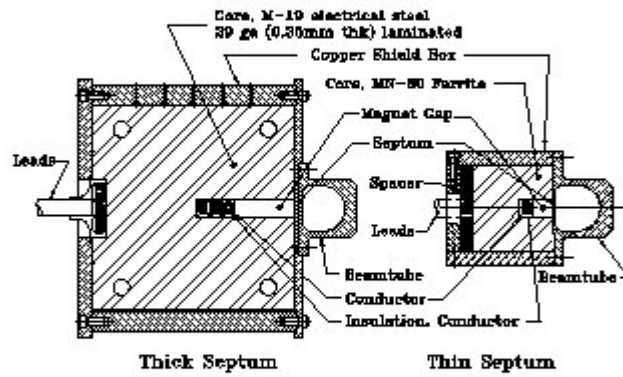


Figure 3.5-14: Thick (left) and thin (right) Septa cross sections – (needs to be resized)

Parameter	Thick	Thin	unit
Magnet vertical gap	1.5	1.5	cm
Magnet Horizontal Gap (varies along length)	4.9-7.0	1.7-2.7	cm
Mag., Total Lengths, L_m, L_o	0.89, 0.91	0.6, 0.62	cm
Number of turns in coil	3	1	
Required Good Field Width	4-6	1.8	cm
Good Field Width distance from Septum	1	0.5	mm
Required Field Uniformity	2×10^{-3}	$2 * 10^{-3}$	T/T
Conductor cross section dimensions, W x H	0.7 x 1.06	0.7 x 1.06	cm
Magnet AC Resistance, R	1.15@4kHz	4.5@25kHz	m Ω
Magnet Inductance, L	36	1.24	μ H
Maximum Pulse Rate	10.0	10	Hz

Table 3.5-4: Thin and Thick septum fixed parameters

	Present	Top-Off	
Maximum Field, B	1.0	1.33	T
Magnet Current, $I_{min.} - I_{max}$	4.0	5.3	kA
Pulse length, t	125 (half sine)	250 (full sine)	μ S
Magnet Voltage, max., V	4.0	5.3	kV
Pulse energy, max., U	270	480	J
Energy loss/pulse, max., Q_t	20	67	J
Temp. Rise, max., steady state	10 (1 Hz)	5 (0.05 Hz)	$^{\circ}$ C

Table 3.5-5: Thick septum operating parameters

	Present	Top-Off	
Maximum Field, B	0.29	0.38	T
Magnet Current, $I_{min.} - I_{max}$	3.5 (4.2)	4.55 (5.46)	kA
Pulse length, t	20 (half sine)	20 (half sine)	μ S
Magnet Voltage, max., V	1.35 (1.62)	1.76 (2.11)	kV
Pulse energy, max., U	8 (9.6)	15 (18)	J
Energy loss/pulse, max., Q_t	0.2	0.4	J
Temp. Rise, max., steady state	10 (1 Hz)	5 (0.05 Hz)	$^{\circ}$ C

Table 3.5-6: Thin septum operating parameters (SR thin septum)

3.5.5.3 Theoretical investigations:

Field quality & current distribution in thick septum at 2.0 GeV

Thick Septum:

The thick septum core is made from M-19 electrical steel laminations each 0.35mm thick. This material retains high permeability even at 1.6 T. The pole-tip fields do not exceed the nominal gap field of 1.33T, except at a very small corner section where the septum plate meets the core. Sufficient thickness throughout the core back leg exists to keep average B in this section below 1.3T. The presence of eddy currents in the iron laminations during the pulse concentrates the field towards the outer surfaces of the laminations, thus requiring more MMF in the core section of the magnetic circuit. To account for this, an eddy current modified B-H curve was generated for M-19 steel specific to this lamination thickness and transient time pulse. Using the eddy current modified B-H curve in a transient finite element model of the magnet cross section (OPERA-2D), it was verified that only slight local saturation at the inside corners of the core back leg occur, behind the conductors. This causes a negligible rise in core MMF and also helps to maintain field uniformity across the gap (by equalizing the core MMF along different flux paths).

Figure 3.5-15 shows a plot of the vertical B field component along the transverse width of the gap at the mid-plane. Three different field levels are shown, 1.0T (present operation) 1.33T (top off nominal) and 1.5T (13% over top-off nominal); with the two higher field levels current normalized by the current factor to the nominal current of present operation for comparison. The magnet efficiency is still quite good at 1.5T, as the field value in the straight line portion is within 0.2% of the lower value. In all cases, a small amount of highly localized saturation occurs at the pole tip corner where it meets the septum, leading to a slight field drop off very close to the septum. This is due to the field penetration into the septum, as the AC skin depth is 1.04 mm @ 4 kHz.

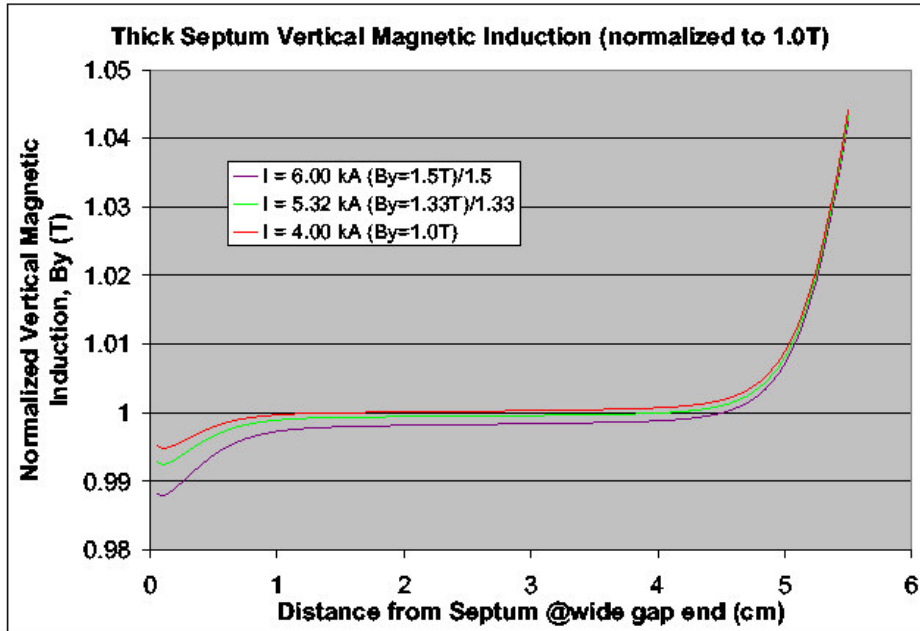


Figure 3.5-15: Vertical B field component along the transverse width of the gap at the mid-plane. For 1.525 GeV, 2.0 GeV, and + 10%

Thin Septum:

Figure 3.5-16 shows similar field plots, with the high current ($B=0.40T$) curve normalized to the present nominal current ($B=0.30T$) across the gap mid-plane, near the narrow end. One can see that the magnet retains a high degree of efficiency at the higher field and also maintains a uniform field closer to the septum. The ferrite used (MN-80) retains high permeability @ 0.48 T so a 20% safety factor is present. The thin septum has an AC skin depth of 0.42mm @ 25 kHz leading to less field falloff close to the septum.

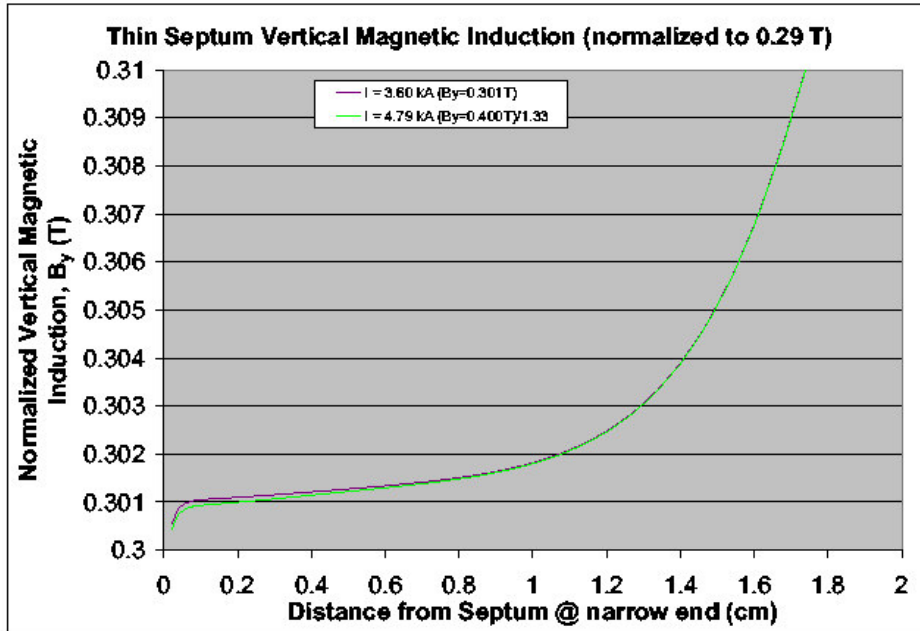


Figure 3.5-16: Thin septum high current ($B=0.40T$) curve normalized to the present nominal current ($B=0.30T$) across the gap midplane, near the narrow end.

The theoretical results for the thick and thin septum show very acceptable field quality with good margins at ‘topoff’ currents levels. Magnet measurements of the thin and thick septa agree with the model results and are discussed in the section “Parameter measurements of septa spares”.

3.5.5.4 Improvements in magnet system topology that improve SR beam stability:

Beam position measurements as shown in Figure 3.5-17 show horizontal and vertical orbit shift in the stored beam during the injection process. Injection studies show that this effect only occurs when the thick septum magnet is firing. It had been surmised that a slowly decaying remnant leakage field penetrates through the eddy current ‘thick’ septum. Our theoretical and experimental investigations described below accurately verify this effect. We also experimentally demonstrate a modification to the thick septum driver that markedly reduces this problem.

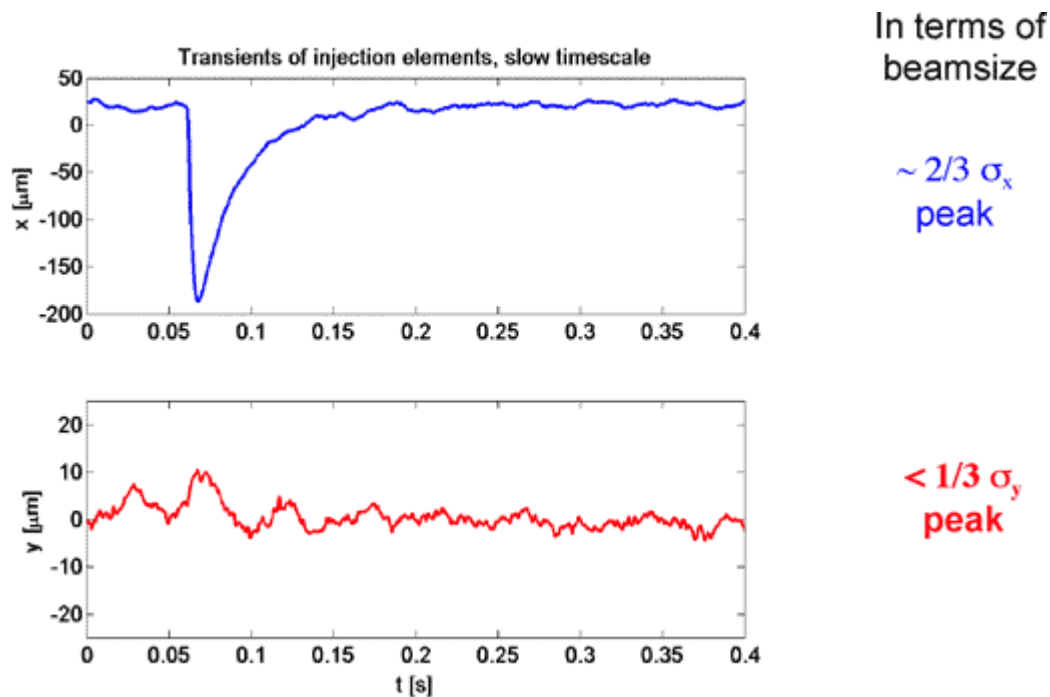


Figure 3.5-17: Beam orbit distortion due to slowly decaying eddy currents in thick septum magnet.

3.5.5.5 Theoretical model eddy current leakages:

The eddy current in the septum plate diffuses into the septum plate over time and the current profile across the septum has the form of an exponentially damped traveling cosine wave. Figure 3.5-18 shows both eddy currents in the thick septum and flux lines in the thick septum at full field ($t=62.5\mu\text{s}$). At the end of the half sine drive pulse ($t=125\mu\text{s}$), even though the total current in the septum is zero, this damped cosine current profile is not zero and forms a very thin vertical dipole B field in the septum, which can be seen in Figure 3.5-19 as flux lines entering the core at the corner. A small portion of the total flux circulates around the left side of the septum (not shown) to produce a stray field along the circulating beam path. This dipole current has its own L/R decay time constant which is relatively long, and, for the thick septum, the stray field causes a beam orbit distortion shown in Figure 3.5-17. The thin septum stray field is smaller and is shielded by thick iron plating inside the beam tube and has little effect on the beam. Figure 3.5-20 shows the thick septum stray field at its maximum value, which occurs at 1.0 msec after the start of the half sine current pulse. The stray field intensity is a function of transverse distance from the septum, and a field integral of ~ 500 G-cm maximum integrated along the beam path is predicted. Figure 17 shows the predicted time history of this stray field integral. Under top-off mode this persistent stray field would be present about every 30 sec.

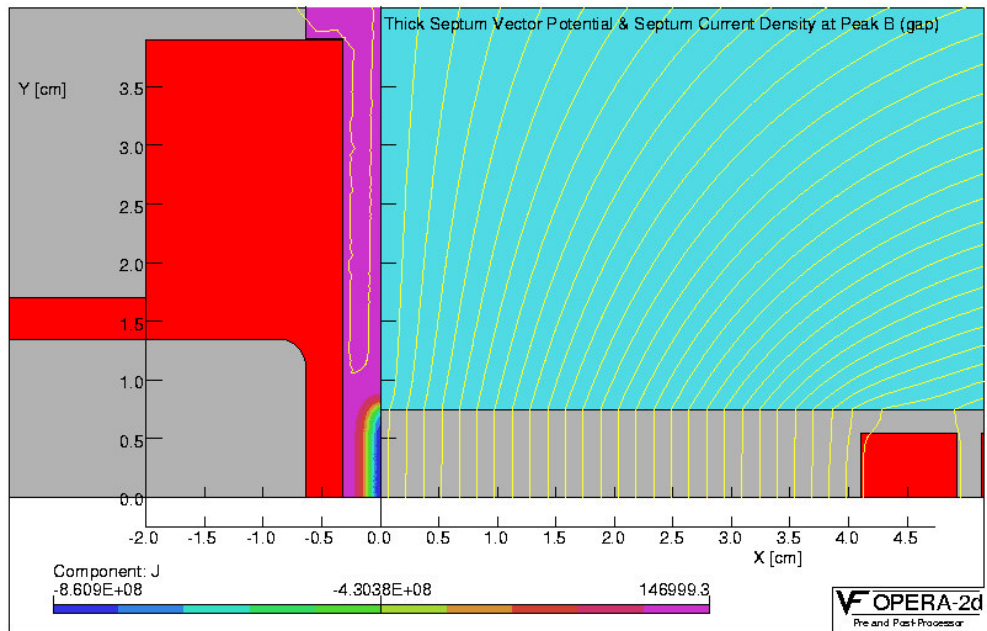


Figure 3.5-18: Thick septum at peak field (1.33 tesla) of half sine pulse

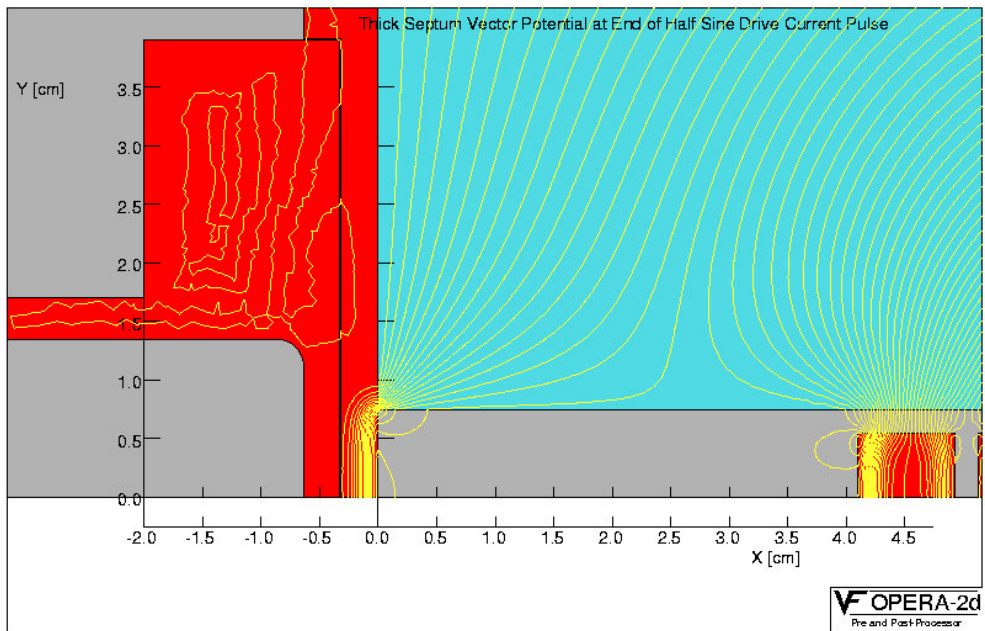


Figure 3.5-19: Thick septum at zero field at end of half sine pulse

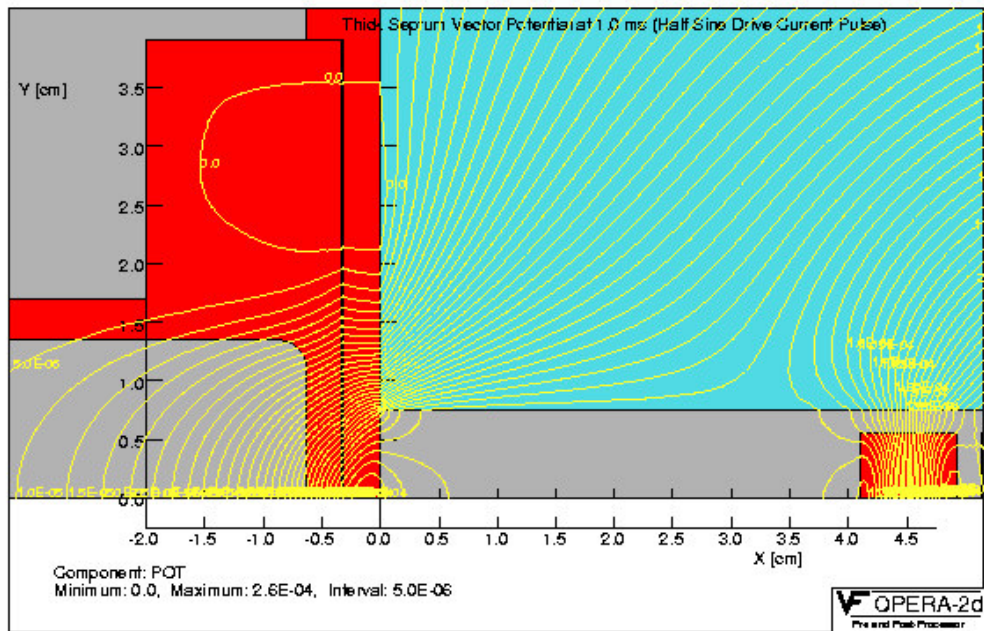


Figure 3.5-20: Thick septum stray field at its maximum value at 1.0 msec after the start of the ‘half sine’ current pulse.

3.5.5.6 Reducing the leakage using a full sine ring:

By using a full sine pulse instead of a half sine pulse, a second “following” dipole eddy current of opposite polarity is created which can reduce both the magnitude and the long time duration of the stray field. Figure 3.5-21 shows the flux lines at the end of a damped full sine current pulse using a damping factor as measured on the installed magnets (93.5% voltage reversal) and Figure 3.5-22 shows the time history of the resulting predicted stray field integral.

3.5.5.7 Experimental results of full ring test:

To test this prediction the present pulse driver was reconfigured to produce a full sine drive current pulse and the effect on the stored beam was measured, the beam deflection time-history and FEA calculated time history of the stray field integral are shown in Figure 3.5-22. This reduced stray field integral meets the requirements for top off operation.

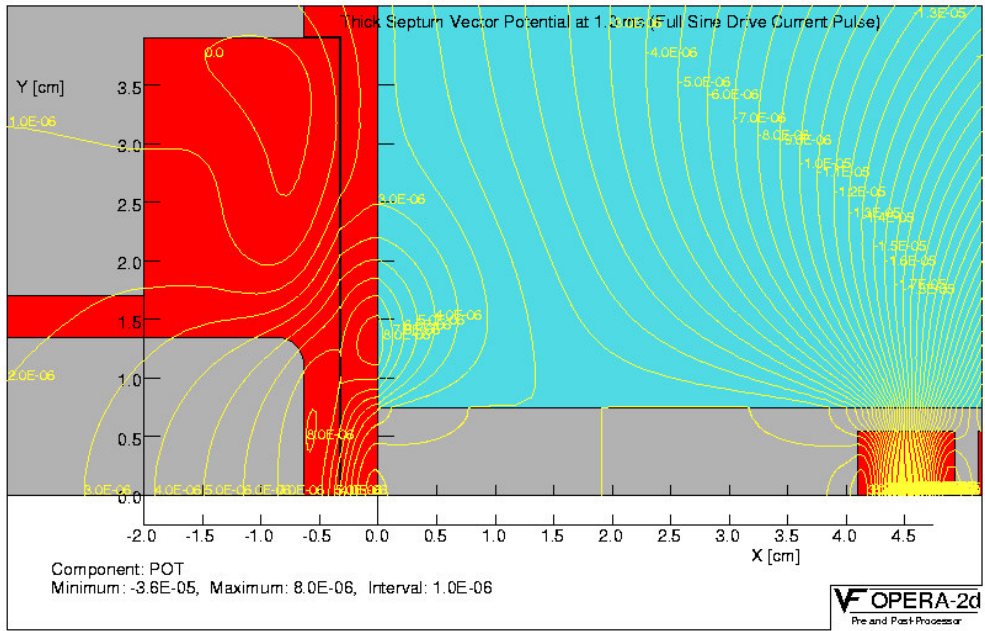


Figure 3.5-21: Flux lines at the end of a damped ‘full sine’ current pulse using a measured damping factor of (93.5% voltage reversal)

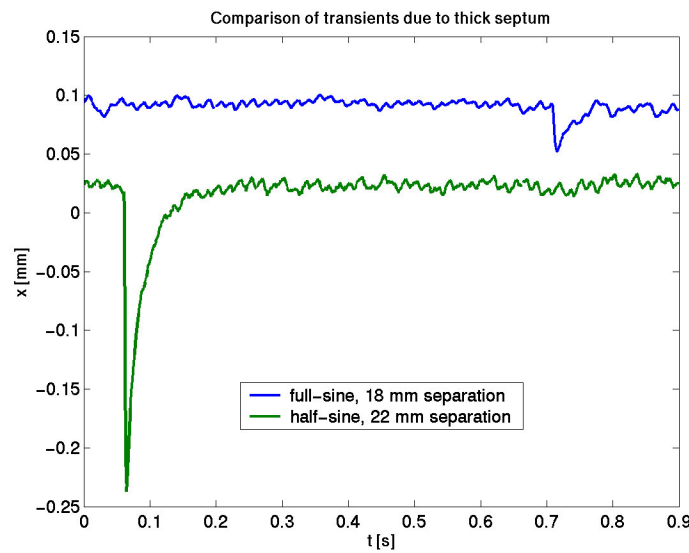
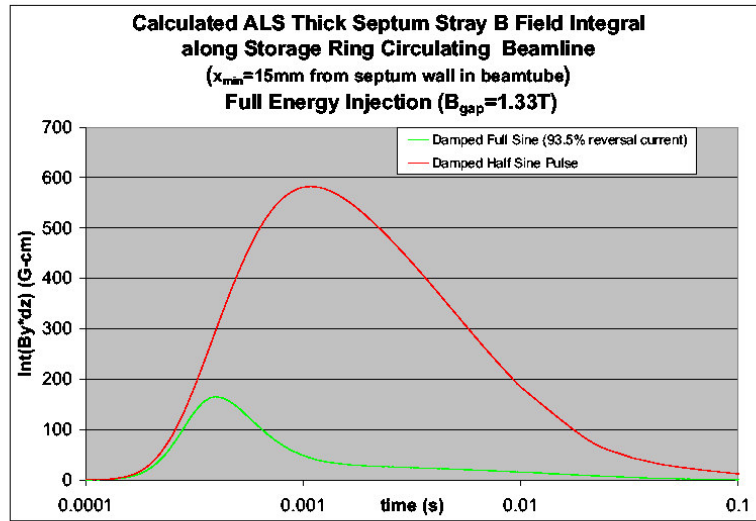


Figure 3.5-22: Predicted time history of this stray field integral along the beam axis and measured orbit distortion for half-sine and damped full-sine case.

3.5.5.8 An estimate of the reliability of magnets and expected contingencies:

Lifetime requirements for magnets:

An upper limit of the maximum number of pulses the magnets will endure in the ‘top-off’ mode would be: 3 shots/min. * 60min./hr. * 6000hr/year * 10 years = $10.8 * 10^6$ pulses. The existing magnets which have been in operation since 1992 without failure may have very approximately: 400shots/6hr. * 6000hr./year * 12years + 1.2 (special mode) = $5.7 * 10^6$ shots. We acknowledge that estimated life left in the existing magnets is unknown. In the following text we

will attempt to identify any factors that might accelerate the degeneration of the magnets and will propose a contingency plan in the event of a magnet failure.

The key factors that could lead to an accelerated failure of the magnets would be high voltage breakdown at the core to conductor edges, repetitive magneto-strictive shock, increased heat load of the septum or the cores and radiation damage to the Epoxy.

Higher voltage breakdown at the core to conductor edges:

The magnet coil is insulated with 2 mm of epoxy/fiberglass insulation. At each end of the magnets the coil projects past the core edges which have a sharp corner; they were not radiussed before winding the coil. The core can be considered to be at ground potential as it makes intimate contact with the copper shield box along the top, bottom and back sides of the core (a thin Kapton sheet was inserted between the septum and the core. A high electrical field gradient occurs at the start and end of each half sine pulse between the coil and ground. A possible fix is the addition of a stainless steel "field smoothing piece". The coil voltage at these locations is close to the full voltage across the leads. 10.6 million 'full ring' pulses can be very re-scaled in time to 60 hrs of 50 Hz AC excitation. This test would be a much more stringent stressor of the voltage hold-off capabilities of the magnet material. The peak 5.5 kV voltage across 2mm of laminate is equivalent to ~20 kV/cm RMS. Figure 3.5-23 shows a chart⁶ of rod(sharp-edged)-plane discharge tests of epoxy/fiberglass laminates. An epoxy/fiberglass laminate of similar thickness (1.5mm) should survive ~6 months of 50 Hz operation. In the lower chart (Figure 3.5-23), we extrapolate the 1.5mm 20 deg.C curve to the left in the lower chart we also find that the discharge inception voltage could be as little as 10% of the applied voltage in order to survive the 60 hrs.

Given the very short duration of our pulse voltage (< 20μsec) the possibility of a corona discharge and breakdown seems unlikely.

⁶ Chart 9.4a, High Voltage Technology, L.L.Alston

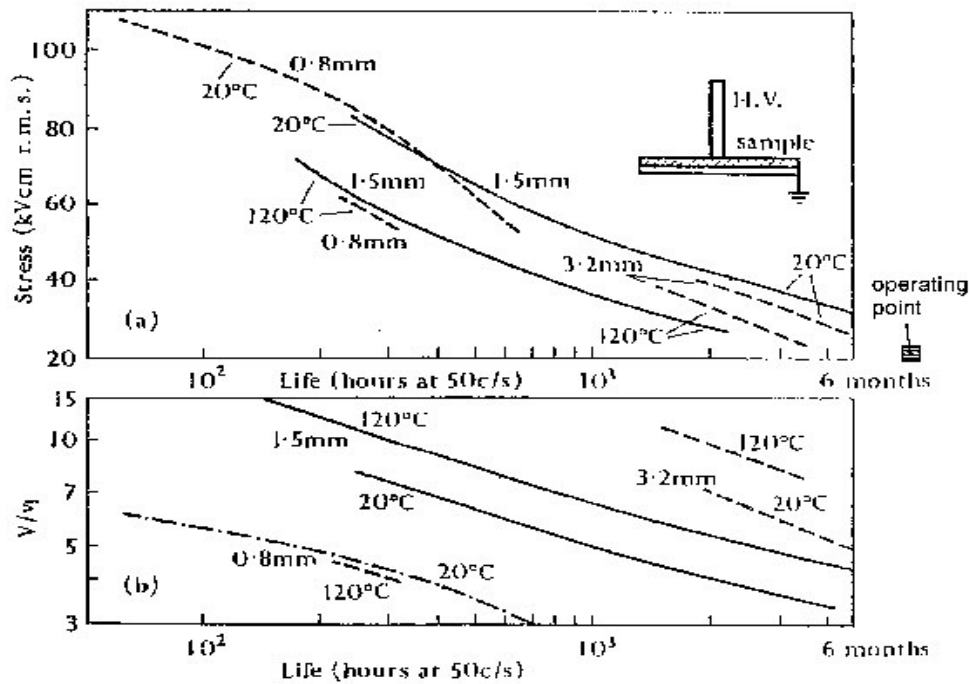


FIG. 9.4. The effect of discharges on the life of epoxy-glass laminates (Mason). (a) Life versus stress. (b) Life versus voltage applied/discharge inception voltage.

Figure 3.5-23: Rod-plane insulation tests from Alston

Higher forces:

During the pulse, the septa have a magnetic pressure on them that is directed outward from the core. A full sine current pulse will generate two such outward pulses. The pressure

against the thin septum is 0.64 bar @0.4T, for the thick septum 7.0 bar @ 1.33T. The thin septum is 1mm thick and the maximum stress associated with this pressure is +/- 3500 psi (27.8 Mpa); this is primarily a bending stress. The thick septum is 6.4 mm thick but has a section on one end of 3.2 mm thick; maximum stress here is +/- 4400psi (33.3 Mpa). A typical fatigue endurance limit stress for 1100 Copper alloy is 10 ksi (69Mpa) (for 10^7 cycles), so there is a factor of safety of over two on fatigue.

Increased heat loading:

In the thick septum original operating design, the nominal 1.0T gap field 100 microsec half sine pulse produces 35 J/pulse Joule loss in the coil. For top-off the pulse will be a full sine 1.33T gap field of 250 microsec duration. Joule losses in the coil rise to 155J/pulse, or 155 Watts @1 Hz pulse rate. At present the coil is conductively cooled to the core to which it ostensibly remains bonded to. Magnetic forces tend to push the conductors towards the back leg of the core, however potential debonding of the coil from the core cannot be discounted. For this reason forced air or water cooling will be used on the thick septum. A water flow rate of 0.12GPM is indicated to keep coil temp rise below 5 deg. C. The cooling channel is 4mm dia.; such a flow rate will have negligible pressure drop. Due to the high voltage, water conductivity may need to be higher than the ALS LCW supply; if so a dedicated system will be supplied for these magnets. Coil losses are much less in the thin septum coil (0.44W@ 0.4T, 1 Hz) and this magnet will remain conductively cooled.

Septum heating: Joule heating indicates negligible temperature rise in the septums for continuous pulsing at 1 Hz. For the thick septum a Joule heating of 11 W/m produces a 20mKdeg steady state temp rise between the horizontal midplane of the septum and the bulk of the shield. For the thin septum a Joule heating of 0.26 W/m gives a steady state temp rise of 1.3 mK between the horizontal midplane of the septum and the bulk of the beamtube.

Core heating: From a chart of core loss as a function of high frequency AC B field excitation, core total losses in the thick septum are 40W for full sine (250 microsec) operation @ 1.33T 1 Hz pulse rate, up from 8W at 1.0T half sine 100 microsec operation@ 1 Hz as originally calculated.

The magnet is cooled conductively to ambient temperature of the vacuum box through the three aluminum pads of the baseplate which the magnets sit on, and are bolted down to. The actual contact pressure and fit are unknown so, assuming a thin 0.003" layer of air is present between the magnet and these feet (which would then be the dominant thermal resistance), a maximum possible temperature rise of 3.5 deg. K is indicated. In reality the fit is likely to be better and temp rise may be much lower than this.

Radiation damage to the Epoxy binder:

This has not been assessed but is not expected to be a problem, since the radiation dose for all existing equipment is not expected to increase with the addition of a collimation/scraper system to localize losses away from sensitive equipment.

3.5.5.9 Contingency plans and modifications septa magnets:

We've attempted to assess the key factors that could lead to an accelerated failure of the septa pulse magnets. The assessments are speculative at best and given the critical dependence of

the ALS on proper septum magnet function, we are preparing a detailed mechanical procedure for the rapid change out of any of the septa magnets with ‘machine ready’ spares. The spares were upgraded to a ‘machine ready’ condition during R&D phase of this CDR. The plan will identify the diagnostic equipment and procedures needed to quickly determine the fault condition after replacement with a the machine spare.

Replacement of any of the septa magnets with a spare is procedurally complex and labor intensive. In particular the replacement of the SR thin septa is the most difficult. Given the exigencies of machine ‘down time’ this procedure will also attempt quantify the maximum time required to replace the SR thin septa with it’s requisite spare. We have been advised that the canonical maximum down time for unscheduled machine operations is one week. After careful analysis it is hoped that we will be able to meet this time limit.

Electronic ‘windowing’ circuitry will be added to sense any significant changes in a magnets current waveform. A progressive insulation failure i.e. a turn-to-turn or turn-to-ground short can be quickly sensed and stopped in one cycle. Given the relatively low stored energy in these magnets it is fairly likely that coil may be saved from significant damage and will be repairable ‘on the core’. This would save many man-months of effort needed to procure conductor and insulation, and to re-commission the coil winding and potting apparatus.

For example the damage caused by an electrical failure at the sharp core-conductor edge as discussed above may be repaired without winding another coil. The insulation can be removed by hand in the breakdown area by judicious hand filing and a small half round stainless steel “field smoothing piece” can be electrically bonded to the core at the corner thus reducing the local field concentration. The repaired area would be vacuum repotted with fiberglass and epoxy.

Another concern is core delamination in the thick septa magnets. Our stress calculations suggest this an unlikely event but the magnet shield box end plates could be easily modified to accommodate the addition of longitudinal core compression plates (actuated by springs or bolts) that would limit or otherwise negate the effect of delamination. Delamination caused by accelerated damage to the epoxy from synchrotron radiation has not been assessed.

3.5.5.10 Parameter measurement plan:

As discussed in ‘contingency plan and modifications’ section above the thin and thick septum spares have been upgraded to a ‘machine ready’ condition. The spare storage ring beam tube has been located and fastened to the gap face of the thin septum magnet. Both magnets have been mounted on a granite table and will be driven by a new higher voltage spare driver that has already been constructed for testing the magnets and as a ready spare for the existing septa pulse magnets.

The key measurements will include stress and heating tests, magnetic field measurements in the gap and adjacent beam tube, and short life tests. The stress and heating tests will include a coil-to-ground high voltage (Hi-pot) test, corona breakdown signatures, local conductor heating at nominal power and repetition rate, calorimeter measurements at nominal operation, constant voltage vs. current test to measure total head load, and sonic spectra measurements with attached accelerometer. The magnetic field measurement will be made using a ‘electrically isolated’ long longitudinal Bdot probes and compared against point measurements made with ad hoc broadband Hall probes manufactured by SENSIS GmbH. The short life tests will include operating the magnets at an accelerated pulse rate at nominal 1.95 GeV field parameters for ~1% of their 10 year lifetime or 10.8×10^4 shots.

3.5.5.11 Further critical studies to do:

As discussed in Table 3.5-6 the SR thin septum magnet is presently overdriven by 20%. Operation at 2.0 GeV will increase the overdrive condition to ~50%. The reasons for the overdrive condition are not understood at this time. A beam injection analysis could be performed to determine if the angle and position into the thick septum could be incorrect. As a result the thin septum is driven harder to correct for this condition. It has been noted that the booster to storage ring transfer line has never been surveyed.

3.5.5.12 Summary of study:

Our theoretical and empirical results indicate that the existing BR/SR thick and thin septa will have the desired field quality for operation at 2.0 GeV operation. Modification of the SR thick septum driver to a 'full ring' mode will bring the amplitude of the septum leakage field within acceptable limits. High μ laminated shielding will further improve the leakage fields. Estimates of possible failure modes caused by the increased operational stresses suggest that the probability of a magnet failure is relatively low. To mitigate the stresses we plan to add water or air-cooling of both magnets.

However we will have two 'ready spare' magnets which will be life tested and coupled with a well defined magnet swap-out plan that should cover the most likely failure contingencies. Further investigations of the thin septum overdrive need to be made.

3.5.6 Storage ring 'fast' bump magnets

Two microseconds before the beam is transferred from the booster to the storage ring a set of four 'fast' dipole magnets are energized to produce a four-turn local closed-orbit distortion in the stored beam. The location of the Bump Magnets in the storage ring is shown in Figure 3.5-2. (Storage Ring injection area) and are labeled as SR01S_BUMP1 to BUMP4. Each of the four bump magnets is identical and their design and construction very similar to the booster ring 'fast' kicker magnets. Larger than the kicker magnets they are single-turn ferrite loaded (MN8CX) window frame magnets designed to easily accept a sinusoidal current waveform of several kilo amperes peak and a half sine period of four microseconds.

3.5.6.1 Existing driver design:

Great care was taken to minimize any potential offset in the beam closed orbit during the injection cycle. Precise magnetic field correspondence between the two magnet groups was accomplished through the precise construction of each magnet and the series-parallel connection of the magnet to the discharge modules. In addition the 'downstream' set of magnet have an additional 5.3 ft of cable to make up for the electron 'time of flight' between the two magnet groups.

The sinusoidal current wave form is generated by the resonant discharge of a low inductance capacitor bank through an SCR switch array into the predominantly inductive four bump magnetic load. The bump magnets are connected by a very low inductance transmission network to four parallel bipolar SCR-capacitor discharge modules. The basic topology of a discharge

module is shown in Figure 3.5-24. Each module has sixteen high voltage SCRs (eight + and eight -) which are charged by opposite polarity high voltage (10 KV max) power supplies. There are four discharge modules which gives a total of sixty four SCRs in the pulse chassis. The series parallel lattice of SCR's is necessary to accommodate the high standoff voltages and provide the high di/dt capability required to survive a 7000 kA, 4 us pulse. The current system has been in operation since 1992.

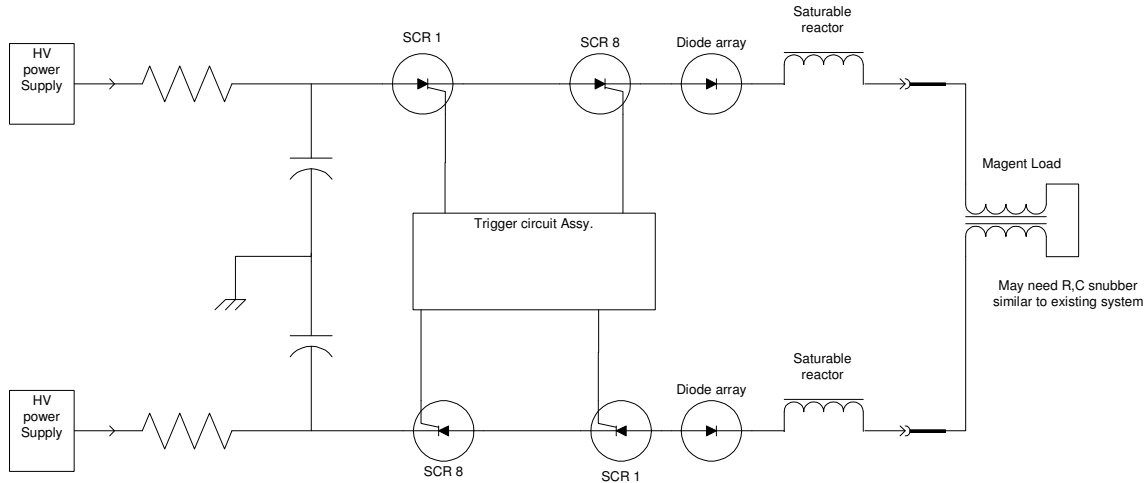


Figure 3.5-24: One of four bipolar switch modules

3.5.6.2

3.5.6.3 Topoff upgrade issues, experiments and results:

Mechanical offset of injection septa magnets:

Operational measurements have demonstrated that the bump driver system cannot quite reach the required orbit offset for optimal beam injection. Since the driver power supplies are at or near their voltage limits a simple solution has been the addition of slight (1 – 2 mm) orbit correction of the stored beam towards the injection septa during the normal injection process. During our Top-off investigations it was realized that the entire injection vacuum assembly could be moved laterally +/- 10mm. This capability has offered two advantages:

- 1) The injection orbit correction can be permanently removed.
- 2) Bump drivers and magnets do not have to be redesigned for 1.9 GeV injection.

Several machine experiments have successfully demonstrated both capabilities.

Vertical and horizontal kicks caused by the injection bumps:

Great care was taken to minimize any potential offsets in the beam closed-orbit but some observable problems still exist. Based on prior beam measurements the amount of stored beam distortion when the bump magnets are operating is presently acceptable for users. It does suggest further investigation for future Topoff beam stability improvements. These observed problems suggest some future experiments and system upgrades.

- 1) An observed >100um vertical kick during bump operation may be caused by systematic magnet misalignments.
 - a. This problem may be correctable by re-alignment of the bump magnets.
- 2) An observed horizontal kick of similar magnitude during bump operation may be due to inductive mismatch between the 'upstream' and 'downstream' magnet groups. This kick may be caused by the missing 'backend' compensation coil
 - a. The compensation coil should be reinstalled to confirm this theory
- 3) Both vertical and horizontal kicks could be greatly reduced by the construction of closely matched individual solid state drivers for each bump magnet.

Summary:

Successful experimental results have shown that storage ring driver and bump magnets do not need to be upgraded for 'top-off' operation. However there are transient orbit distortions caused by the SR bump system that may be correctable through magnet realignments or hardware modifications.

3.5.7 *Summary of pulse magnets study:*

Our measurement results have shown that for 2.0 GeV operation the booster ring bumps reach the nominal B fields with sufficient headroom. Higher field measurements indicate some nonlinear effects in the measurements but this is well above the nominal operating point. Conversion to water cooling is not necessary. We recommend that the capacitors in all the pulse drivers be replaced for the upgrade and if necessary the charging supplies be replaced with modern commercially available models.

Modeling and calculations have shown that the existing magnets in the Booster fast extraction kicker are adequate for 2.0 GeV. Additionally the kicker magnet drivers can be easily modified to operation with the higher voltage requirements as discussed in the booster fast extraction kicker summary.

Theoretical and empirical results indicate that the existing BR/SR thick and thin septa will have the desired field quality for operation at 2.0 GeV. Modification of the SR thick septum driver to a 'full ring' mode will bring the amplitude of the septum leakage field within acceptable limits. High μ laminated shielding will further improve the leakage fields. Estimates of possible failure modes caused by the increased operational stresses suggest that the probability of a magnet failure is relatively low. To mitigate the stresses we plan to add water or air-cooling both magnets.

However we will have two 'ready spare' magnets which will be life tested and coupled with a well defined magnet swap-out plan that should cover the most likely failure contingencies. Further investigations of the thin septum overdrive need to be made

Successful experimental results have shown that storage ring driver and bump magnets do not need to be upgraded for 'topoff' operation. However there are transient orbit distortions caused by the SR bump system that may be correctible through magnet realignments or hardware modifications.

3.6 DC and Slow Ramped Magnets

To accommodate the goal of increasing the Booster Ring energy to 1.95 GeV, the various Booster Ring DC and ramped magnets and power supplies must be incremented in current in approximate proportion to the energy increase, 1.95/1.5 or about 30%.

These increases naturally put additional stresses on the existing magnets, power supplies, DC wiring, and AC utilities. Fortunately, the magnets themselves were designed with 1.95 GeV operation in mind, so this section will address the power supply, and wiring issues.

It is desired to avoid the high costs of upgrading the AC utilities serving the Booster Bend and QD/QF power supplies. Toward that goal, the Booster cycle period will be extended from 1 second to 3 seconds. This will reduce the ramping rate requirements for these magnets, thus minimizing the increase of peak and average AC RMS currents over 1.5 GEV values. The ramp will be a near linear triangular envelope that will dwell at zero current for the last 20% of the period. The dwell at zero reduces RMS heating in the AC and DC side wiring so that existing cabling can continue to be used.

We are looking into the use of Switching Mode power supplies. Here, the potential exists for further lowering the AC demands by discharging the ramping magnets into a capacitor bank instead of pushing that energy back into the AC line. This technique will significantly reduce the RMS heating in the AC wiring and utility transformer as well as to soften the impact on the utilities of pulsing this megawatt load.

3.6.1 Power Supplies

Magnet System	Present	Required	Action	Est. Cost
B Bend 1 Hz 0.5 Hz 0.33 Hz	1175V @ 800 A	2065V @ 1050A 1422V @ 1050A 1208V @ 1050A	Must replace with more powerful unit.	450 k\$ 300 k\$
QD Quadrupoles 1 Hz	110V @ 265A Cont. 270V @ 460A Peak	234V @ 520A Pk	Must replace with more powerful unit.	100 k\$
QF Quadrupoles 1 Hz	110V @ 265A Cont. 270V @ 460A Peak	287V @ 520A Pk	Must replace with more powerful unit.	100 k\$
S Sextupoles (8)	Not in use	45 V @ 10 A	Must replace with more powerful unit.	5k\$/ea
BTS Bends (4)	33V @ 820 A	47V @ 900A	Must replace with more powerful unit.	50k\$/ea
BTS Quads (9)	40V @ 130 A	36.6V @ 110A	No action required	0

BTS Q2.2/Q3.1	15V @ 50 A	15V @ 50A	No action re- quired	0
BTS HCM (9)	30V @ 8 A	30V @ 8 A	No action re- quired	0
BTS VCM (9)	30V @ 8 A	30V @ 8 A	No action re- quired	0

Table 3.6-1: List of all mayor dc and ramped power supplies in the booster and BTS including upgrade requirements.

List of some of the main features of the power supplies:

- New power supplies will be switchmode systems with;
- Increased efficiency over SCR systems.
- Ethernet control.
- 14 bit resolution (16 bit for BTS PS's).
- Arbitrary waveform generator (for ramping supplies).
- 0.05% repeatability (for ramping supplies).
- 300 ppm stability (for continuous supplies).
- Capacitor bank for energy recovery (dipole).
- Reduced I²R heating of 12 KV transformer & AC wiring.
- Reduced 12 KV transformer mechanical stress.
- Reduces peak AC current demand.

3.6.2 DC Cabling

Magnet System	Present Capacity	Required (20% zero dwell)	Action	Est. Cost
B Bend	585 A RMS	542 A RMS	No action re- quired	0
QD Quadrupoles	285 A RMS	268 A RMS	No action re- quired	0
QF Quadrupoles	285 A RMS	268 A RMS	No action re- quired	0
S Sextupoles	Not in use	-----	No action re- quired	0
BTS Bends (4)	1000 A RMS	900 A RMS	No action re- quired	0
BTS Quads (9)	150 A RMS	110 A RMS	No action re- quired	0
BTS Q2.2/Q3.1	75 A RMS	50 A RMS	No action re- quired	0
BTS HCM (11)	20 A RMS	8 A RMS	No action re- quired	0
BTS VCM (11)	20 A RMS	8 A RMS	No action re- quired	0

Table 3.6-2: List of capability of DC cables for all mayor booster and BTS power supplies.

3.6.3 AC Power

Magnet System	Present Capacity	Required (40% Duty Cycle) 1 Hz, 85% Eff.	Action	Est. Cost
B Bend	800 A RMS	772 A RMS (0.5 Hz)	No action required	0
QD Quadrupoles	125 A RMS	109 A RMS	No action required	0
QF Quadrupoles	125 A RMS	89 A RMS	No action required	0
S Sextupoles	10 A RMS	5 A RMS	No action required	0
BTS Bends (4)	125 A RMS	60 A RMS	No action required	0
BTS Quads (9)	20 A RMS	14 A RMS	No action required	0
BTS Q2.2/Q3.1	20 A RMS	7 A RMS	No action required	0
BTS HCM (11)	10 A RMS	5 A RMS	No action required	0
BTS VCM (11)	10 A RMS	5 A RMS	No action required	0

3.7 Timing System

3.7.1 *Injector Timing*

The ALS Timing System was designed to operate the Booster Ring at 1, 2, 5, and 10 PPS. The existing Rep-Rate module cannot be modified for the anticipated rep-rates of 0.33, 0.5, and 1 PPS so a new module must be designed and fabricated.

In current operation, the Booster Bend Magnets are allowed to ramp up at their L/R time constant, the Timing System controls the duration of the ramp by means of the Gauss Clock. Proposed operation will replace this with a programmed ramp applied to the magnet power supply, however, the Timing System will still be responsible for triggered the start of the Bend, QD, and QF ramps. A new Magnet Control module must be designed and fabricated to support this new mode of operation.

Various minor changes and adjustments to other Timing System modules may be required to accommodate the increased periods and higher magnetic field strength measurements.

3.7.2 *User Gating System*

A new system is required to give Users advanced notice of an Injection Cycle so that they can gate their data collection if necessary. Notification would consist of:

- a). A coarsely timed pulse significantly advanced from the injection event.
- b.) A more precisely timed pulse immediately prior to the event.
- c.) A precisely timed gate that fully encloses the perturbed time space with minimal overlap.

The system would be designed with a central chassis located at the Timing System racks and satellite chassis located convenient to the users. Signal distribution will be identical to the pre-existing User Timing System with fiber optic trunk lines from the central chassis to distribution chassis's as required. Each distribution chassis handles wired distribution to the individual satellite chassis.

3.8.1.1 Beam Loading Effect in the 50MeV ALS LINAC Structure

In ALS Top-Off operation mode, to insure more uniform storage ring beam fill pattern, the injector might deliver up to 10 bunches in each injection cycle. What impact will this have on the LINAC output beam energy spread?

The ALS LINAC has uniform parameters along its length (constant impedance structure). The fill time for a constant impedance structure is given by:

$$T_f = \frac{L}{v_g} = \tau \cdot \left(\frac{2 \cdot Q}{\omega} \right) = 393\text{ns} \quad (3.8-1)$$

where:

- L - length of single linac section (2m)
- v_g - energy group flow velocity
- τ - attenuation parameter (0.285 per 2m section)
- Q - linac structure quality factor (Q=13000)
- ω - angular operational frequency ($\omega=2*\pi*2.998\text{GHz}$)

Since the filling time of the linac accelerating structure is much longer than the bunch spacing (393ns \gg 8ns), the beam can be represented as a DC pulse with its width equal to the length of the pulse train when determining the beam-cavity interaction. The formula for the beam-induced voltage in a traveling wave LINAC structure as developed by P.B. Wilson [28] is:

$$V_b(x) = I_0 \cdot r_{sh} \cdot L \left[\left(1 - \frac{1}{\tau} \right) \cdot (1 - e^{-\tau \cdot x}) + x \cdot e^{-\tau \cdot x} \right] \quad (3.8-2)$$

where:

- x - bunch length parameter: $x=t/T_f$ (t- length of the bunch train)
- $V_b(x)$ - beam induced voltage
- I_0 - linac beam current
- r_{sh} - linac shunt impedance (53M Ω /m)
- L - length of single LINAC section (2m)

The beam-induced voltages were calculated for the two cases listed below:

1. Current multibunch operation mode: 3 bunches; total charge per injection cycle $Q_{tot}=1e^{-9}[C]$; $I_0=62.5[mA]$; $t=16[ns]$; $x=0.041$; $\tau*x=0.0117$
2. Proposed multibunch mode for top-off operation: ten bunches total charge per injection cycle- $Q_{tot}=1e^{-9}[C]$; $I_0=13.9[mA]$; $t=72[ns]$; $x=0.183$; $\tau*x=0.0522$

The results are as follows (for entire LINAC -2 sections):

Case #1,	$V_b=150\text{kV}$	energy spread: $\sigma E/E= 0.3\%$
Case #2	$V_b=136\text{kV}$	energy spread: $\sigma E/E= 0.27\%$

The conclusion reached is that the beam loading effect in ALS LINAC injector is not a significant problem for the proposed top-off mode of operation. No compensation is required for the proposed ALS main ring injection rate. The energy spread for 10-bunch LINAC operation is 10% lower than for 3-bunch operation, for the same total beam charge.

3.8.1.2 Beam Loading Effect in the Booster Ring.

Beam loading effect during beam injection from ALS LINAC into the Booster can cause a fast (at the rate of the cavity's time constant) cavity voltage amplitude and phase change and as an effect, this can lead to significant beam losses.

Beam loading effect in the booster ring could be corrected by:

- initial detuning of the RF cavity prior to the beam injection moment
- increasing the power source-to-RF cavity coupling coefficient (more power from RF source required)
- increasing the RF cavity voltage during beam injection (results in larger synchrotron tune changes that may lead to a synchrotron resonance problem).

3.8.1.3 Synchrotron Oscillations in ALS Booster Ring.

Coupling between transverse and longitudinal oscillations gives rise to excitation of resonances for tunes, which satisfy the following equation:

$$k \cdot Q_x + l \cdot Q_y + m \cdot Q_s = n \quad (3.8-3)$$

where Q_x , Q_y and Q_s are horizontal, vertical and synchrotron tune values and k , l , m and n are integers.

For the given lattice parameters horizontal and vertical tunes are constant (for ALS booster ring $Q_x=5.82$ and $Q_y=2.72$). From a logical point of view, the simplest way to avoid the synchrotron resonances problem is to choose the optimum Booster Ring operation conditions, which includes maintaining the synchrotron tune value constant over entire Booster energy ramp. This can be done by maintaining a constant ratio of beam energy to cavity voltage.

3.8.2 Booster RF Power Requirements for Top-Off Mode of Operation

In Top-Off mode of operation, the Booster RF system has to accelerate the electron beam up to the full ALS Storage Ring energy (1.9GeV). The dominant mechanism, which dictates the minimum required RF bucket height is the quantum emission of energetic photons by the electron beam (quantum lifetime). The quantum lifetime τ_q is a steep function of the electron beam energy and according to Sands [29] and [30] is given by:

$$\tau_q = \frac{\tau_e}{\eta_\sigma^2} \exp\left(\frac{\eta_\sigma^2}{2}\right) \quad [3.8-4]$$

where:

τ_q -quantum lifetime
 τ_e -longitudinal damping time

$$\eta_\sigma = \frac{\text{relative} \cdot \text{bucket} \cdot (\text{half}) \cdot \text{height}}{\text{relative} \cdot \text{energy} \cdot \text{spread}} \quad [3.8-5]$$

Table 3.8-1 shows the quantum lifetime, synchrotron tune, cavity cell power and effective ALS Booster cavity voltage (for cavity shunt impedance $R_{sh}=5M\Omega$) as a function of η_σ parameter for 1.9GeV electron beam energy.

η_σ	Quantum Lifetime	Synchrotron Tune	Cavity Cell Power	Cavity Voltage
-	[s]	-	[kW]	[kV]
3	0.017	0.0120	19.0	436
3.5	0.065	0.0129	22.8	477
4	0.319	0.0137	27.3	522
4.5	2.14	0.0146	32.8	573
5	18.8	0.0155	39.3	627
5.5	216.2	0.0164	47.0	686
6	3203	0.0172	56.0	748
6.5	61373	0.0181	66.5	815
7	1600000	0.019	78.9	888

Table 3.8-1: ALS Booster RF parameters as a function of η_σ parameter.

Booster RF parameters for proposed ramp (constant synchrotron tune value) are presented in Table 3.8-2. Calculations were done for 4mA (1nC total beam charge) booster current, cavity-to-power source coupling factor $\beta_c=2$ (cavity tune into the resonance prior to beam injection moment).

Beam Energy	Synchr. Tune	RF Cell Power	Cavity Voltage	Stationary Bucket Half Height	Dynamic Bucket Half Height	Cavity Detuning (by beam)	Cavity Voltage (detuned by beam)	Synchrotron Radiation losses
MeV	-	kW	kV	keV	keV	deg	keV	keV
50	0.0181	0.054	23.2	382	340	-29.8	20.2	0.000133
100	0.0181	0.175	41.8	723	689	-17.7	39.9	0.0021
200	0.0181	0.67	81.9	1430	1403	-9.3	80.8	0.034
300	0.0181	1.5	122.5	2142	2116	-6.2	121.8	0.172
400	0.0181	2.6	161.2	2838	2808	-4.7	160.7	0.544
500	0.0181	4.1	202.5	3556	3516	-3.8	202.1	1.33
600	0.0181	5.9	242.9	4266	4208	-3.1	242.5	2.76
700	0.0181	8.0	282.8	4792	4882	-2.7	282.5	5.1
800	0.0181	10.5	324.0	5690	5550	-2.3	323.8	8.7
900	0.0181	13.3	364.7	6402	6190	-2.1	364.5	14.0
1000	0.0181	16.2	402.5	7090	6775	-1.9	402.3	21.3
1100	0.0181	19.7	443.9	7808	7356	-1.7	443.7	31.2
1200	0.0181	23.8	487.9	8550	7919	-1.6	487.7	44.1
1300	0.0181	27.7	526.3	9243	8378	-1.4	526.1	60.8
1400	0.0181	32.4	569.2	9976	8818	-1.3	569.1	81.7
1500	0.0181	37.5	612.4	10710	9189	-1.2	612.2	107.7
1600	0.0181	44.0	663.3	11512	9558	-1.1	663.2	139.5
1700	0.0181	50.0	707.1	12252	9759	-1.0	707.0	177.7
1800	0.0181	58.0	761.6	13084	9968	-1.0	761.5	233.4
1900	0.0181	66.0	812.4	13884	10018	-0.9	812.3	277.3

Table 3.8-2: Booster RF parameters for proposed energy ramp for ALS Top-Off mode of operation.

The stationary and dynamic 1.9 GeV ALS Booster RF buckets for 66 kW cavity cell power and the single bunch with the population of 1000 electrons and the normal energy distribution are shown in Figure 3.8-2. Figure 3.8-3 shows 10 LINAC bunches with the total energy spread of 136keV captured by 54W Booster RF bucket at injection (the energy spread inside each LINAC microbunch is neglected). The difference between the static and dynamic buckets in this case is the result of the cavity detuning due to the beam loading effect.

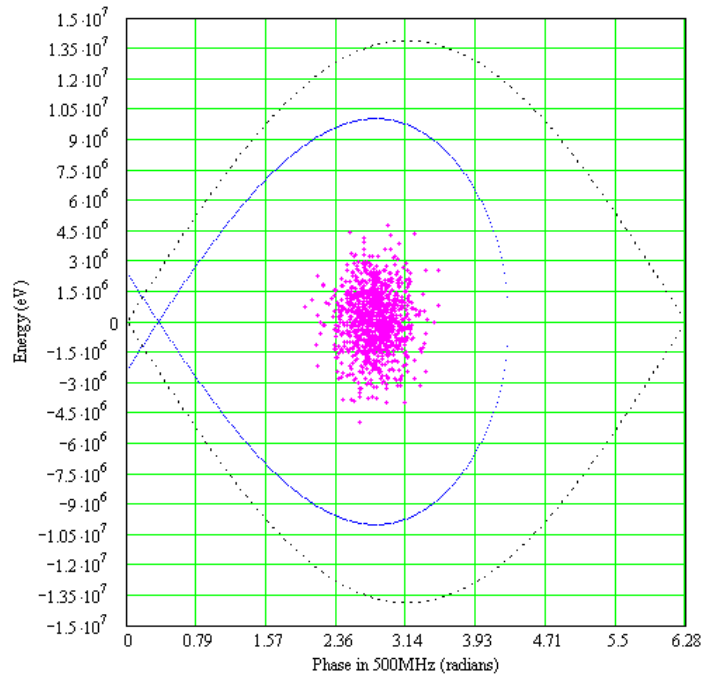


Figure 3.8-2: RF buckets and particle distribution in ALS Booster at 1.9 GeV.

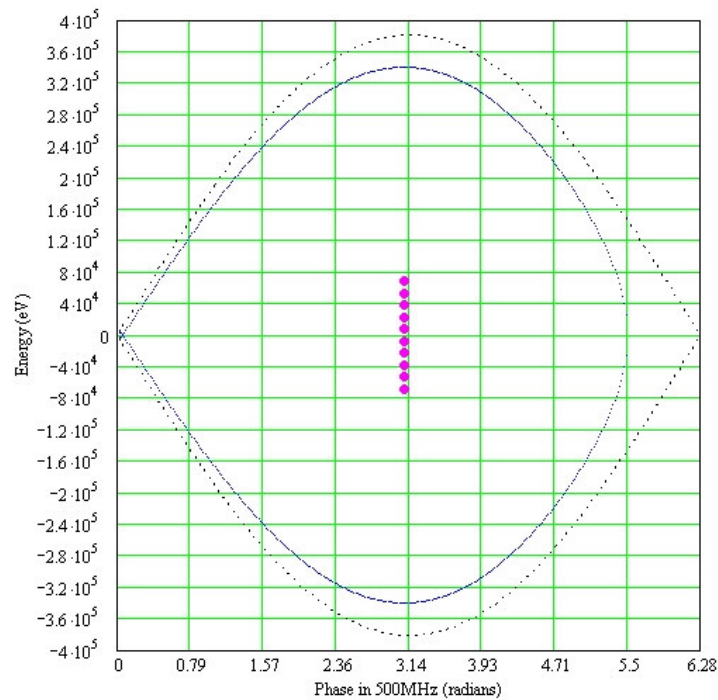


Figure 3.8-3: RF buckets and 10 injected linac bunches into ALS Booster at 50 MeV.

Table 3.8-3 shows the current and proposed Booster Ring RF Parameters.

Parameter	Current	Proposed
Frequency (MHz)	499.64	499.64
Harmonic number	125	125
Peak effective voltage (kV)	300	813
Beam current, multibunch mode (mA)	4	4
Synchrotron radiation loss, dipoles (kW)	2	5
Total effective shunt impedance, ZT^2 (M Ω)	5	5
Fundamental-mode cavity dissipation (kW)	7.8	66
Waveguide and other losses (kW)	1	11
Total RF power required (kW)	8.8	77
Total RF power installed (kW)	22	80

Table 3.8-3: RF parameters for current and Top-Off mode.

3.8.3 Final Amplifier/Transmitter with Controller

It has been determined, as noted above, that the existing final amplifier –transmitter can not produce the output power needed, so we plan to replace it with a higher output power final amplifier-transmitter based on an inductive output tube (IOT). We came to this conclusion after first exploring two possible upgrade paths for the existing transmitter. First we looked at replacing the existing klystron with a higher power klystron. However the poor efficiency of the larger klystron and the maintenance of an aging electro-mechanical transmitter system dissuaded us from this option. Second we looked at replacing the klystron with a higher power IOT. However, with this option we were faced with installing a crowbar system and with considerable rework of the existing transmitter’s power supplies, relay controls and interlocks during an ambitious installation shutdown period. Additionally the maintenance of an aging electro-mechanical transmitter system dissuaded us from this option.

In the end we opted to replace the final amplifier-transmitter, which will be IOT based and have an integrated class A solid state drive amplifier, integrated thyatron crowbar system, fiber optic isolated metering, and an integrated microprocessor based control system. The maximum output power is 80 kW CW. This higher output gives us sufficient operating headroom above the required power level to ensure reliable operation for all three modes (50 MeV to 1.5 GeV @ 1 Hz, 50 MeV to 1.9 GeV @ 0.5 Hz, and 77 kW CW). The higher operating efficiency (>70% expected) will pay back the initial capital cost difference, as compared to a klystron upgrade, in a 3-4 year time frame.

3.8.4 High Voltage Power Supply

The current high voltage power supply (HVPS) is rated at 22 kV @ 2.4 A DC. It is a dry type, (no oil) air-cooled unit located inside of Bldg. 6 under the old dome section. We looked at three HVPS types as possible replacement candidates; a Pulse Step Modulator (PSM), a SCR input controlled 6-pulse rectifier power supply cooled by oil, or a SCR input controlled 6-pulse recti-

fier power supply cooled by air. We felt the PSM design though capable added a considerable amount of complexity to the overall transmitter system, an amount of uncertainty with regard to audio band noise injection and it put pressure on our budget due to its higher cost. The oil cooled power supply would have been our next choice because of its compactness but we are unable to introduce a significant flammable source without greatly increased installation costs. Locating an oil-filled power supply outside of Bldg. 6 was also looked at, but without a dedicated wire-way we would have incurred considerable installation costs and possible disruption of beamline operation in the area during installation. Ultimately we chose the SCR input controlled 6-pulse rectifier power supply air-cooled version, which minimized the fire hazard and installation costs.

The HVPS's maximum output will be 37 kV @ 4.0 A DC with a typical output of 36 kV @ 3.3 A DC for all modes of operation of the Booster RF System. The HVPS will be fabricated in an all-metal enclosure with a step-start contactor and a complete self-protecting interlock system. The HVPS will have a Star Point SCR controller on its input and a capacitor tuned specifically for the typical output load noted above, which will set the power factor to ≥ 0.92 .

3.8.5 RF Cavity Window

The RF power delivered is to the cavity via an aperture-coupling cylindrical window made of aluminum-oxide. This window must reliably deliver the expected 60 kW of power needed by the cavity to satisfy the quantum lifetime requirements without multipactor, arcing, or overheating. LBNL has designed, fabricated, anti-multipactor coated with titanium-nitride in-house, and power tested to 66kW (the maximum of our RF teststand) several windows that operate in the storage ring at power levels approaching 50 kW without beam. We plan to reuse this proven design and build 2 new windows (one spare) for this upgrade project.

3.8.6 RF Transmission Line

The existing transmission line is primarily 3 1/8" coaxial line consisting of a mixture of types as rigid, clamp line, 3" air dielectric Heliac, 3 1/8" to 6 1/8" adapters (for the existing 75 kW circulator), and WR1800 (for interfacing to the cavity). The current transmission line is rated for 16.8 kW average, however since the upgraded system is required to deliver a ramped power profile from < 1kW up to 77 kW over a 1/2 second ramp the average power (19.3 kW) will exceed the reliable operating range for this 3 1/8" line therefore it needs to be replaced. Additionally, the existing line will not support the 70kW CW test/maintenance mode.

The new transmission line will be primarily 6 1/8" rigid coax but it will contain 2 short sections of 4 1/16" rigid and clamp line coax. The output of the IOT is 4 1/16" EIA transmission line with forward and reverse power couplers. Upon exiting the transmitter cabinet the line will transition to 6 1/8" line to a SPDT 6 1/8" coaxial switch. The switch selects between an 80 kW CW 6 1/8" load or the Booster cavity. Following the switch is a length of 6 1/8" line, which connects to the existing 75 kW circulator. The circulator has an 80 kW CW 6 1/8" load on one port with the cav-

ity connected on the other port via 6 1/8” line and adapter to WR1800. There is an existing bi-directional WR1800 coupler located at the cavity to measure cavity forward and reverse power.

3.8.7 Controls & Interlocks

The existing Control and Interlock chassis are typical single purpose custom relay chassis that are expensive to modify and difficult to work on. We will likely replace these chassis with an Ethernet capable Programmable Logic Controller (PLC) rated Safety Integrity Level 3 (SIL3) with a local pc and monitor providing a local control station at the equipment. The SIL3 rating is necessary for inclusion in the Booster Ring Personnel Safety System. By installing this PLC system in addition to the embedded microprocessor based system supplied with the transmitter, we will be able to replace all but two Intelligent Local Controllers (ILC), the now obsolete workhorse of the ALS Control System. There are sufficient expansion capabilities to accommodate the channels on the remaining two ILC’s. The new PLC systems will interface to the existing EPICS based control system via MODBUS over Ethernet. This will allow us to leverage existing MODBUS code already in use at the ALS.

3.8.8 Utilities

The replacement of the transmitter and HVPS sub-systems impacts the 480/120 VAC and LCW plants. There is sufficient installed capacity to accommodate the upgrade. See Table 3.8-4 below for current and projected capacities.

System	Current Installation			Proposed Installation		
	120/208 VAC	480 VAC	LCW (gpm)	120/208 VAC	480 VAC	LCW (gpm)
Transmitter	30A	-	32	-	225	25
HVPS	-	80	-	-		-
Xmtr Test Load	-	-	5	-	-	12
Circulator	-	-	5	-	-	4
Circulator Load	-	-	5	-	-	12
Cavity	-	-	5	-	-	30
Cavity Window	-	-	1.4	-	-	2.5
Cavity Tuner	-	-	0.8	-	-	1.5

Table 3.8-4: Electrical power and LCW requirements for current installation and upgrade condition.

Transmitter LCW Circuit



Cavity LCW Circuit



The current transmitter LCW requirement is 37 gpm and the new requirement is also 37 gpm. The current cavity LCW requirement is 7.2 gpm (the circulator, circulator load and cavity are in series) and the new requirement is 50 gpm.

3.8.9 Structure Core Drilling

The existing Booster Ring roof penetration accommodates the 3 1/8" coax transmission line and two – 1" hoses for cooling the circulator and its load. The requirement for higher average power transmitted to the cavity translates into a larger coax line as mentioned above. We will need to re-drill the roof penetration to ~ 8" and we will also need to drill at least one more new hole to fit the hoses supplying LCW to the circulator and its load. The existing and any new holes will not be centered over the beam axis therefore satisfying the radiation safety engineer. Additionally, an existing unused roof block hole directly centered over the cavity will be filled with concrete to remove the direct line of sight to the cavity.

3.8.10 Spares

The components that can cause a significant down time if they fail are the IOT, solid-state drive amplifier, RF cavity-coupling window, and various PLC components. We will need to have these items in hand at the beginning of our commissioning.

3.9 Diagnostics

3.9.1 *Booster Diagnostics*

The diagnostics in the Booster will play a major role during the commissioning and operation of the Booster in the top-off mode. Injection efficiency together with short and long term stability of the booster operation conditions are fundamental requirements for the proper operation in this new mode.

At the present time, the booster is operated with sextupoles off and without any orbit control. Long-term drifts are compensated by readjustments by the operators. In top-off operation, tolerances for the injection parameter fluctuations are much tighter requiring more efficient diagnostics systems. Some examples, synchro-betatron resonance control is required during the energy ramping, closed orbit and current monitoring are necessary for preserving the injection efficiency, bunch cleaning requires accurate control of tunes, chromaticities and orbit.

In the next paragraphs, a description of the proposed new tune measurement system and of the refurbishing and/or upgrade for the orbit system is presented as well as the description of the proposed bunch cleaning system.

3.9.1.1 Orbit Monitoring System.

The Booster ring has 32 beam position monitors distributed along the circumference. They are equipped with the original ALS electronics that allows for both single and multi turn measurements. The all orbit system has been rarely used for several years and requires significant refurbishing.

The requirements for this system during the topoff operation can be distinguished in two main phases. During the commissioning, single turn or few turns measurements will be required. Being the larger of the betatron tunes greater than 6, about 13-14 BPMs should be equipped with single turn electronics. During topoff operation, in order to maintain an efficient injection and bunch cleaning, a regular monitoring of the orbit is also required. Again, about 13-14 BPMs equipped now with multi turn electronics will be sufficient for the task.

For this topoff upgrade, we are proposing to refurbish the existing electronics for the single turn measurement and to buy the electronics for a reliable orbit monitoring during operation.

A high level application, similar to the one existing for the ALS storage ring, should be developed for allowing an easy monitoring of the orbit in the booster.

3.9.1.2 Bunch Cleaning System

Introduction and system description.

In the present operation of the ALS, about 4 weeks per year are dedicated to the so-called “two-bunches mode of operation”. In such a special mode, only two diametrically opposite buckets, over the 328 available, are filled with relatively high current (~ 30 mA/bunch). The distance in time between these buckets (~ 330 ns) is large enough to allow for experiments with long relaxation time. The “two-bunches” users’ community is continuously growing and the sci-

entific quality of their work is of very high level, making a top priority maintaining the quality of these runs even with the top-off operation.

In order to avoid contamination of the experimental data, it is fundamental to have high levels of “bunch purity”. In other words, it is extremely important that undesired particles in the nominally empty buckets are kept down to a level lower than $\sim 0.01\%$ relatively to the particle number in the main two bunches. Several mechanisms, during the injection process, can contribute in contaminating the filling pattern in the storage ring and even when injection is tuned at its best, a contamination level of the order of 0.1% can still happen. For this reason, a bunch cleaning procedure is always required.

At the present time, the cleaning is performed in the storage ring after every injection and energy ramping to 1.9 GeV. The beam impedance of the ALS vacuum chamber induces betatron tune shift on current, so that the small current parasitic bunches have a tune significantly different from the one of the two high current main bunches. By exciting the beam at the betatron frequency of the parasitic bunches, one can generate large transverse oscillations of the undesired bunches with minor effects on the main ones. The insertion of a scraper kills the oscillating particles allowing for the cleaning. Unfortunately, the whole procedure requires about 4 minutes and perturbs the main buckets making it incompatible with top-off operation.

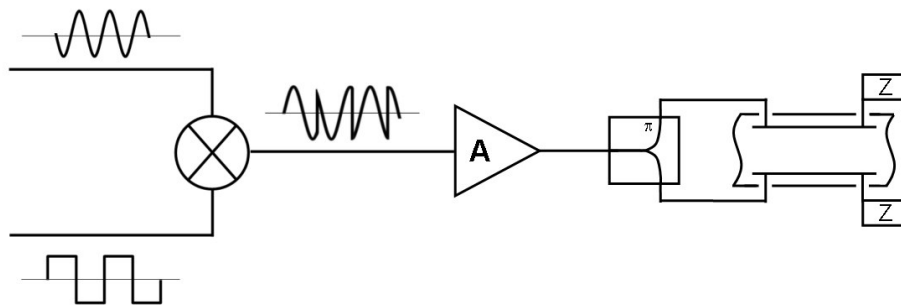


Figure 3.9-1: Bunch cleaning system schematics

A convenient solution consists in performing the cleaning in the booster before injecting in the storage ring. A possible scheme [31] [32] is based on the idea of resonantly exciting large transverse oscillations in all the bunches except the ones you want to save. With reference to Figure 3.9-1, two signals, a sinusoidal wave at the frequency of one of the betatron sidebands and a square-like wave that switches polarity synchronously with the transit of the bunches to be saved, are mixed together. The resulting signal is still an excitation at the betatron tune but with always zero amplitude at the passage of the “good” bunches. The signal is then amplified and sent to a transverse kick for the beam excitation. A scraper in the plane of the excitation will increase the efficiency of the cleaning and reduce the power requirement for the amplifier.

Cleaning in the Booster requires that no contamination happens when injecting from the booster to the storage ring. The technique described above is already in routine operation at Spring 8 [33] in Japan and under final test at the ESRF [34] in France. Here at the ALS, we have tested in the storage ring the complete cleaning procedure with successful results.

Table 3.9-1 shows the system parameters for the ALS Booster. The cleaning is tuned for the maximum efficiency at the beam energy of 300 MeV. The excitation in the vertical plane will be applied for few tens of ms during the energy ramp around the energy of 300 MeV. Ideally, chromaticity should be corrected to zero in order to avoid spread of tunes with energy. A non-

properly corrected chromaticity will require more excitation power for maintaining the required oscillation amplitude within the beam energy spread range.

Table 3.9-1: Cleaning system parameters for the ALS Booster.

Beam energy at cleaning	300 MeV	Natural vertical chromaticity	- 4.61
Booster revolution period (T_0)	250.2 ns	Operation vertical chromaticity	0.0 ± 0.1
RF frequency	500 MHz	Vertical Tune	2.72
Harmonic number	125	Vert. excitation frequency	~ 1.12 MHz
Long. Damp. time @ 300 MeV	~ 400 ms	Max tune variation at $\Delta E/E = 0.5\%$ ($\Delta \nu_y$)	$\sim 5 \times 10^{-4}$
Transv. damp. time @ 300 MeV (τ_d)	~ 800 ms	Vertical kick angle ($\Delta\theta$)	~ 6.3 μ rad
Vertical beta function at scraper position (β_{Sc})	~ 10 m	Kicker type	stripline
Vertical beta function at the kicker position (β_K)	~ 10 m	Kicker transverse shunt impedance	~ 9000 Ω
Distance vertical scraper-reference orbit (Δy)	10 mm	Amplifier power (P)	~ 200 W
Energy spread at 300 MeV (rms) (assuming 1% rms linac energy spread @ 50 MeV)	$\sim 1.7 \times 10^{-3}$	Amplifier bandwidth	> 200 MHz

The parameters in the table have been evaluated according to the criteria presented in reference [32]. In particular, the following expressions have been used (the symbols in the following equations are defined in Table 3.9-1):

$$\Delta y \cong \frac{1}{2} \frac{\Delta\theta \frac{\tau_d}{T_0} (\beta_K \beta_{Sc})^{1/2}}{\left[1 + \left(2\pi \frac{\tau_d}{T_0} \Delta \nu_y \right)^2 \right]^{1/2}} \quad (3.9-1)$$

or, as in our case, where $\tau_d/T_0 \gg 1/(2\pi\Delta\nu_y)$:

$$\Delta y \cong \frac{\Delta\theta (\beta_K \beta_{Sc})^{1/2}}{4\pi \Delta \nu_y} \quad (3.9-2)$$

where $\Delta\theta = eV_k/E$, with e and E the electron charge and energy respectively and V_k is transverse kick voltage given by:

$$V_k = \sqrt{2PR_{\perp}} \quad (3.9-3)$$

Here P is the power applied to the kicker and R_{\perp} is its transverse shunt impedance. The amplifier bandwidth has been chosen in order to clean out parasites contiguous to the main buckets (2 ns distance).

Equations (3.9-1) and (3.9-2) do not include the tune shift on amplitude that the particles will experience for large oscillations. The resulting additional tune spread would require extra excitation power for maintaining the amplitude of the oscillation at the same level. In our proposed scheme, the inclusion of a vertical scraper in the booster allows, by setting properly Δy , to control such effects without dramatically increase the power requirements for the amplifier. It is worth reminding that the scraper position must trade between an efficient cleaning and an efficient injection in the booster.

In the next paragraphs, the new systems required for the cleaning implementation are described.

3.9.1.3 Kicker system

The kicker for booster bunch cleaning will be a copy of the storage ring vertical transverse feedback system kicker. The kicker is a vertical stripline pair with 30 cm long electrodes each subtending 120 deg of the beam. Driven differentially, the transverse shunt impedance of the kicker is given by:

$$R_{\perp} = 2Z_L \left(\frac{2g_{\perp} \sin(kl)}{kd} \right)^2 \quad (3.9-4)$$

where Z_L is the stripline characteristic impedance, $k = \omega/c$, l is the electrode length, d is the electrode diameter and $g_{\perp} = (4/\pi)\sin(\Delta\Phi/2)$ with $\Delta\Phi$ the electrode subtend angle. The values for these quantities for the ALS kicker are shown in Table 3.9-2. Using such values, the calculated shunt impedance at low frequencies for the ALS kicker is $R_{\perp} = 8938$ ohms which compares favorably to bench measurements of about 10 k Ω .

Table 3.9-2: ALS-like stripline kicker characteristics.

Electrode length (l)	30 [cm]	Electrode diameter (d)	70 [mm]
Electrode subtend angle ($\Delta\Phi$)	120 [deg]	Characteristic impedance (Z_L)	50 [Ω]

The azimuthal position of the vertical kicker in the ring must be as close as possible to the central defocusing quadrupole of the cell (cell symmetry point) where the vertical beta function has a local maximum.

The power amplifiers for driving the kicker will be identical to the storage ring transverse feedback system amplifiers. They are 250 watt, 250 MHz instantaneous bandwidth RF power amplifiers.

Nominally, one would use two amplifiers to drive the electrodes separately at opposite phases with a total available power of 500 watts. Recently, a bunch cleaning experiment was performed in the ALS storage ring at 1.9 GeV using the transverse feedback system amplifiers and kickers. In this case, only one electrode was driven with one amplifier. In such configuration the effective shunt impedance is about half that given by Eq. (3.9-4) resulting in a $\sqrt{2}$ reduction in kick. In this experiment, a 125 MHz sine wave modulated by a vertical betatron tune line was used to clean every other bunch in the ring. For 100 watts of drive power and nominal scraper depths, perfect bunch cleaning within the approximate 1% resolution of our instrumentation was obtained. In addition, the cleaning process was essentially instantaneous as opposed to the present technique that takes several minutes.

Depending on the final position that the scraper in the Booster will have during the top-off operation, it could be that the more economical single electrode drive scheme will be adequate for cleaning in the booster. The current plan is to buy and install two amplifiers for the booster kicker but possibly operate only one of them reserving the other as an online spare. A commercial arbitrary function generator for general bunch cleaning will replace the 125 MHz sine wave used in the experiment.

3.9.1.4 Vertical Scraper

A single blade vertical scraper, as the one presently installed in the ALS storage ring, will be installed in the Booster as well. The azimuthal position of the scraper in the ring must be as close as possible to the central defocusing quadrupole of the cell (cell symmetry point) where the vertical beta function has a local maximum.

3.9.1.5 Storage Ring Cleaning System Upgrade

In some particular conditions, a high purity injection alone could not be sufficient. In fact, specifically if the dynamic aperture of the storage ring is larger than the RF bucket size, diffusion of particles from the main bunches to the near buckets could happen. In that case, a periodic cleaning in the storage ring will be required as well. We propose to include in the storage ring a cleaning system similar to the one in the Booster, specially taking into account that most of the more expensive system components are already present in existing subsystems in the ring.

The system will be identical to the one in the Booster but using the existing transverse feedback system amplifiers and kickers jointly with the existing vertical scraper. An additional arbitrary function generator is required.

3.9.1.6 Transverse Tune Measurement System.

The Booster tune measurement system will utilize the bunch-cleaning kicker and power amplifiers for exciting the beam at chosen vertical betatron tune frequencies. For horizontal coverage an additional horizontal kicker will need to be fabricated and installed and an additional

power amplifier will need to be purchased. The measurement itself will be performed with a fast broadband oscilloscope utilizing FFT to obtain frequency spectrums.

The azimuthal position of the horizontal kicker in the ring must be as close as possible to the last focusing quadrupole before the cell symmetry point, where the horizontal beta function assumes a local maximum.

3.9.2 *BTS Diagnostics*

3.9.2.1 Injection chain beam transmission monitor.

In the existing configuration the ALS complex has several beam charge monitors: the linac and the LTB transferline are equipped with three, the Booster has two monitors, the BTS three and the Storage Ring has one. Table 3.9-3 summarizes the situation.

We are proposing the development of a high level application that collects all the charge information and presents them in a single window for an easy at a glance control of the transmission efficiency along the injection chain.

Table 3.9-3: Beam charge monitors in the ALS complex.

Name	Type	Location	Present control status
BIM1	Resistive wall current monitor	Linac: downstream electron gun	Multiplexed to a scope
ICT1	Integrating current transformer	LTB: Linac end	Not connected
ICT2	Integrating current transformer	LTB: before booster injection septa	Controlled
FCT1	Fast current transformer	Booster ring	Multiplexed to a scope
DCCT1	DCCT	Booster ring	Controlled
ICT3	Integrating current transformer	BTS: downstream Booster extraction septa	Controlled
BIM2	Resistive wall current monitor	BTS central part	Multiplexed to a scope
ICT4	Integrating current transformer	BTS: before storage ring injection septa	Controlled
DCCT2	DCCT	Storage ring	Controlled

From the last column of Table 3.9-3, one can see that 5 of the 9 monitors are already controlled and the FCT in the Booster is a fast monitor for special measurements and does not need to be included in our proposed application. So only 3 monitors (BIM1, ICT1 and BIM2) need upgraded electronics allowing for their integration in the control system.

3.9.2.2 Synchrotron Radiation Monitors

The two synchrotron radiation monitors in the BTS will allow for the non-destructive and continuous monitoring of the beam in the final part of the injection chain. The monitors will ex-

exploit the visible and part of the infrared portions of the synchrotron radiation emitted in two bending magnets among the four identical 20 deg dipoles present at the BTS. The higher dispersion in the first point source, will allow for the control of the energy variations in the beam extracted from the booster, while the second point, in a lower dispersion region, will be more suitable for beam emittance measurements. But the fundamental idea is that a quick glance at the two monitors will give the complete information about the status of the injector chain. A similar scheme is already in operation at ESRF in Grenoble with quite satisfactory results [35].

Figure 3.9-2 shows the optical functions and the beam sizes along the BTS with the position of the two source points.

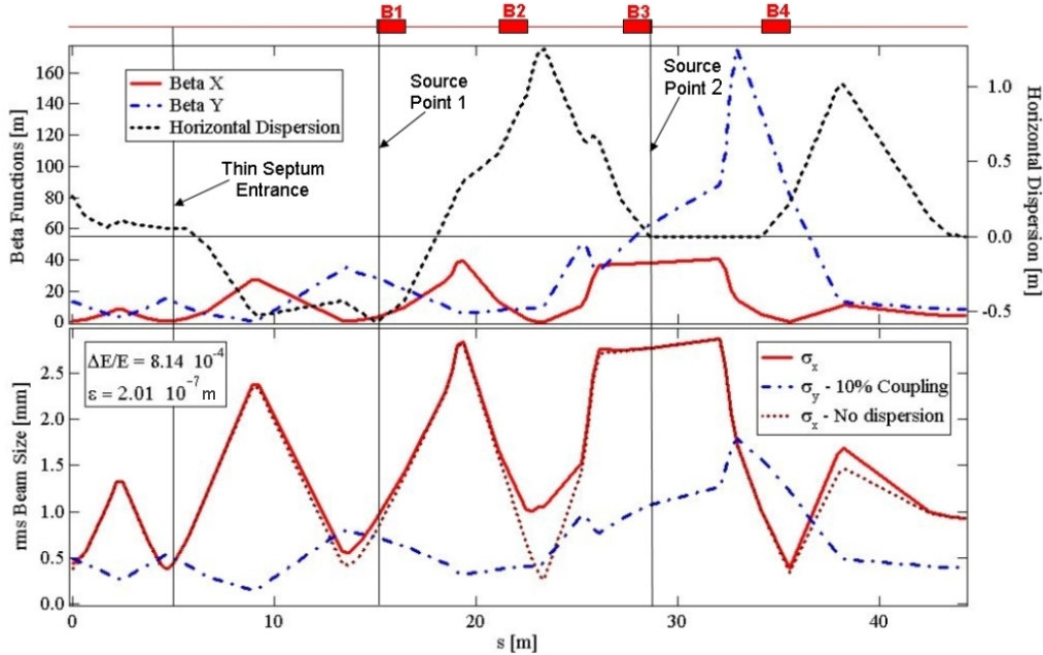


Figure 3.9-2: BTS optical function, beam sizes and SR source point positions.

Source Point 1 exploits an already existing port on the vacuum chamber of the first bend B1 of the BTS, see Figure 3.9-3. At the present time, the port is equipped with a TV system (fluorescent screen) and in the new configuration, it will be sufficient to replace the existing screen with a metallic mirror to bring the synchrotron radiation out of the chamber.

The synchrotron radiation characteristics of the Source Point 1 are given in Table 3.9-4.

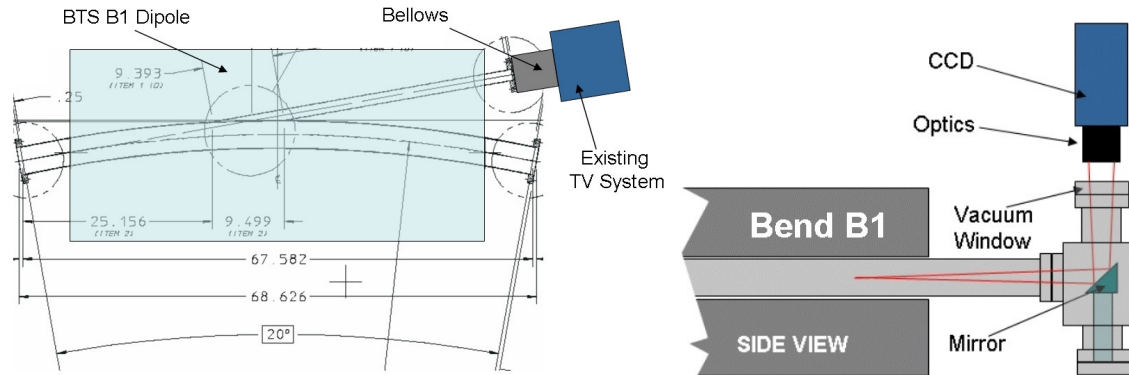


Figure 3.9-3: Synchrotron radiation monitor at BTS bend B1.

Table 3.9-4: Source Point 1 synchrotron radiation characteristics

Photons per beam passage (between 250 – 700 nm)	$\sim 1.3 \times 10^8$	Horizontal acceptance (total chamber aperture)	~ 18 [mrad]
Energy deposited in the mirror per passage (whole SR spectrum)	$\sim 8.0 \times 10^{-7}$ [J]	Minimum vertical acceptance (total)	10 [mrad]
Bunch charge (1.5 mA in the Storage Ring)	9.84×10^{-10} [C]	Mirror angle	45 [deg]

Source Point 2 will be located downstream bend B3 of the BTS. In this case, a new vacuum chamber segment will allow extracting the synchrotron radiation, see Figure 3.9-4 and Figure 3.9-5. The linear actuator shown in Figure Figure 3.9-4 is not strictly required but its presence will allow positioning the mirror at the proper distance from the actual electron beam orbit.

The synchrotron radiation characteristics of the Source Point 2 are given in Table 3.9-5.

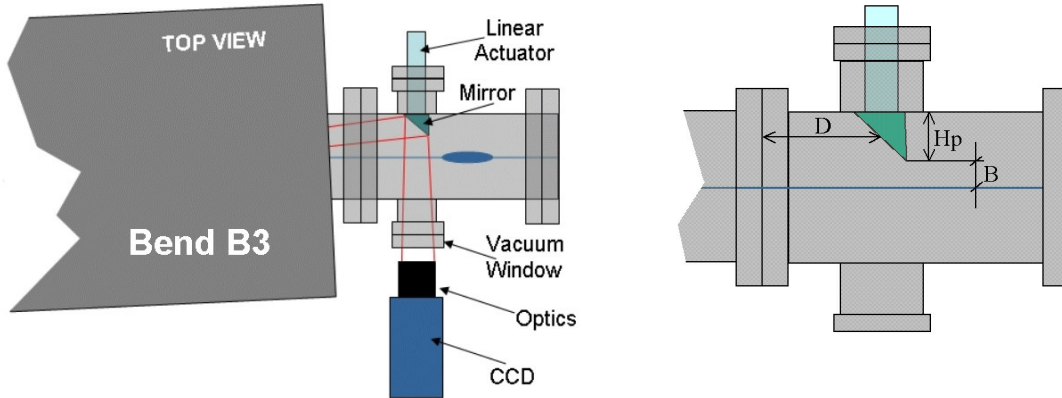


Figure 3.9-4: Synchrotron radiation monitor at BTS bend B3 and detail of the mirror area. For the symbols in the figure see Table 3.9-5.

Table 3.9-5: Source Point 2 synchrotron radiation characteristics

Photons per beam passage (between 250 – 700 nm)	$\sim 6.8 \times 10^8$	Distance mirror-B3 vacuum chamber flange (D)	10 [cm]
Energy per shot (whole SR spectrum)	$\sim 4.0 \times 10^{-6}$ [J]	Mirror projected horizontal size (Hp)	35 [mm]
Bunch charge (1.5 mA in the Storage Ring)	9.84×10^{-10} [C]	Mirror minimum vertical height (total)	10 [mm]
Mirror angle	~ 41 [deg]	Distance mirror edge-beam axis (B)	10 [mm]

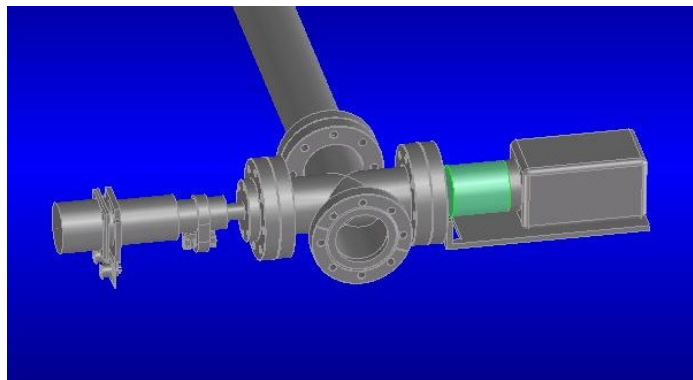


Figure 3.9-5: Synchrotron radiation monitor at BTS bend B3, a 3D CAD view.

Alternatively, the Source Point 1 could be moved and placed at the end of dipole B2, with a geometry of the monitor similar to the one downstream B3. The advantages are: a larger dispersion and a larger dispersion to horizontal beta function ratio, see Figure 3.9-2. The disadvantages are a larger distance from the Booster (less effective diagnostics of the booster extraction status), a tighter space downstream B3 and additional engineering and construction effort with increased costs.

For all the cases, the photon flux is high enough to allow the use of standard CCD cameras with a sensitivity of ~ 1 lux.

The synchrotron radiation heat load in both the metallic mirrors is negligible and no water-cooling is required for that. In the case of the monitor at B3, a wrong orbit could bring the electron beam on the mirror, the induced heat load will be approximately ~ 0.1 J per beam passage. This number has been estimated for an aluminum 5 mm thick mirror and for the nominal bunch charge indicated in Table 3.9-5. Assuming an operation at currents ten times larger and 1 Hz repetition rate, the mirror needs to be designed in order to dissipate an average power of ~ 1 W.

3.9.2.3 Beam Stopper for Injection Tune-up

We are proposing the insertion of an extractable beam stopper at the end of the BTS transfer-line, just before the first injection septum of the storage ring. Such a beam stopper, when inserted, will allow for the complete tuning of the accelerator injection chain without perturbing the beam stored in the storage ring.

The beam stopper should have a thickness of ~ 10 radiation lengths in order to efficiently stop the beam particles. The structure can be very compact if high atomic number and high density materials are used. For example, if tungsten is used the required thickness will be ~ 4 cm. The maximum heat load will be smaller than 10 W (1 Hz and 5 nC charge). Long term activation of the beam stopper needs to be estimated.

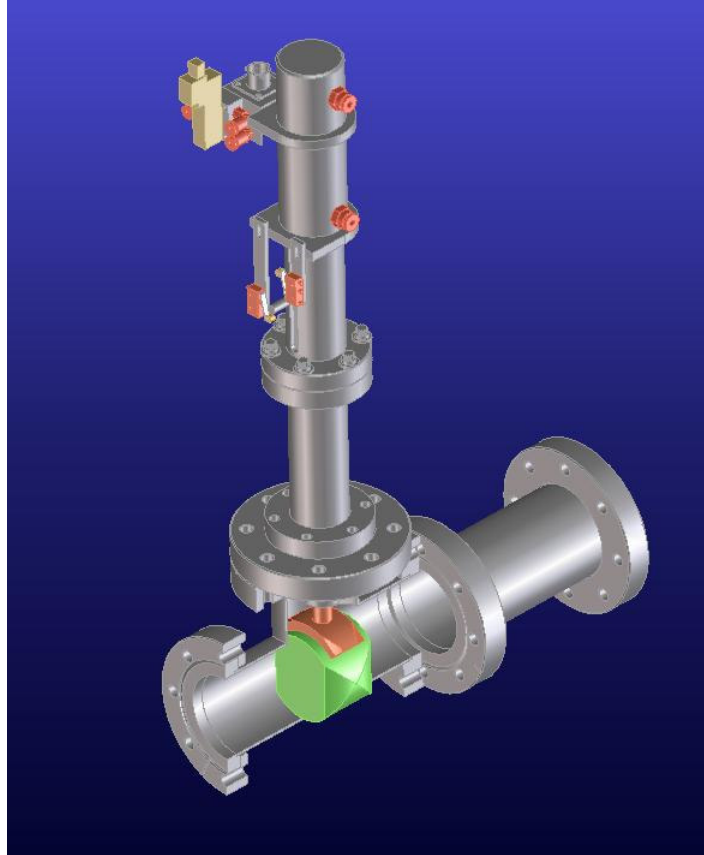


Figure 3.9-6: CAD drawing of the BTS diagnostic beam stop. A tungsten block being inserted vertically into the beam path.

3.9.3 *Storage Ring Diagnostics*

3.9.3.1 Storage Ring Bunch Purity Monitor

During the two bunches mode of operation, bunch purity in the storage ring must be measured. At present during two-bunch operation, we set up a simple BPM-digital scope system with a resolution (ratio between the charge in the main bunch and the one in the parasite bunch) of a few units in the 10^{-3} range.

For the top-off upgrade, we propose a dedicated bunch purity monitor with a higher resolution ($<10^{-4}$) that will permit an easier and more reliable control of the bunch cleaning procedure. The proposed system is based in a photon counting scheme using the synchrotron radiation emitted by the bunches. The block diagram of the system is shown in Figure 3.9-7.

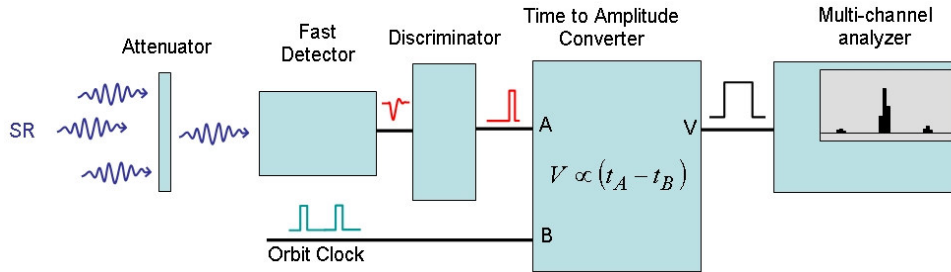


Figure 3.9-7: Bunch Purity Monitor Block Diagram.

The attenuator is required to go in the so-called single photon count regime, where a single photon is detected every few hundred passages of the bunch. This is fundamental for avoiding photons pile-up and for ensuring a linear response of the system. The detector must be fast enough to discriminate between contiguous bucket (2 ns) at a resolution smaller than 10^{-4} . This requirement is kind at the limit with what can be achieved using synchrotron radiation in the visible range (PMT, MCP, ...) while it is well in the range of performance for x-ray detectors like avalanche photo diodes. The signal coming from the detector is properly formed by a discriminator and is compared in time with an orbit clock by a time to amplitude converter. The output signal of the converter will have an amplitude proportional to the time difference between the orbit clock and the arrival of the detector signal. Finally, an amplitude analyzer will present the results in the shape of amplitude histograms.

The visible option is simpler because it can use the synchrotron radiation already available in some of ALS beam lines (BL3.1 or BL7.2), while for the x-ray case a new port with a thin beryllium window must be placed somewhere for taking out the x-ray from the vacuum chamber.

3.9.3.2 Storage Ring Bunch-by-Bunch Current Monitor

There are several operational aspects that require an accurate measurement of the beam current in all individual bunches in the ALS storage ring. One is the desire of users for specific fill patterns tailored to their needs. Others are accelerator physics issues like lifetime and instabilities related to bunch current or details of the fill pattern. This issue is more critical in top-off, where just random injection timing could lead to a slow but continuous deterioration of the fill pattern. The ALS already has a bunch-by-bunch current monitor, however, the current system is not dedicated for this purpose, uses a signal with poor signal quality and is not user friendly.

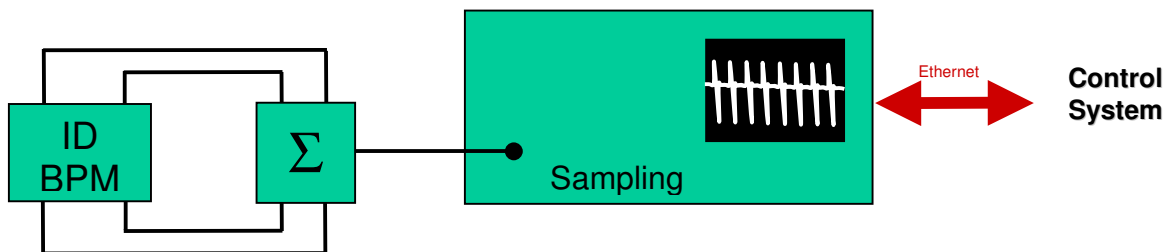


Figure 3.9-8: Schematic of a bunch-by-bunch current monitor for the ALS Storage Ring.

Therefore, an upgrade of the existing system will be implemented: The signal quality of the Beam Position Monitor signal will be improved. A dedicated scope with higher bandwidth will be used. The signal processing software will be included as a reliable application at a lower level in the control system and a new high-level operator interface will be implemented.

3.10 Computer Control System

The computer control system (CS) for the ALS consists of distributed controllers installed in the proximity of the accelerator hardware which are linked by networks to the ALS control room (CR). In the CR, standard workstations, both Windows and UNIX/Linux based, provide the higher level control of the facility. These workstations, known as *console computers*, are configured with specialized applications developed in-house to meet the needs of accelerator operations for controlling and monitoring all the ALS subsystems. The subsystems include magnet power supplies, electron beam diagnostics, RF, vacuum valves and ion gauges, and insertion devices. The control requirements for these subsystems differ somewhat between the electron gun, LINAC, booster, storage ring and transfer lines, but since maintenance costs increase in proportion to the to these differences, the goal in specifying CS hardware and software is to maintain as much commonality as possible between similar subsystems.

The original design of the CS described in the 1-2 GeV Synchrotron Radiation Source Conceptual Design Report (LBL PUB-5172), has greatly evolved over the almost 20 years since the design was completed. The CS is now in the midst of a migration from controls based on in-house developed local controllers, Intelligent Local Controllers (ILCs) linked by RS-485-based serial networks, to commercial bus-based (VME and cPCI) controllers, Input Output Controllers (IOCs), linked by standard Ethernet networks. This hardware migration enables a migration of the CS software to the EPICS system currently in use at most other light sources such as the Advanced Photon Source at Argonne National Lab and the Swiss Light Source.

The detailed CS plan for the Booster Top-off effort is driven both by the requirements of the changing hardware, such as new magnet power supplies and the RF subsystem and the by goals for the CS at large; namely the goal to minimize the differences in control interfaces between similar subsystems and the goal to continue the migration of the CS hardware and software to off-the-shelf solutions in the interest of maintainability over the long life span of the booster.

The control requirements for each of the subsystems affected by the booster upgrade will be discussed followed by a discussion of the software effort. Finally, an inventory of the new control system i/o crates and their functions are discussed.

3.10.1 Magnet Power Supplies

The booster magnet power supplies have the property that their currents must change together to maintain the electron orbit as the energy of the booster is changed. The booster supplies are divided into *large* supplies: the main bend (1) and the quadrupoles (4) and the *small* supplies: the sextupoles (8) and the correctors (32).

The current scheme for ramping these magnets is based on following the field of the main bend magnet using a gauss clock to generate an interrupt to the controllers about every 100ms as the field increases. Due to inflexibility of this scheme and the wide availability and low cost of digi-

tal controls, a new system is envisioned that will drive the ramp profile with programmable waveform generators. We expect to follow the industry trend in control of the large supplies by specifying integrated vendor-supplied PLC based controls with a digital interface to the CS and an internal waveform generator for ramping the current. Integrating the controls in the power supply reduces the wire count and simplifies the software effort significantly. Software effort can be reduced further by specifying a well supported wire-protocol such as MODBUS/TCP which is supported by many PLC vendors. This protocol is already in use in the CS and can be efficiently extended to power supply controls.

The large number (40) of small supplies and their individual cost do not warrant the expense of digital interfaces. These supplies would be controlled in the traditional analog fashion by the addition of some 5 additional IOCs identical to the ones already in use in the storage ring. Ramping of these supplies would require an external timing signal supplied to each IOC.

The *fast* magnet power supply category includes the thin and thick septum magnets and the kicker magnets in the booster and the thick and thin septum magnet and the bump magnets in the storage ring. There is no change expected in the control requirements for these magnets.

The BTS bend magnets are large supplies for which the digital controls identical to the large supplies in the booster (minus the waveform generator) would be used.

3.10.2 *BTS Diagnostics*

There will be two **synchrotron light monitors** at two bending magnets in the BTS, each with a CCD camera. In addition, a linear actuator will allow the positioning of a mirror inside the vacuum chamber for reflecting synchrotron light. Control of these cameras and the linear actuator will be done by a dedicated PC, similar to the system already deployed in the 7.1 beamline.

An insertable **beam stop** at the very end of the BTS will allow operating the injector for tune-up without injecting in the storage ring. The actuator position, either in or out of the beam, will be remotely controlled from the control room.

The existing current monitors, both the **Integrated Current Transformers** (ICT) in the BTS and the **wall current monitors** (WC) in the booster, will require ADCs (6) for measurement of peak or average current. These measured values should be displayed in the control room by a new application.

3.10.3 *Booster Diagnostics*

A **bunch cleaning** system will be installed in the booster. It uses an arbitrary function generator and a RF synthesizer. They will be placed somewhere inside the ALS dome and should be remotely controlled.

A single-blade **beam scraper** will be added to the booster. Micrometric control of the scraper position is required.

3.10.4 Booster RF

The controls for the RF will also be integrated into the hardware and a digital interface, ideally with the same MODBUS/TCP wire-protocol used for the large magnet supplies, provided to the CS.

3.10.5 Radiation Protection

The CS never takes an active role in Radiation Protection or any form of personnel safety. There will be modifications to the existing CR alarm monitoring application that will be required in response to the expected hardware changes however.

3.10.6 Collimation Controls

There will be motor-controlled collimators added to both the BTS and storage ring. Control of these motors will require the addition of 2 IOCs with motor control boards identical to those used for the current scraper controls in the storage ring.

3.10.7 Software Effort

Software Effort falls into 2 main categories: IOC software development and Control Room (CR) application development.

3.10.8 IOC software effort

The software effort can be greatly reduced by reducing the different types of interfaces to accelerator equipment. The standard digital interface should be Ethernet based and should support MODBUS/TCP for communications with the IOCs.

There will be IOC development effort for controlling the new digital supplies (both ramped and non-ramped). This effort will start with the development of interface specifications for the type of PLC and the communication mechanism (serial or Ethernet) and the communication protocol. Then an IOC template for the PS must be developed that handles PS process variables. For testing this template it will be essential to procure some version of the digital control hardware from the vendor early.

There will also be an IOC software development effort required for the analog controlled ramped supplies. Interrupt driven software must be written to respond to the incoming 'ramp step' interrupt generated by the timing system as the booster is ramped to full energy.

Two IOCs will be used to control the new booster RF system. The transmitter is a commercial unit with internal digital controls (similar to the large PSSs) with a serial or, preferably, an Ethernet interface using the MODBUS protocol (again similar to the large PSSs). A PLC based RF Interface Chassis will also be controlled by an IOC.

3.10.9 Control Room Application Development

Many of the changes and additions made to the booster instrumentation also require changes and additions to CR applications. Development of CR typically includes testing during dedicated machine time for both development and application commissioning. Application commissioning typically involves a team consisting of a controls group member, the instrumentation lead engineer or accelerator physicist and an accelerator operator. Although they have not been established, the need for the following applications has been identified:

- Booster RF Controls.
- Booster Tune-up. Insert/Remove BTS beam stop. Display current monitors.
- Booster Bunch Cleaning. Control waveform generator.
- Booster Scraper control.
- Booster BPM.
- BTS Synchrotron Light Monitor.
- Storage Ring collimator controls
- Radiation monitoring.

3.10.10 New IOCs

About 10 new IOCs will be required for the top-off project. The number is dictated mainly by the I/O capacity but also by the requirement that they be located within the proximity of the hardware that they must control. It is also quite important, given the large number of IOCs that need to be managed, that, where possible, these additional crates use hardware and software that is currently used elsewhere in the accelerator.

IOC1 booster (40 PVs)

- Digital magnet supplies (7)

IOC2-5 booster (20 ILC replacements, 300 PVs)

- Booster corrector supplies
- Thick and Thin Septum magnet supplies
- Kicker supply

- Magnet thermocouples (20 PVs/ea)
- IOC6 booster (12 PVs)
- Booster scraper
- IOC7 booster diagnostics (20 PVs)
- Bunch cleaning waveform generator and amp
 - Current transformer ADC (5) (maybe LTB)
 - Wall current monitor readout ADC (1)
- IOC8 booster RF (100 PVs)
- transmitter
 - interface chassis
- IOC9 VME BTS (12 PVs)
- collimator
- IOC10 BTS diagnostics
- beam stop????
- IOC11-12 VME storage ring (12 PVs)
- 2 collimators
 - Radiation monitors???

3.11 AC Power Utilities

3.11.1 AC Power Utilities-Booster Ring

3.11.2 Description-General

The Advanced Light Source Booster Ring AC Power (Bank 303) is derived from a 2MVA, 12.47KV-480Y/277V transformer which feeds a 3200Amp, 480V, 3 phase distribution panel (SS303) located at the ALS Switching Station A3. Reference 4B06E179B for basic one-line diagram.

SS303 currently houses 3 each distribution circuit breakers.

Circuit 1 supplies 480VAC, 400Amp power to Panel 303A1A located within the Booster Pit Area Sector 3 via 1 each 3/C-500MCM cable. Panel 303A1A is the distribution panel used to power the Booster QF and QD Power Supplies. The current load on this panel is approximately ½ of its designed rating. No AC Power Utility upgrade will be required for the new QF and QD Power Supplies which will be required for the Booster Upgrade Project.

Circuit 2 supplies 480VAC, 800 Amp power to the Booster Dipole Power Supply located within the Booster Pit Area Sector 1 via 2 sets of 3/C-500MCM cables. Each set of 3/C-500MCM cables are located within a 4" Conduit. The new Booster Dipole Power Supply will be designed such as the input ac power requirements will not exceed the factory operating characteristic curve of the existing 800Amp feed breaker and input ac power cabling. No AC Power Utility upgrade will be required for the new Booster Dipole Power Supply.

Circuit 3 supplies 480VAC, 400 Amp power to Panel 303A3A located within the Booster Pit Area Sector 3 via 1 each 3/C-500MCM cable. Panel 303A3A is the distribution panel used to distribute 208-120Vac power to each of the Booster Quadrants via 3 each 75KVA (Sectors 1,2,4) and 1 each 112.5KVA (Sector 3) 480V-208V step down transformers located in the Booster Pit Area Sector 3. This power distribution is for all booster ring system support loads requiring lower voltages. No AC Power Utility upgrade will be required in this area for the Booster Upgrade Project.

3.11.3 Booster RF AC Power

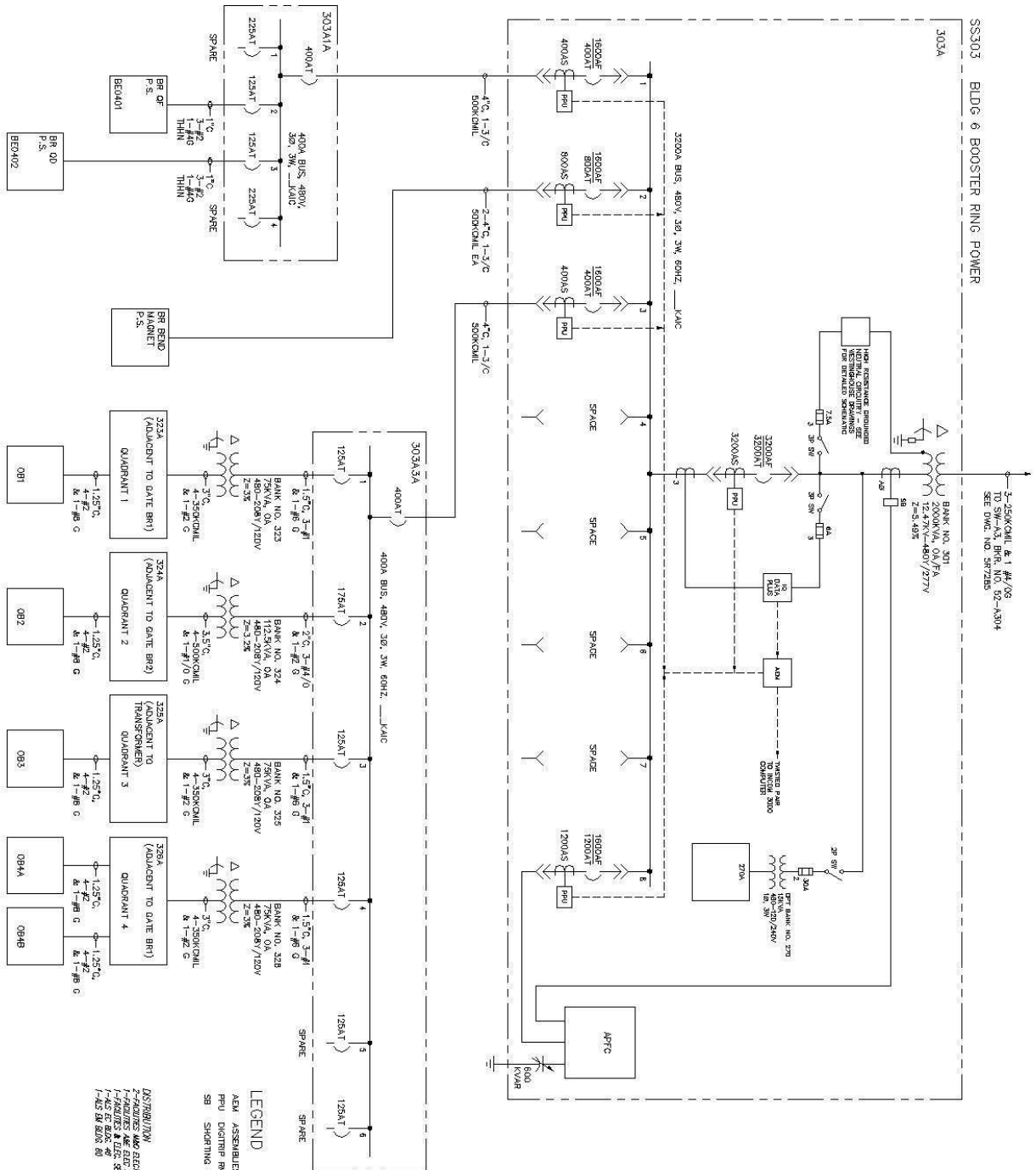
The Advanced Light Source Booster RF AC Power is derived from a 2MVA, 12.47KV-480Y/277V transformer which feeds a 3200Amp, 480V, 3 phase distribution panel (SS302) located at the ALS Switching Station A3.

Reference 4B06E178C for basic one-line diagram.

SS302 circuit 1 supplies 480VAC, 1200Amp power to Panel 302A1A located near the ALS Linac entrance. Panel 302A1A is fed via 3 sets of 3/C-500MCM cables and has a current limit of 1200amps. Circuit 5, 80Amp feed supplies input power to the existing Booster Ring RF Transmitter Power Supply and circuit 6, 60amp feed supplies power to the existing BR RF Cavity Water System. The existing circuit 6 will be removed and a local utility upgrade will be needed for the new ALS Booster RF Transmitter. Panel 302A1A has multiple spare circuits and circuit breakers. No AC Power Utility upgrade will be required for panel 302A1A for the Booster Upgrade Project.

3.11.4 Booster to Storage Ring (BTS)

AC Power for the 4 each BTS Bend Magnet Power Supplies is fed from the Storage Ring/Linac Distribution Power SS 302 circuit 1 via distribution panel 302A1A located near the Linac entrance area. Panel 302A1A circuits 7-10 supply the 480V input power feeds for each of the BTS Bend Magnet Power Supplies. Reference 4B06E178A for basic one-line diagram. No AC Power Utility upgrade will be required for the new BTS Bend Magnet Power Supplies required for the Booster Upgrade Project.



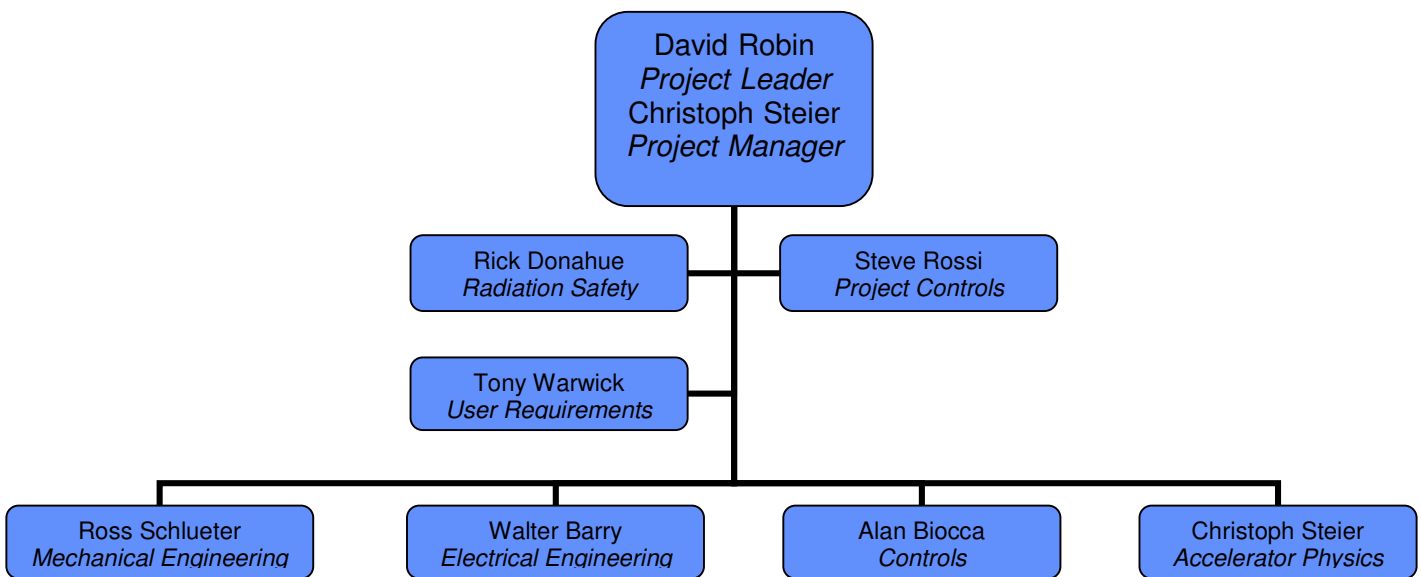
BANK 303										
06	BANK NO. 303				DRAWN BY: AD		DATE: 6/28/2000			
ONE LINE DIAGRAM					CHECKED BY: ROB		DATE: 6/6/2000			
					APPROVED BY: MCG		DATE: 6/9/2000			
					DWG FILE PATH: 00010962					
					SCALE: As Noted					
					DRAWN NO.: 4B06E179B		SHEET: 1 OF 1			
					PROJECT NO.: 000000					

Figure 3.11-1: Diagram of the electrical supply bank 303 at the ALS.

4 COST, SCHEDULE, INSTALLATION

4.1 Project Organization

The Top-off upgrade of the ALS has been treated ALS internally like a project since the project kick-off meeting in October 2003. All applicable project management tools are used. The organization chart of the project is shown below. Everybody listed on the organization chart has full line responsibilities, i.e. safety, technical, cost, and schedule responsibility. The ALS



division directorate provides management oversight and all project decisions are closely coordinated with ALS management.

Identifying risks, analyzing and resolving them was the main emphasis of the conceptual design phase in FY04. The project management identified an initial list of major risk items. Later input was solicited from all project team members. Based on this list, a prioritized list of studies for the conceptual design phase was assembled and all high risk items were studied intensively. At the time of this CDR, most high risk items have been successfully resolved. The few remaining items are currently actively being studied, with positive results so far. After finishing the CDR, the risk analysis will be formalized further and detailed mitigation plans will be documented for all remaining risk items.

With the completion of the CDR, the scope of the top-off upgrade will be frozen and a formal change control process will be put in place. All future changes to the scope, parameter

list/configuration, or requests to use cost or schedule contingency will have to be approved by the project management. Significant changes will also need approval by ALS management.

4.2 Work Breakdown Structure

The Work Breakdown Structure (WBS) was created shortly after the project kick-off in October 2003. It has slightly evolved over time, and so far changes were just informally approved by project management (and discussed with ALS management). Once this CDR is finished, the WBS will be frozen. Afterwards changes will be approved only with a formal change control process. The WBS also includes the conceptual design phase. Therefore there are some WBS items with zero cost in the cost estimate, since all effort in those was in last fiscal year and does not show up in cost-to-complete.

- 1.1 Project Management
- 1.2 Top Off Documentation
 - 1.2.1 User Requirements
 - 1.2.2 Specification
 - 1.2.3 CDR
- 1.3 Linac
 - 1.3.1 EDI
 - 1.3.2 Beam Loading Compensation
 - 1.3.3 Diagnostics
- 1.4 Booster
 - 1.4.1 Power Supplies
 - 1.4.2 Thin Septum Magnet
 - 1.4.3 Thick Septum Magnet
 - 1.4.4 Kicker Magnet
 - 1.4.5 RF
 - 1.4.6 Diagnostics
 - 1.4.7 Bump Magnets
- 1.5 BTS
 - 1.5.1 EDI
 - 1.5.2 Diagnostics
 - 1.5.3 Beam Stopper for Injection Tune-Up
 - 1.5.4 B1-B4 bend power supplies
- 1.6 Storage Ring
 - 1.6.1 Bump Magnets
 - 1.6.2 Thin Septum Magnet
 - 1.6.3 Thick Septum Magnet
 - 1.6.4 Radiation Protection
 - 1.6.6 Diagnostics
- 1.7 Controls and Timing
 - 1.7.1 User Gating Signal
 - 1.7.2 Linac and Booster Timing
 - 1.7.3 Controls
 - 1.7.4 RF Controls

- 1.8 Commissioning
 - 1.8.1 Pre-commissioning
 - 1.8.2 Commissioning/Startup

4.3 Cost Estimate

The cost estimate shows cost to complete from December 2004 on. It includes the full scope of the top-off upgrade as presented in Section 2.2. It includes all necessary spare parts and is based on FY05 craft rates, with full burden. Escalation is not included in the cost estimate. Based on the current schedule of the project, i.e. completion in spring of 2006, escalation costs are relatively small (i.e. about 75 k\$) and will be covered out of contingency.

All effort, including staff people on operations funding is included (e.g. commissioning time). Routine accelerator physics studies part of the precommissioning are not included and instead are funded out of the operations budget. Safety is an integral part of the project. The cost of complying with all applicable OSHA regulations and the electrical code is not shown separately but included everywhere in the cost estimate. EH+S support staff is heavily involved at all stages of the project. Their salaries are paid out of ALS operations funds and are not included in the cost estimate.

Contingency is applied at level 3 of the WBS and the overall contingency is 21%. The complete cost estimate is included as an appendix and can be found in Section 7.2.

Top Off Project Cost Estimate Summary

	Total Material K\$	Total Labor K\$	Total Labor + Material K\$	Overhead Total K\$	Sub Total K\$	Contingency K\$	Total K\$
1.0 ALS Top Off Upgrade	2,092.5	1,416.4	3,508.9	492.7	4,001.5	849.7	4,851.3
1.1 Project Management	0.0	95.4	95.4	19.6	115.0	11.5	126.5
1.2 Top Off Documentation	0.0	3.7	3.7	0.8	4.5	0.5	5.0
1.3 Linac	6.0	16.7	22.7	4.0	26.7	5.3	32.1
1.4 Booster	1,380.5	470.3	1,850.9	229.4	2,080.3	394.1	2,474.4
1.5 BTS	225.2	90.2	315.3	40.2	355.5	77.0	432.5
1.6 Storage Ring	263.5	328.5	592.0	93.0	685.0	144.3	829.3
1.7 Controls and Timing	217.3	389.1	606.4	101.0	707.4	214.3	921.7
1.8 Commissioning and Start Up	0.0	22.5	22.5	4.6	27.1	2.7	29.8

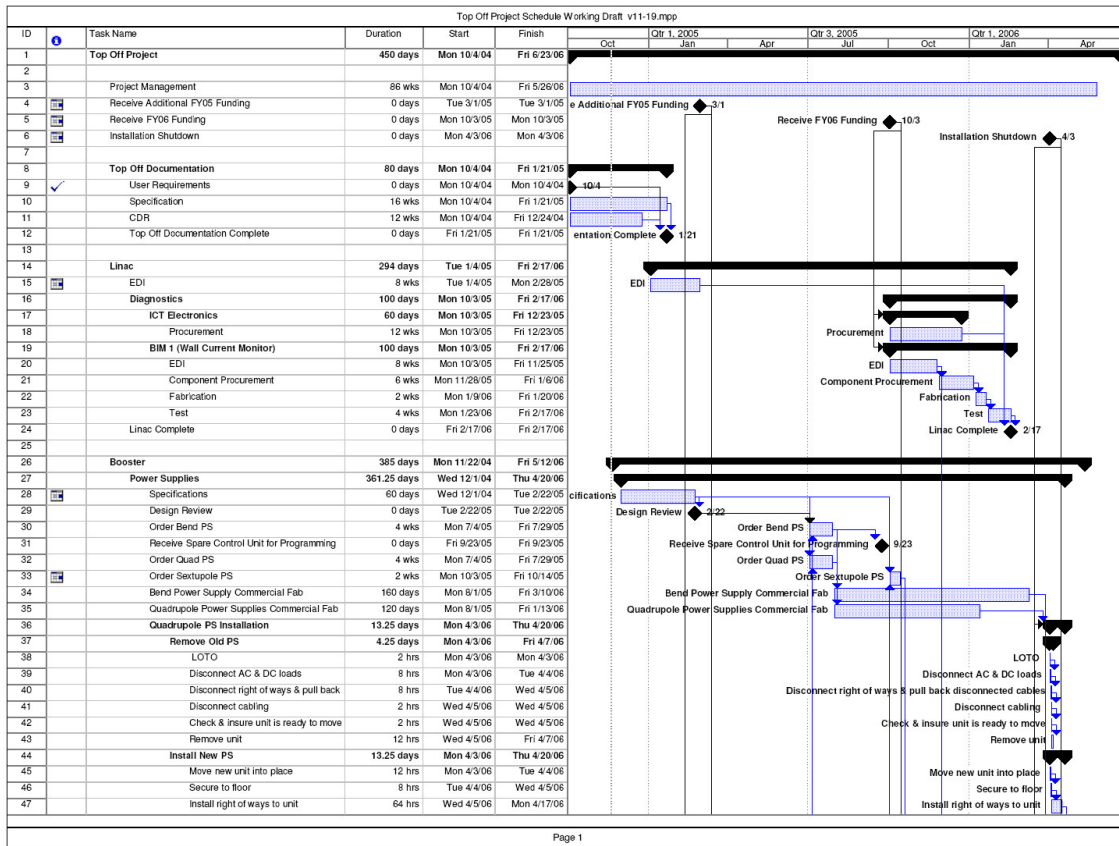
Table 4.3-1: Summary of the cost estimate for the ALS Top-off upgrade as of November 19, 2004.

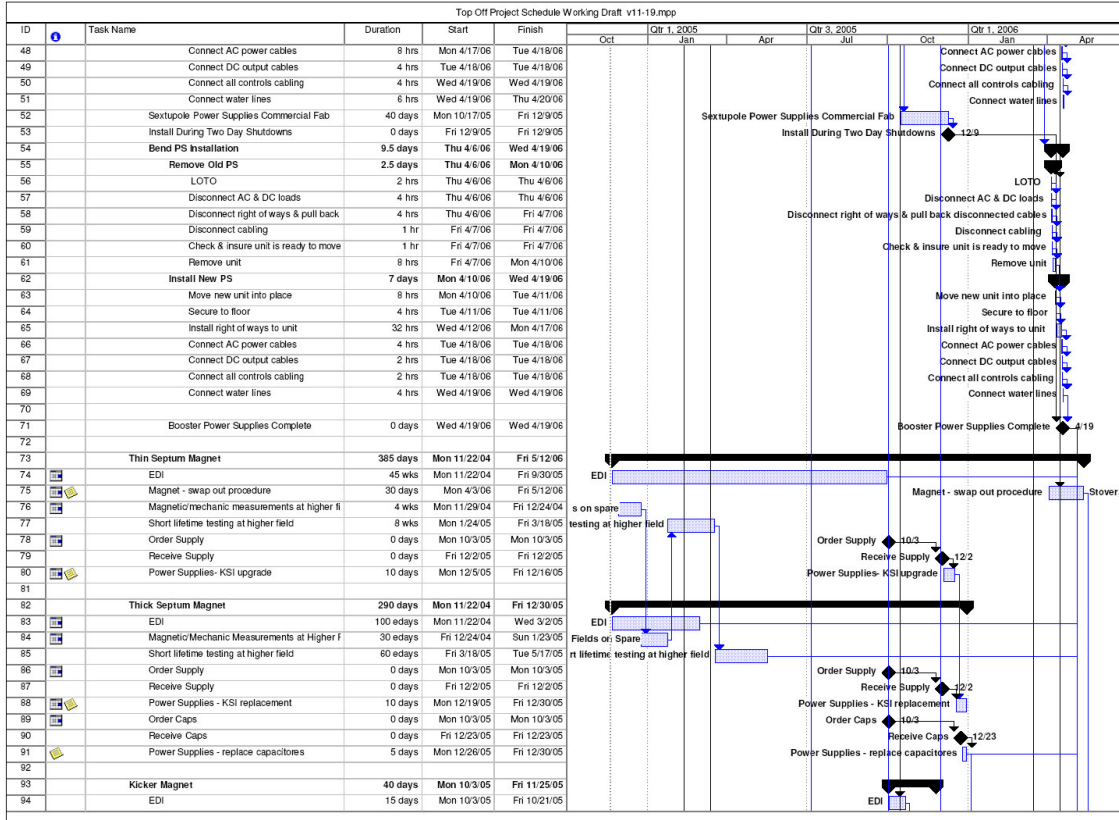
		MATERIAL	LABOR				TOTALS		
		Total	Total	Total	Overhead	Sub	Cntng	Cntng	Totals
Description		Material	Labor	Labor +	Total	Total	%	K\$	K\$
		K\$	K\$	Material					
1	ALS Top Off Upgrade	2,092.5	1,416.4	3,508.9	492.7	4,001.5	21%	849.7	4,851.3
1.1	Project Management	0.0	95.4	95.4	19.6	115.0	10%	11.5	126.5
1.2	Top off Documentation	0.0	3.7	3.7	0.8	4.5	10%	0.5	5.0
1.3	Linac	6.0	16.7	22.7	4.0	26.7	20%	5.3	32.1
1.3.1	Diagnostics	6.0	16.7	22.7	4.0	26.7	20%	5.3	32.1
1.4	Booster	1,380.5	470.3	1,850.9	229.4	2,080.3	19%	394.1	2,474.4
1.4.1	Power Supplies	540.0	18.3	558.3	55.6	613.9	20%	122.8	736.7
1.4.2	Thin Septum Magnet	9.4	28.3	37.7	6.7	44.4	25%	11.1	55.5
1.4.3	Thick Septum Magnet	7.1	8.9	16.0	2.5	18.6	25%	4.6	23.2
1.4.4	Kicker Magnet	7.7	18.6	26.3	4.6	30.9	25%	7.7	38.6
1.4.5	RF	613.2	233.0	846.2	106.9	953.1	15%	143.0	1,096.1
1.4.6	Diagnostics	197.7	159.7	357.4	51.9	409.3	25%	102.3	511.6
1.4.7	Bump Magnets	5.6	3.4	8.9	1.2	10.2	25%	2.5	12.7
1.5	BTS	225.2	90.2	315.3	40.2	355.5	22%	77.0	432.5
1.5.1	EDI	0.0	40.0	40.0	8.2	48.3	25%	12.1	60.3
1.5.2	Diagnostics	12.0	10.2	22.2	3.3	25.4	25%	6.4	31.8
1.5.3	Beam Stopper for Injection Tune Up	3.9	6.2	10.1	1.7	11.8	25%	2.9	14.7
1.5.4	B1 - B4 Bend Power Supplies	200.0	15.9	215.9	22.5	238.3	20%	47.7	286.0
1.5.5	Double Sided Collimators	9.3	17.9	27.2	4.6	31.7	25%	7.9	39.7
1.6	Storage Ring	263.5	328.5	592.0	93.0	685.0	21%	144.3	829.3
1.6.1	Bump Magnets	0.0	4.5	4.5	0.9	5.4	25%	1.4	6.8
1.6.2	Thin Septum Magnet	6.1	7.2	13.3	2.1	15.3	25%	3.8	19.2
1.6.3	Thick Septum Magnet	6.1	8.9	15.0	2.4	17.4	25%	4.4	21.8
1.6.4	Radiation Protection	175.9	286.4	462.3	75.9	538.2	20%	107.6	645.9
1.6.6	Diagnostics	75.5	21.4	96.9	11.7	108.6	25%	27.1	135.7
1.7	Controls and Timing	217.3	389.1	606.4	101.0	707.4	30%	214.3	921.7
1.7.1	User Gateing Signal	31.0	124.4	155.4	28.6	184.0	25%	46.0	230.0
1.7.2	Linac and Booster Timing	1.0	27.0	28.0	5.7	33.7	20%	6.7	40.4
1.7.3	Controls	184.3	223.6	407.9	63.8	471.7	33%	155.6	627.3
1.7.4	RF Controls	1.0	14.0	15.0	3.0	18.0	33%	6.0	24.0
1.8	Commissioning and Start Up	0.0	22.5	22.5	4.6	27.1	10%	2.7	29.8

Table 4.3-2: Cost estimate down to WBS level 3 for the ALS top-off upgrade as of November 19, 2004.

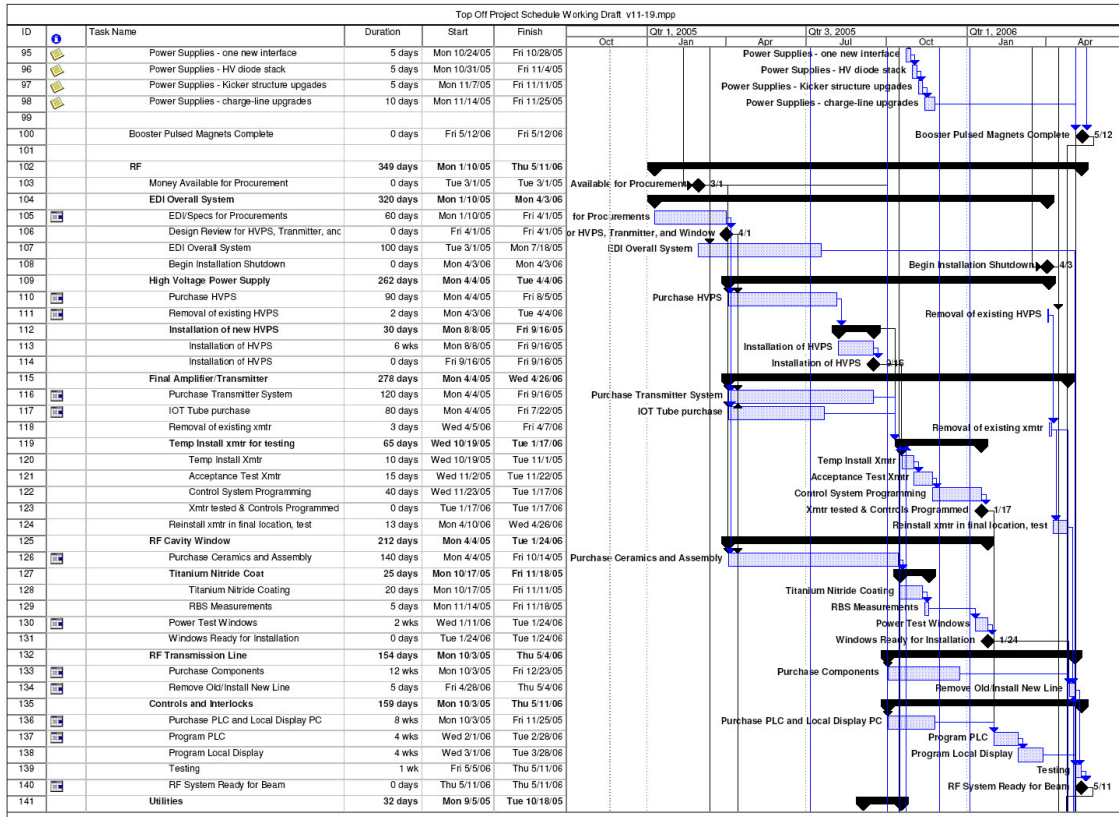
4.4 Draft Schedule

This CDR tries to evaluate the optimum schedule imaginable without funding profile limitations, so that we would be ready independent of what the final profile will be. The optimum schedule assumes availability of significant additional funding in FY05 (starting sometimes around March). This would provide the possibility to purchase long lead items early enough and consequently the project could be completed in FY06. For the schedule and cost estimate presented here, we would need a total of about 2.4 M\$ in FY05, and the rest in FY06. There is uncertainty on a funding profile from DOE at this time. So far 500 k\$ are available for the Top-off upgrade for FY05 (given in FY04).

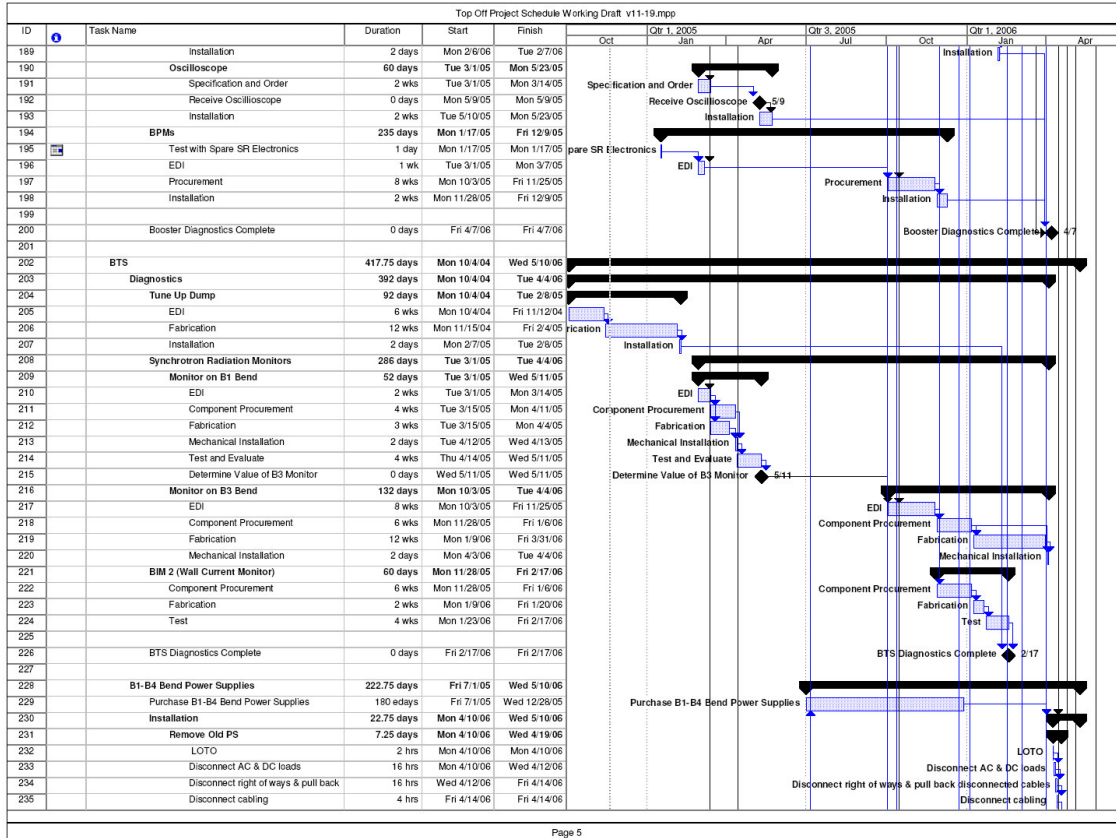
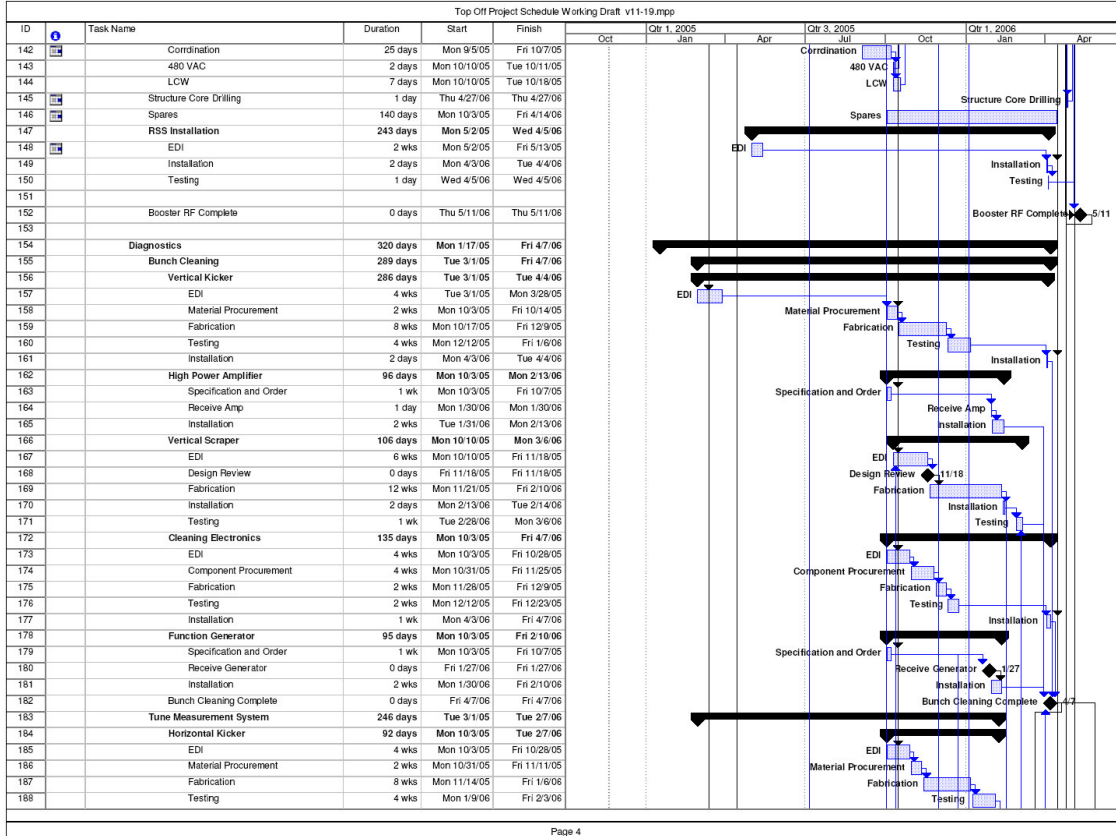


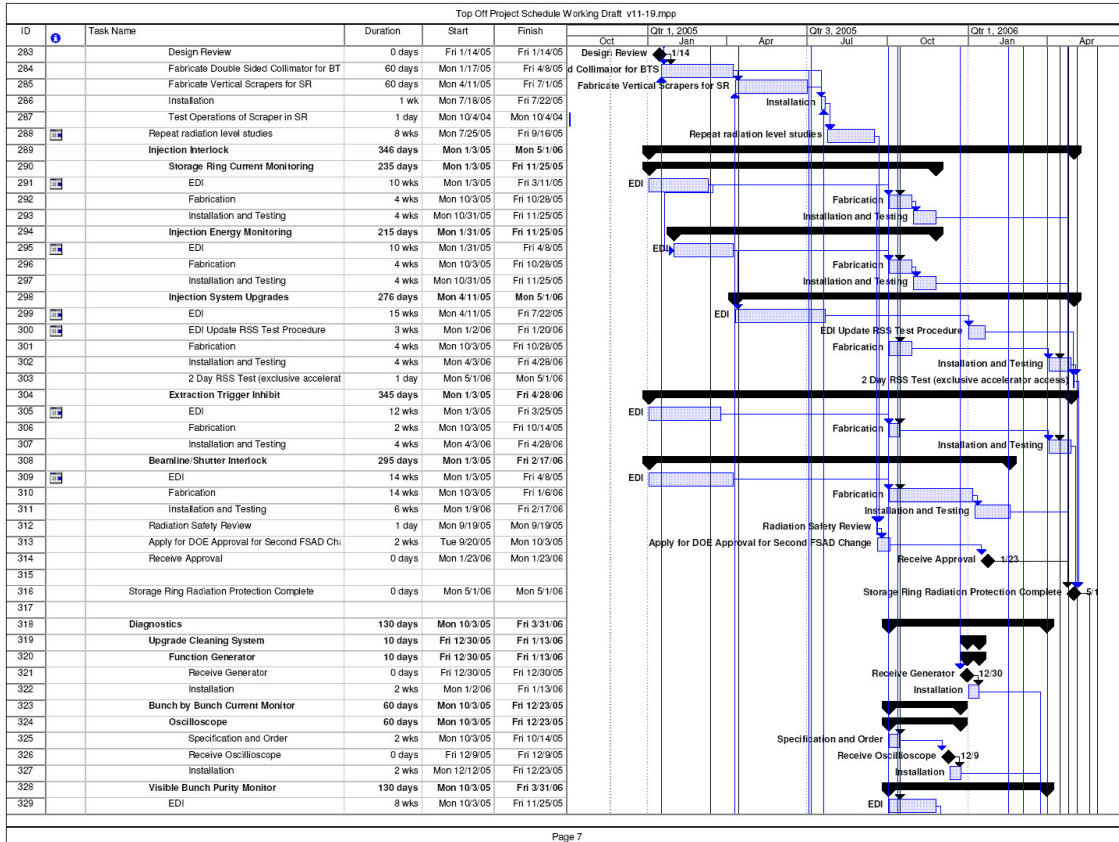
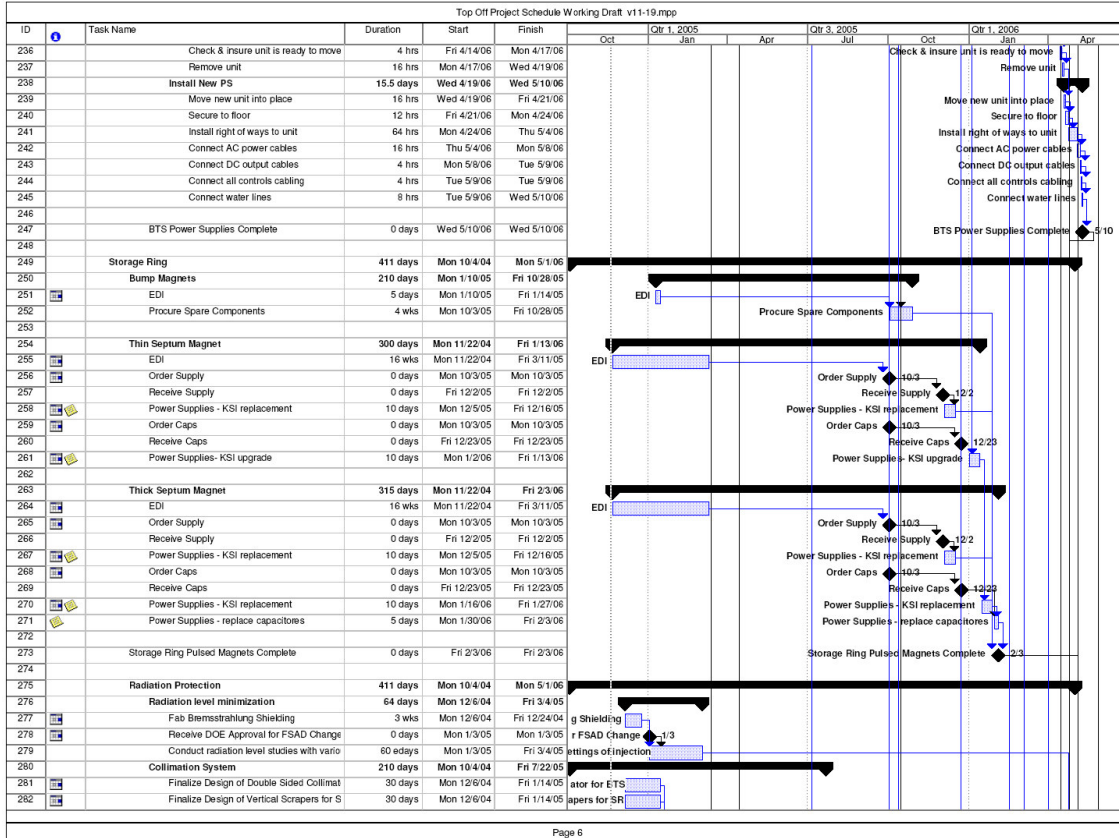


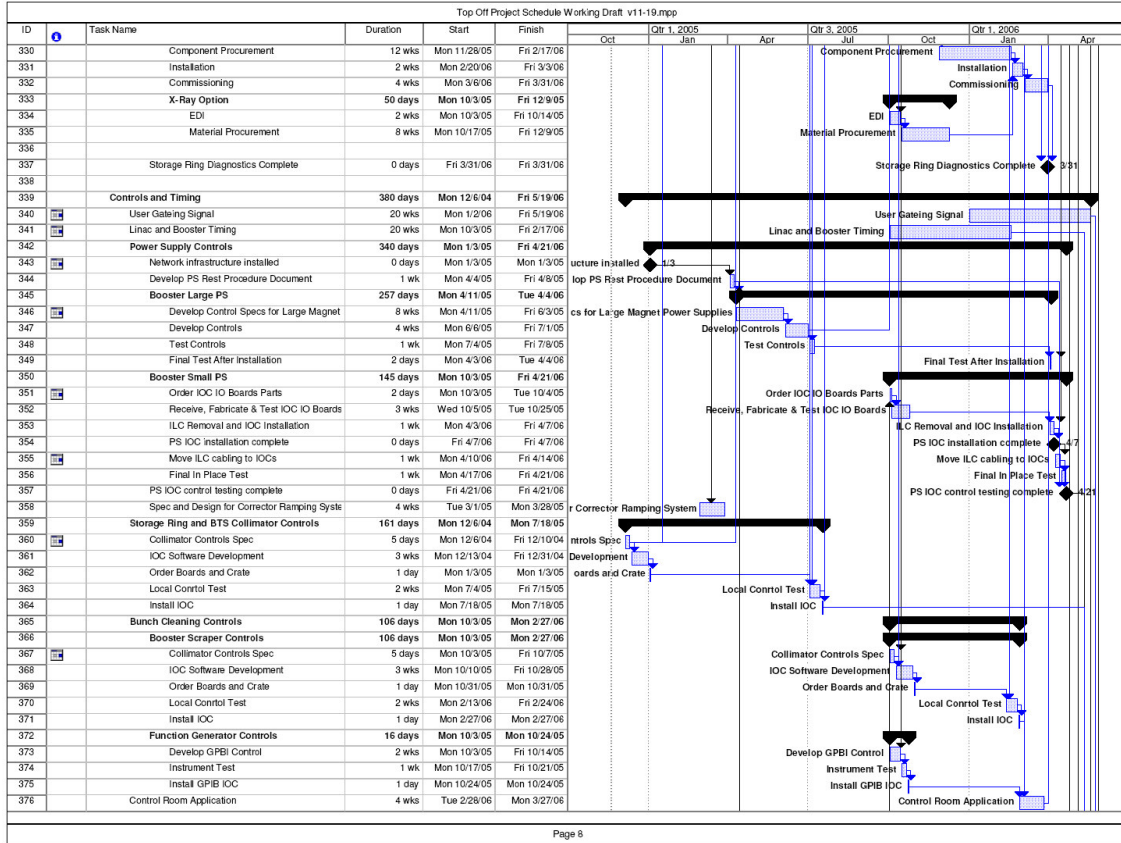
Page 2



Page 3







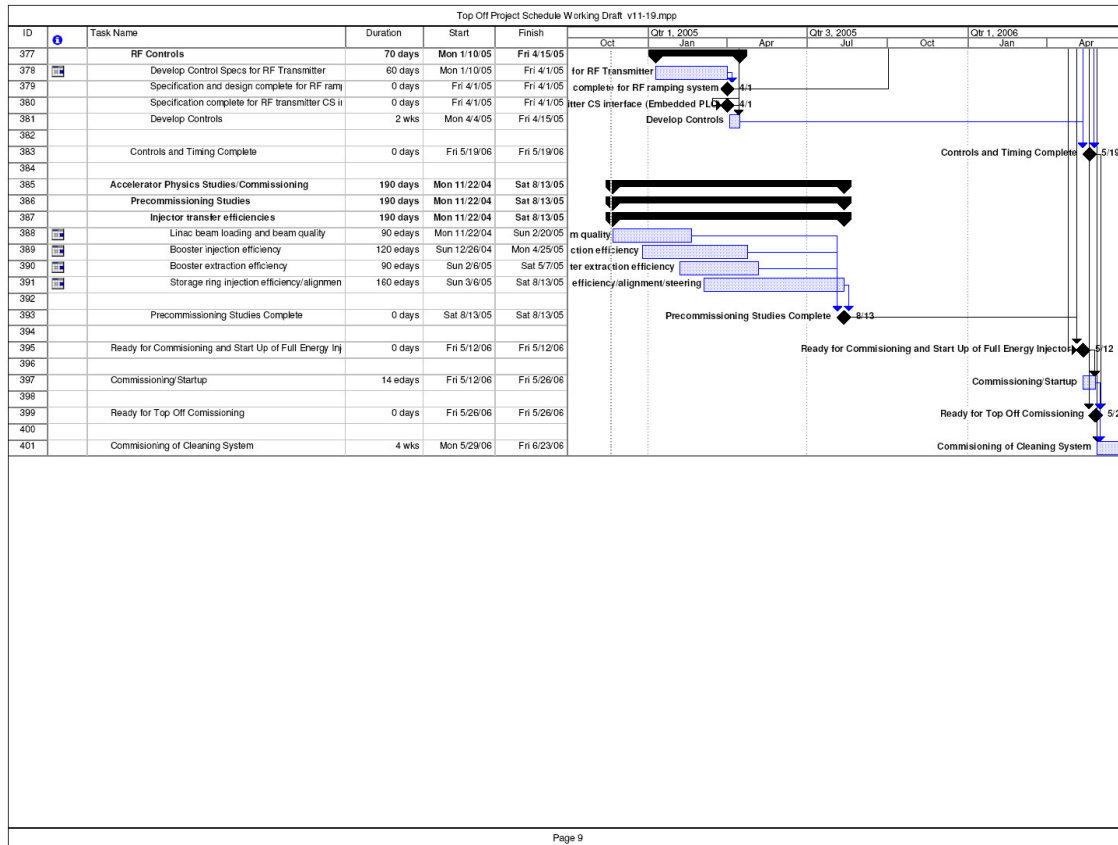


Figure 4.4-1: Complete draft schedule for the ALS Top-off upgrade as of November 19, 2004.

Depending on when and how much money becomes available, a staged approach might be necessary. The possible stages of the project could be:

1. Immediate need is to conclude radiation safety studies so that DOE approval process for Final Safety Analysis Document (FSAD) change can be started.
 - First priority: Install scrapers and collimators
2. Next one could purchase long lead items for booster energy upgrade (RF windows, power supplies, RF transmitter, ...).
3. Then one would complete everything necessary for full energy injection.
4. Next one could install the radiation protection equipment necessary for injection with shutters open (true top-off).
5. Last one would install equipment necessary for bunch cleaning in booster and the corresponding diagnostics equipment.

4.5 Installation

The schedule presented above includes basic installation details for all subcomponents. However, we will develop a separate installation schedule with higher level of detail at a later time. The installation schedule will consolidate the top-off upgrade with all other non top-off upgrade tasks also performed during the same shutdown. Nevertheless, the level of detail present in the schedule right now is sufficient to conclude that the installation of all components in one, about 6 week long, shutdown is possible. The relatively short installation shutdown is facilitated by the fact that very little mechanical work is necessary, very few high power cables need to be re-

routed, and several components can be installed (or test-installed) beforehand (pulsed magnet upgrades, full RF transmitter, etc.). All of these factors minimize the workload in the actual shutdown. Furthermore, nearly all smaller equipment (amplifiers, diagnostics, collimators, scrapers, etc.) will be installed in routine (2 day) shutdowns before big installation shutdown. The main schedule drivers for the length of the shutdown are the installation and final tests of the new booster RF transmitter, as well as the installation and test of all new slow/ramped power supplies for the booster and the BTS line.

4.6 Commissioning

In order to ensure a smooth final transition period with low commissioning risk and minimal teething period for the users, precommissioning is an integral part of project plan. The main tasks that will be investigated during the early precommissioning phase were described in the radiation safety and accelerator physics sections.

The actual commissioning period will intrinsically include time without beam, to test coordinated control and ramping of all new components. A commissioning period of about 2 weeks seems very reasonable, given sufficient pre-commissioning studies:

- Many beam diagnostics elements are already there. Enabling a complete set of reference measurements to be taken.
- Pulsed magnets will be upgraded beforehand.
- RF transmitter will be fully tested months before.

The first 5 days of commissioning will be without beam. The next 5 days will be dedicated to injector commissioning with beam. The final 4 days consist mostly of routine storage ring startup. The commissioning of the true top-off operation with beamline shutters open would be done incrementally in normal accelerator physics shifts during the months following the initial commissioning.

The minimum goal at the end of the commissioning is to return to the nominal 1.5 GeV injection used up to the installation shutdown with comparable performance. However, it is expected and a goal of the project, to provide 1.9 GeV full energy injection without any ramping by the end of the initial commissioning period.

The move to injection with shutters open, higher beam currents and smaller beamsizes on the other hand is planned to be implemented gradually and in close cooperation with all users over the months following the initial commissioning period. It is expected that the full implementation will probably take several months. Operation at the nominal upgrade parameters is expected to be possible about 6 months after the initial commissioning.

5 ACKNOWLEDGMENTS

The editors wish to acknowledge the many members of the ALS staff who contributed to the formulation of these upgrade plans, particularly the members of the top-off project team who wrote large sections of this design report. We are very grateful to the ALS management for its strong support of the upgrade plans and the close cooperation in implementing them. Finally we are very grateful to the colleagues who reviewed the top-off project in November 2004 and who helped to fine tune our upgrade plans.

This work was supported by the Director, Office of Science, Office of Basic Energy Sciences, of the U.S. Department of Energy under Contract No. DE-AC03-76SF00098.

6 REFERENCES

- [1] A. Lanzara, et al., "Evidence for ubiquitous strong electron-phonon coupling in high-temperature superconductors," *Nature* 412, 510 (2001).
- [2] A.D. Gromko et al, "Mass-renormalized electronic excitations at $(\pi, 0)$ in the superconducting state of $\text{Bi}_2\text{Sr}_2\text{CaCu}_2\text{O}_{8+x}$ " *Physical Review B* 68, 174520 (2003).
- [3] *Workshop on "Soft X-Ray Science in the Next Millenium: The Future of Photon-In/Photon-Out Experiments,"* (Pikeville, Tennessee, March 15 - 18, 2000), prepared by Oak Ridge National Laboratory for the U.S. Department of Energy.
- [4] A. Scholl et al., "Observation of antiferromagnetic domains in epitaxial thin films," *Science* 287, 1014 (2000).
- [5] J. Stohr et al., "Images of the antiferromagnetic structure of a NiO(100) surface by means of x-ray magnetic linear dichroism spectromicroscopy," *Phys. Rev. Lett.* 83, 1862 (1999).
- [6] F. Nolting et al., "Direct observation of the alignment of ferromagnetic spins by antiferromagnetic spins," *Nature* 405 (6788), 767 (2000).
- [7] H. Ohldag et al. "Spectroscopic identification and direct imaging of interfacial magnetic spins," *Phys. Rev. Lett.* 87, 247201 (2001).
- [8] H. Ohldag et al., "Spin reorientation at the antiferromagnetic NiO(001) surface in response to an adjacent ferromagnet," *Phys. Rev. Lett.* 86, 2878 (2001), and references therein to ALS magnetic microscopy.
- [9] J. Feng et al., "An Aberration Corrected Photoemission Electron Microscope at the Advanced Light Source," *AIP Conf. Proc.* 705, 1070 (2004).
- [10] S.A. Wolf et al., "Spintronics: A spin-based electronics vision for the future," *Science* 294, 1488 (2001).
- [11] R. Schoenlein, "Femtosecond x-rays from relativistic electrons: New tools for probing structural dynamics," *Comptes Rendus de l'Academie des Sciences Serie IV Physique Astrophysique* 2, 1373 (2001); P. A. Heimann, H. A. Padmore, and R. W. Schoenlein, "ALS Beamline 6.0 For Ultrafast X-ray Absorption Spectroscopy," *AIP Conf. Proc.* 705 (1), 1407 (2004).
- [12] J. Miao, "High-resolution 3D x-ray diffraction microscopy," *Phys. Rev. Lett.* 89, 088303 (2002).
- [13] S. Marchesini et al., "X-ray image reconstruction from a diffraction pattern alone," *Phys. Rev. B* 68, 140101(R) (2003).
- [14] J. Chavanne, P. Elleaume, and P. Van Vaerenbergh, "Recent developments of insertion devices at the ESRF," in *Proceedings of the 1999 Particle Accelerator Conference*, New York, 1999.
- [15] T. Hara, T. Tanaka, T. Tanabe, X.M. Marechal, S. Okada, and H. Kitamura, "In-vacuum undulators of SPring-8," *J. Synchrotron Rad.* 5, 403 (1998).
- [16] R. Schlueter, S. Marks, S. Prestemon, and D. Dietderich, "Superconducting undulator research at LBNL," *Synchrotron Radiation News* 17(1), 33 (2004).

- [17] S. Prestemon, D. Dietderich, S. Marks, and R. Schlueter, "NbTi and Nb₃Sn Superconducting Undulator Designs," *AIP Conf. Proc.* 705, 294 (2004).
- [18] C. Steier, D. Robin, A. Wolski, G. Portmann, and J. Safranek, "Coupling Correction and Beam Dynamics at Ultralow Vertical Emittance in the ALS," in *Proceedings of the 2003 Particle Accelerator Conference*, 3213-3215.
- [19] L. Emery and M. Borland, *Proceedings of the 1999 Particle Accelerator Conference (1999)* 200-202
- [20] M Boege, *Proceedings of the 2002 European Particle Accelerator Conference (2002)* 39-43
- [21] H. Tanaka et al, *Proceedings of the 2004 European Particle Accelerator Conference*
- [22] H. Nishimura, "The Horizontal Orbit When SR08C SuperBend is Tripping", LSAP Note # (2004)
- [23] M. Borland and L. Emery, *Proceedings of the 1999 Particle Accelerator Conference, New York* 2319 – 2321 (1999)
- [24] L. Favraque, Private Communication
- [25] Engineering Note: Light Source – Booster Extraction Bump Magnets. AL0323, M6852
- [26] G.Stover "Comparison of Booster ring "Bump magnet" B field measurements vs. calculations @ 1.522 and 2.0 Gev." ALS Top-Off Project Note 04/19/2004
- [27] S.Kwiatkowski "Do we need to modify the Booster fast extraction kicker for Top-Off operation?" ALS Top-Off Project Note 02/20/2002
- [28] "High Energy Linacs": Applications to Storage Ring RF Systems and Linear Colliders, Perry B. Wilson SLAC Publication 1991
- [29] M.Sands. "Observation of Quantum Effects in an Electron Synchrotron." International Conference on Accelerators, CERN, 1959
- [30] M.Sands. "Physics of Electron Storage Rings." SLAC Report No. 121 (1970).
- [31] N. Sereno, *Proceedings of the 1999 Particle Accelerator Conference, New York, US, 1999*, p. 2322.
- [32] H. Suzuki, *et al.*, *Nuclear Instruments and Methods in Physics Research A* 444 (2000) 515-533.
- [33] T. Aoki, *et al.*, *Proceedings of the 2003 Particle Accelerator Conference, Portland, US, May 2003*, p. 2551.
- [34] E. Plouviez, ESRF Machine Technical Note 01-04/MDT.
- [35] E. Plouviez, P. Ellaume, private communications.

6.1 List of Figures

Figure 1.2-1: Parameters of top-off injection after the upgrade with reduced vertical emittance. . 9

Figure 1.2-2: Brightness comparison of new ALS insertion devices to current insertion devices.	10
Figure 1.3-1: Beamlines at the ALS. In the upgrade, the five “workhorse” 4.45-m-long U5, U8, and U10 undulators would be replaced with nine shorter, small-gap devices with higher brightness in an orderly, phased manner to minimize disruption of the experimental program.	11
Figure 2.1-1: Layout of our present injection system.....	14
Figure 2.1-2: Booster ramping cycle.	15
Figure 3.1-1: Heating induced focusing error on sagittally focusing mirror.	20
Figure 3.1-2: Fast (vertical and horizontal) oscillation of the beam, due to mismatch of the bump magnets. This lasts less than 1 ms.	22
Figure 3.1-3: Slower (horizontal) closed orbit distortion, due to the septum magnet eddy currents, that lasts about 0.1 s.	23
Figure 3.1-4: Injection transients causing an intensity fluctuation during a horizontal line scan in STXM at beam line 11.0.2 (second test 7 Dec 2003). Septum magnet turned off. One horizontal line scan takes 60 ms.	24
Figure 3.2-1: Locations of Radiation Monitors at the ALS.	26
Figure 3.2-2: Active Radiation Monitors: Interlocked Neutron/Gamma Monitors (left) and Optics Gamma Monitors (right).	27
Figure 3.2-3: Passive Radiation Monitors: In-close dosimeters (left) and Peripheral dosimeters (right).	27
Figure 3.2-4: Passive Dose equivalent at 30 cm of one injected pulse of electrons carrying 1 nC of charge striking a high Z material.	30
Figure 3.2-5: Geometry of x.1 beamline. Rays A-D mark the extremes in angle and offset that still pass through the frontend apertures. Ray N marks the nominal center of a x.1 beamline.	31
Figure 3.2-6: Maximum distance injected back to SR injection point.	32
Figure 3.2-7: Trajectories of several important particles.....	33
Figure 3.2-8: Jackson hole locations on arc sector	34
Figure 3.2-9: Closed orbit distortion following rf trip.	35
Figure 3.2-10: Beam loss at SR02 JH6 and SR03 JH1 as a function of JH half gap height.....	36
Figure 3.2-11: CAD drawing of the double sided horizontal collimator for the BTS transfer line.	37
Figure 3.2-12: A pair of vertical scrapers installed in the so-called Jackson holes of one of the storage ring arc vacuum chambers.....	38
Figure 3.2-13: Drive system, cooling and inner structure of vertical scrapers.	39
Figure 3.2-14: Potential operational modes and logic for transitioning between them both for the current ALS operation and for top-off. B1 and B2 are the first two bending magnets in the booster to storage ring (BTS) transfer line.	41
Figure 3.2-15: Logic of a (potential) beam line radiation monitor interlock system.....	43
Figure 3.3-1: Histograms showing the results of simulated vertical emittance and dispersion correction for 100 randomly misaligned error seeds.	46
Figure 3.3-2: Horizontal/vertical beamsize and beam tilt as calculated from calibrated machine model using orbit response matrix analysis. The blue case is before coupling correction, the green one after one iteration.	47

Figure 3.3-3: Vertical beamsize for two four day periods. Using a global vertical dispersion wave to increase the vertical emittance (right) leads to a much better beamsize stability than excitation of the coupling resonance (left).....	48
Figure 3.3-4: Measured lifetime of the ALS versus half aperture in one straight for three different cases: excited coupling resonance (red), corrected coupling and vertical dispersion (green), vertical dispersion wave (blue). The two cases with excited coupling resonance and dispersion wave were measured for identical vertical emittance.....	49
Figure 3.3-5: Lifetime of the ALS versus half aperture in one straight, measured using a scraper: The lifetime reduction for a lattice with corrected coupling and vertical dispersion wave to increase the vertical emittance is small down to a full vertical aperture of about 5 mm.....	50
Figure 3.3-6: Dependence of ALS injection efficiency (without re-optimization) on insertion device settings. Only the W11 wiggler reduces the injection efficiency significantly. Because the integration time of the storage ring current monitor is not exactly matched to the injector period, the measurements have some jitter around the correct values. This also explains why some of the measurements indicate injection efficiencies above 100%.....	51
Figure 3.3-7: Dependence of ALS injection efficiency on the vertical physical aperture in the storage ring without any re-optimization. The aperture was changed by opening and closing two vertical scrapers in straight 3 at a beta function of about 6 m.	52
Figure 3.3-8: Reduction in radiation dose at first optics in beamline 4.0 due to ALS beam dump using a vertical collimator at the end of straight 3. The vertical axis shows average count rates of radiation monitors and the horizontal axis is time in minutes. Shown are 3 (intentional) beam dumps with equal stored beam current. After the first dump with scraper open, the scraper (at a vertical beta function of about 6 m) was set to a full aperture of 8 mm for the second, and 5 mm for the third beam dump.	53
Figure 3.5-1: Booster extraction magnets.	60
Figure 3.5-2: Storage Ring injection area.	61
Figure 3.5-3: Timing diagram for booster/storage extraction/injection magnets. Time periods not to scale	62
Figure 3.5-4: Location of booster extraction magnets.	63
Figure 3.5-5: Bump Magnets core and coil geometry	64
Figure 3.5-6: Basic discharge circuit	64
Figure 3.5-7: Waveform pictures taken at peak drive current of 312 amps	66
Figure 3.5-8: Field versus current transfer function for the second booster extraction bump magnet.....	66
Figure 3.5-9: INSOFT Half magnet simulation of B field @ 2.0 Gev	69
Figure 3.5-10: Drawing of kicker test stand arrangement.	70
Figure 3.5-11: Basic discharge circuit for the thin and thick septum magnet	72
Figure 3.5-12: Basic discharge circuit waveforms for the thick septum magnet.....	73
Figure 3.5-13: Top view of Septa magnet layout – SR straight. Each magnet sectioned through the horizontal midplane.....	75
Figure 3.5-14: Thick (left) and thin (right) Septa cross sections – (needs to be resized)	75
Figure 3.5-15: Vertical B field component along the transverse width of the gap at the mid-plane. For 1.525 Gev, 2.0 Gev, and + 10%	78
Figure 3.5-16: Thin septum high current (B=0.40T) curve normalized to the present nominal current (B=0.30T) across the gap midplane, near the narrow end.....	79

Figure 3.5-17: Beam orbit distortion due to slowly decaying eddy currents in thick septum magnet.....	80
Figure 3.5-18: Thick septum at peak field (1.33 tesla) of half sine pulse.....	81
Figure 3.5-19: Thick septum at zero field at end of half sine pulse.....	82
Figure 3.5-20: Thick septum stray field at its maximum value at 1.0 msec after the start of the ‘half sine’ current pulse.	83
Figure 3.5-21: Flux lines at the end of a damped ‘full sine’ current pulse using a measured damping factor of (93.5% voltage reversal)	84
Figure 3.5-22: Predicted time history of this stray field integral along the beam axis and measured orbit distortion for half-sine and damped full-sine case.	85
Figure 3.5-23: Rod-plane insulation tests from Alston.....	87
Figure 3.5-24: One of four bipolar switch modules.....	91
Figure 3.8-1: Principal drawing of Booster RF system.	98
Figure 3.8-2: RF buckets and particle distribution in ALS Booster at 1.9 GeV.....	103
Figure 3.8-3: RF buckets and 10 injected linac bunches into ALS Booster at 50 MeV.....	103
Figure 3.9-1: Bunch cleaning system schematics	109
Figure 3.9-2: BTS optical function, beam sizes and SR source point positions.....	114
Figure 3.9-3: Synchrotron radiation monitor at BTS bend B1.	115
Figure 3.9-4: Synchrotron radiation monitor at BTS bend B3 and detail of the mirror area. For the symbols in the figure see Table 3.9-5.	116
Figure 3.9-5: Synchrotron radiation monitor at BTS bend B3, a 3D CAD view.	116
Figure 3.9-6: CAD drawing of the BTS diagnostic beam stop. A tungsten block being inserted vertically into the beam path.....	118
Figure 3.9-7: Bunch Purity Monitor Block Diagram.....	119
Figure 3.9-8: Schematic of a bunch-by-bunch current monitor for the ALS Storage Ring.....	119
Figure 3.11-1: Diagram of the electrical supply bank 303 at the ALS.	128
Figure 3.11-2: Diagram of the AC supply bank 302 at the ALS.	129
Figure 4.4-1: Complete draft schedule for the ALS Top-off upgrade as of November 19, 2004.	139

6.2 List of Tables

Table 1.2-1: Comparison of Present and Future Storage-Ring Parameters	9
Table 1.2-2: Comparison of Present and Future Brightness (photons/sec/0.01%bw /mm ² /mrad ²)	10
Table 2.2-1: Difference between present operation and operation after the top-off upgrade.....	18
Table 3.1-1: Operational parameters chosen as goal for the ALS top-off upgrade.	20
Table 3.2-1: A January 2004 summary report of the in-close gamma and neutron monitors.	28
Table 3.2-2: Geometry parameters of the apertures for a x.1 beamline.	31
Table 3.4-1: Injection System Faults/Failures 1 Oct 03 to 1 Oct 04.....	56
Table 3.5-1: Current and future operation parameters for booster extraction bump magnets.....	65
Table 3.5-2: Thick septum operational parameters for higher fields:.....	73
Table 3.5-3: Thin septum operational parameters for higher fields (SR thin septum*):	73
Table 3.5-4: Thin and Thick septum fixed parameters	76
Table 3.5-5: Thick septum operating parameters	76

Table 3.5-6: Thin septum operating parameters (SR thin septum).....	76
Table 3.6-1: List of all mayor dc and ramped power supplies in the booster and BTS including upgrade requirements.....	95
Table 3.6-2: List of capability of DC cables for all mayor booster and BTS power supplies.....	95
Table 3.8-1: ALS Booster RF parameters as a function of η_{σ} parameter.	101
Table 3.8-2: Booster RF parameters for proposed energy ramp for ALS Top-Off mode of operation.	102
Table 3.8-3: RF parameters for current and Top-Off mode.....	104
Table 3.8-4: Electrical power and LCW requirements for current installation and upgrade condition.	106
Table 3.9-1: Cleaning system parameters for the ALS Booster.	110
Table 3.9-2: ALS-like stripline kicker characteristics.	111
Table 3.9-3: Beam charge monitors in the ALS complex.	113
Table 3.9-4: Source Point 1 synchrotron radiation characteristics	115
Table 3.9-5: Source Point 2 synchrotron radiation characteristics	116
Table 4.3-1: Summary of the cost estimate for the ALS Top-off upgrade as of November 19, 2004.....	132
Table 4.3-2: Cost estimate down to WBS level 3 for the ALS top-off upgrade as of November 19, 2004.....	133

7 APPENDICES

7.1 Parameter List

7.1.1 Storage Ring Performance Parameters

Beam Energy	1.0 – 1.9 GeV (1.9 GeV nominal)
Beam Current (multibunch)	10-500 mA (500 mA nominal)
Number of bunches (multibunch)	250-320
Beam Current (two bunch)	10-60 mA (50 mA nominal)
Bunch purity (two bunch)	$< 10^{-4}$
Beam Current (single camshaft bunch)	< 12 mA (10 mA nominal)
Bunch purity (camshaft)	$< 10^{-4}$
Natural horizontal emittance	< 6.75 nm (nominal 6.3 nm at 1.9 GeV, W11 closed)
Vertical emittance	10 – 150 pm (nominal 30 pm, 1.9 GeV, multibunch)
Beam Energy Spread	$0.97 \cdot 10^{-3}$ (1.9 GeV, multibunch)
Bunch length	20-50 ps (rms, 1.9 GeV multibunch, nominal 30 ps)
Touschek lifetime (multibunch)	> 2 h (1.9 GeV, 500 mA, 6.3 nm, 30 pm)
Current stability in top-off (typical)	$3 \cdot 10^{-3}$ (multibunch, 1.9 GeV, i.e. 1.5 mA out of 500 mA)
Typical time between injections	30 s
Stored beam transients due to injection elements	Horiz.: < 400 μ m peak for less than 200 μ s, < 50 μ m peak for less than 100 ms Vert.: < 100 μ m peak for less than 300 μ s, < 10 μ m peak for less than 100 ms
Injection efficiency	$> 60\%$

7.1.2 Booster Performance Parameters

Injection Energy	50 MeV
Extraction Energy	1.0 – 1.9 GeV (nominal 1.9 GeV)
Number of bunches	1-10
Maximum Charge	3.3 nC
Cycle Rate	0.005-1 Hz (nominal 0.33 Hz at 1.9 GeV for initial injection, 0.033 Hz for top-off)
Injected beam emittance	1.1 μ m

Injected longitudinal emittance ($6\pi\sigma_E\sigma_\tau$)	$3.9*10^{-4}$ eVs
Natural horizontal emittance	230 nm (1.9 GeV)
Energy spread	$0.8*10^{-3}$ (1.9 GeV)
Bunch purity at extraction	$<10^{-4}$

7.1.3 Technical Parameters

Booster maximum bending field	1.622 T (1.95 GeV)
Corresponding dipole current	1019 A
Dipole power supply repeatability	0.05 %
Booster maximum quadrupole field	19.79 T/m (1.95 GeV)
Corresponding quadrupole current	500 A
Quadrupole power supply repeatability	0.05 %
Booster maximum sextupole current	10 A
Sextupole power supply repeatability	0.1 %
Maximum klystron RF power installed	>75 kW
Maximum dissipated cavity cell power	<70 kW (nominal 66 kW)
Booster Extraction bumps maximum field	0.5 T (0.47 T nominal)
Corresponding bump current	306 A
Booster extraction kicker maximum voltage	17 kV
Booster thin septum maximum field	0.38 T
Corresponding septum current	4550 A
Booster thick septum maximum field	1.3 T
Corresponding septum current	5210 A
BTS bend magnets (B1-B4) maximum field	1.677 T (1.95 GeV)
BTS bend magnets (B1-B4) maximum current	846 A
Power supply stability	300 ppm
Storage ring injection bumps maximum current	7000 A
Storage ring thin septum maximum field	0.38 T
Corresponding septum current	5460 A
Storage ring thick septum maximum field	1.3 T
Corresponding septum current	5210 A
Nominal physical aperture at injection point	> 15 mm

7.2 Full Cost Estimate

November 19, 2004

Description	MATERIAL				LABOR							Total Labor + Material	Overhead Total	Sub Total	TOTALS		
	Unit Meas	Material No.	Cost Basis	Unit Cost	Total Material K\$	Labor No. Units	Labor Unit Hours	Labor Total Hours	Craft Code	Labor Rate \$/Hr.	Total Labor K\$				Total %	Cntng K\$	Totals K\$
1	ALS Top Off Upgrade				2,092.5						1,416.4	3,508.9	492.7	4,001.5	21%	849.7	4,851.3
1.1	Project Management				0.0						95.4	95.4	19.6	115.0	10%	11.5	126.5
	Project Management	ea	0	eu	0	0.0	1	624	624	ap	93.65	58.4	58.4				
		ea	0	eu	0	0.0	1	624	624	pc	59.18	36.9	36.9				
1.2	Top off Documentation				0.0						3.7	3.7	0.8	4.5	10%	0.5	5.0
1.2.1	Complete Top Off Documentation	ea	0	eu	0	0.0	1	40	40	ap	93.65	3.7	3.7				
1.3	Linac				6.0						16.7	22.7	4.0	26.7	20%	5.3	32.1
1.3.1	Diagnosics					6.0					16.7	22.7	4.0	26.7	20%	5.3	32.1
1.3.1.1	EDI																
1.3.1.1.1	Integrating Current Transformer EDI	ea	0	eu	0	0.0	1	40	40	ee	80.23	3.2	3.2				
1.3.1.1.2	Beam Intensity Monitor EDI	ea	1	eu	1	0.0	1	120	120	ee	80.23	9.6	9.6				
1.3.1.2	Integrating Current Transformer	ea	1	eu	1000	1.0	1	40	40	ei	48.28	1.9	2.9				
1.3.1.3	Beam Intensity Monitor	ea	1	eu	5000	5.0	1	40	40	ei	48.28	1.9	6.9				
1.4	Booster				1,380.5						470.3	1,850.9	229.4	2,080.3	19%	394.1	2,474.4
1.4.1	Power Supplies					540.0					18.3	558.3	55.6	613.9	20%	122.8	736.7
1.4.1.1	EDI																
1.4.1.1.1	Bend EDI	ea	0	eu	0	0.0	1	30	30	ee	80.23	2.4	2.4				
1.4.1.1.2	Quadrupole EDI	ea	0	eu	0	0.0	1	30	30	ee	80.23	2.4	2.4				
1.4.1.1.3	Sextupole EDI	ea	0	eu	0	0.0	1	20	20	ee	80.23	1.6	1.6				
1.4.1.2	Bend Power Supply	ea	1	eu	300000	300.0	0	0	0	ee	80.23	0.0	300.0				
1.4.1.3	Quadrupole Power Supplies	ea	2	eu	100000	200.0	0	0	0	ee	80.23	0.0	200.0				
1.4.1.4	Sextupole Power Supplies	ea	8	eu	5000	40.0	0	0	0	ee	80.23	0.0	40.0				
1.4.1.5	Installation	ea	0	eu	0	0.0	3	10	30	ei	48.28	1.4	1.4				
		ea	0	eu	0	0.0	12	6	72	rg	48.95	3.5	3.5				
		ea	0	eu	0	0.0	3	4	12	ru	48.40	0.6	0.6				
		ea	0	eu	0	0.0	3	40	120	ei	52.88	6.3	6.3				
1.4.2	Thin Septum Magnet					9.4					28.3	37.7	6.7	44.4	25%	11.1	55.5
1.4.2.1	EDI	ea	0	eu	0	0.0	1	40	40	ee	80.23	3.2	3.2				
1.4.2.2	Power Supplies - KSI Replacement	ea	2	eu	3300	6.6	1	2	2	ec	69.74	0.1	6.7				
1.4.2.2.1	Build New PS Interface & Upgrade Glassm	ea	1	eu	250	0.3	1	80	80	ei	48.28	3.9	4.1				
1.4.2.2.2	Replacement Capacitors	ea	10	eu	250	2.5	1	40	40	ee	80.23	3.2	5.7				
1.4.2.3	Magnet Swap Out	ea	0	eu	0	0.0	1	80	80	ee	80.23	6.4	6.4				
		ea	0	eu	0	0.0	1	80	80	me	70.49	5.6	5.6				
		ea	0	eu	0	0.0	1	80	80	ma	73.18	5.9	5.9				
1.4.3	Thick Septum Magnet					7.1					8.9	16.0	2.5	18.6	25%	4.6	23.2
1.4.3.1	EDI	ea	0	eu	0	0.0	1	20	20	ee	80.23	1.6	1.6				
		ea	0	eu	0	0.0	1	20	20	ec	69.74	1.4	1.4				

